AN ABSTRACT OF THE THESIS OF

Liang-Ju Lai for the degree of Doctor of Philosophy in Mechanical Engineering presented on February 2, 1999. Title: Rebound Predictions of Mechanical Collisions.

Redacted for Privacy

Abstract approved: _____

Charles E. Smith

Predictions of mechanical collisions between two bodies frequently cannot be completed by the impulse-momentum equation together with a complete description of the motion of the system at the initial contact. Additional account must be taken of the deformations and frictional interaction induced by the impulsive reaction force, where the bodies contact one another, as these play an important role in the outcome of the collision.

During the time the bodies are in contact, elastic, friction and inertia properties combine to produce a complex variation of sliding and sticking through out the contact surface. For accurately predicting the impulse and velocity changes during contact, a considerably simplified, coupled, conservative model, which captures the essential characteristics of the elastic-friction interaction during contact loading, is investigated in this thesis. In this simplified model, the interface between two colliding bodies resembles the behavior of a pair of mutually perpendicular, non-linear springs which react independently with the exception that the stiffness of the tangential "spring" is influenced by the normal displacement. These elastic properties, in combination with

inertial properties derived from generalized impulse-momentum laws, form a "spring-mass" system for which numerical integration yields the prediction of rebound velocities.

For comparison, an explicit non-linear finite element code, DYNA3D, developed at Lawrence Livermore National Laboratory for analyzing the transient dynamic response of three-dimensional solids, is used to predict the responses of an elastic sphere and elastic rod, each colliding with a rigid plane with varying initial velocities and configurations. Results are also compared with results of a complex analysis of collisions of spheres by Maw, Barber, and Fawcett (1976).

Rebound Predictions of Mechanical Collisions

by

Liang-Ju Lai

A THESIS

submitted to

Oregon State University

in partial fulfillment of
the requirements for the
degree of

Doctor of Philosophy

Presented February 2, 1999
Commencement June 1999

Doctor of Philosophy thesis of Liang-Ju Lai presented on February 2, 1999

APPROVED:

Redacted for Privacy

Major Professor, representing Mechanical Engineering

Redacted for Privacy

Chair of Department of Mechanical Engineering

Redacted for Privacy

Dean of Graduate School

I understand that my thesis will become part of the permanent collection of Oregon State University libraries. My signature below authorizes release of my thesis to any reader upon request.

Redacted for Privacy

Liang-Ju Lai, Author

TABLE OF CONTENTS

TABLE OF CONTENTS (Continued)

LIST OF FIGURES

LIST OF FIGURES (Continued)

LIST OF FIGURES (Continued)

LIST OF FIGURES (Continued)

LIST OF TABLES

Rebound Predictions of Mechanical Collisions

1. INTRODUCTION

Since the collision of the bodies within mechanical systems often do not deform any of the bodies significantly, a widely used approach for modeling of mechanical collisions is to treat the two objects that contact as rigid bodies. At the present time, most predictions of collisions between two bodies make use of this assumption, treating the bodies as rigid, with contact at a single point. Each body is assumed to exert an instantaneous impulse on the other at the contact point. When a system S is involved in a collision beginning at time t_1 and ending at time t_2, the motion of S at time t_2 cannot be determined by use solely of the impulse-momentum equation and description of the motion of S at time t_1. This is because the equations of rigid body kinetics are three too few to predict the six components of impulse and separation velocity. Generally, in the absence of detailed knowledge of the deformations and related normal and friction forces induced where the bodies contact one another, additional assumptions about the nature of the reaction must be made. In the other words, if the stress, strain and displacement of the interaction are fully analyzed properly for the contact region of colliding bodies, those additional assumptions are unnecessary.

Because the post-collision motion depends so heavily on the unknown impulse, the assumptions that form a "contact law" to supplement equations of rigid body mechanics, have a profound effect on the predicted motion. Usually the simplifying assumptions are based on speculations about such things as sliding with friction and the

capacity of the bodies to return energy of deformation. Assumptions such as known "coefficient of restitution", a ratio that must be estimated before the prediction can be completed, are usually incorporated in simplified procedures for predicting post-collision motion. The coefficient of restitution, widely believed to have a value of one for a perfect elastic body and zero for a pure plastic body, has been considered as a material property from which changes of velocities can be computed. However, the coefficient of restitution is dependent on the configuration of system, approach angle and the coefficient of friction (Liu, 1991). But there still is no reliable method of evaluation of these quantities available.

The elastic deformations that occur during the impact of colliding bodies may be small in comparison to their actual dimensions, but they play an important role in mechanical collisions. The theory of elasticity permits the examination of wave propagation in impact problems and a specification of stress distributions at the contact point. During the time the bodies are in contact, elastic, friction and inertia properties combine to produce a complex variation of sliding and sticking through out the contact surface. Although detailed analysis of this contact interaction is quite tedious, it would be seen to be necessary for accurately predicting the impulse and velocity changes that occur during contact.

Because such detailed analysis is very complicated and tedious, a simplified, yet acceptably accurate, procedure for predicting post-collision motion is desirable. Therefore, the investigation of the local deformation of the contact area of two colliding bodies, with the objective of developing an accurate simplified method, is made in this thesis. As known previously, the interface conditions between the two bodies is more

complex than might be expected. A considerably simplified model that captures the essential characteristics of the elastic-friction interaction during contact loading will predict the impulse and velocity changes. In this simplified model, the interface between two colliding bodies resembles the behavior of a pair of mutually perpendicular, non-linear springs which react independently against each of the bodies, with the exception that the stiffness of the tangential "spring" is influenced by the normal compliance. If the local deformations between colliding bodies were expressed in terms of spring stiffness in the normal and tangential directions, then the collision process could be solved as a spring-mass system.

The past research and investigations will be discussed in chapter 2. The background of the simplified prediction of planar collisions is focused on the generalized impulse-momentum relationship, which formulated the inertia, M, of the colliding system and the modeling stiffness, K, of local deformation of the contact area and are presented in chapter 3. In chapter 4, the contact mechanics of elastic bodies is described. The simplified model is discussed in chapter 5 in detail. The simulation using the DYNA3D finite element code is represented in chapter 6. The conclusion and the summary of the results are discussed in chapter 7.

2. LITERATURE REVIEW

Newton furnished not only his laws of motion but also the notion of the coefficient of restitution, which is still widely employed, though of questionable fundamental significance. Poisson's hypothesis separates the impact into a compression phase followed by a restitution phase. The former begins at the first contact of the bodies and terminates at the moment of greatest compression. The latter begins at the moment of greatest compression and terminates when the bodies separate. Recent attempts have been made to study impact in the presence of friction. Some theories derived from Poisson's impact hypothesis, involving the tangential component of the contact impulse have some limitations, as discussed in the following.

Whittaker's (1904) theory, derived from Newton's law and Poisson's hypothesis, violates energy conservation laws in some cases. Whittaker assumed the tangential component of separation velocity, w_t, is zero if the magnitude of the tangential impulse is less than the coefficient of friction, μ, times the magnitude of the normal impulse, g_n and that the separation velocity, w, will have a tangential component, w_t, if the magnitude of the tangential impulse, g_t, equals the coefficient of friction, μ, times the magnitude of the normal impulse, g_n. Then, the tangential component, w_t, is computed from impulse-momentum and kinematics relationships. Whittaker's method is correct only when the initial slip does not stop and keeps constant direction throughout the collision.

Kane and Levinson (1985) use the same criteria as Whittaker, but distinguish between coefficients of static and kinetic friction and are more specific about direction, stating that if and only if

$$|g_t| \le \mu_0 |g_n|, \tag{2.1}$$

then

$$w_t = 0, \tag{2.2}$$

and if the inequality is violated, we will have

$$g_t = -\mu |g_n| \frac{w_t}{|w_t|} \tag{2.3}$$

in which μ_0 is the coefficient of static friction and μ is the coefficient of kinetic friction. When applied to a double pendulum striking a fixed surface in certain configurations, these criteria predict an increase of kinetic energy. That means this theory violates the law of energy conservation. When the bodies slip with friction at the beginning of a collision and stop slipping during the collision, some assumptions used in conjunction with Newton's impact law violate energy conservation laws. Keller (1986) and Brach (1989) explained the pendulum striking a fixed surface leading to an increase of kinetic energy that it is due to reverse slip during the impact, but the difficulty in using his theory arises in calculation.

Several recent papers check for energy conservation. Smith (1991) proposed an alternative contact law that gives a more realistic estimate of the rebound. Smith used the kinematics definition of the coefficient of normal restitution, and a frictional impulse that is defined using an intuitively appealing weighted average of the pre-collision and post-collision tangential components of the relative velocities. Smith showed that this model is guaranteed not to create kinetic energy in a collision. With $\boldsymbol{g}_t$ and $\boldsymbol{g}_n$ designating the tangential and normal components of impulse and $\boldsymbol{v}_t$ and $\boldsymbol{w}_t$ designating the tangential components of the pre-collision and post-collision relative velocities respectively, Smith's frictional relationship is stated as

$$\boldsymbol{g}_t = -\mu |\boldsymbol{g}_n| \frac{|\boldsymbol{v}_t| \boldsymbol{v}_t + |\boldsymbol{w}_t| \boldsymbol{w}_t}{|\boldsymbol{v}_t|^2 + |\boldsymbol{w}_t|^2}. \tag{2.4}$$

This, together with the kinematics definition of the coefficient of restitution e,

$$\boldsymbol{w}_n = -e\, \boldsymbol{v}_n, \tag{2.5}$$

and the impulse-momentum relationship, permit estimation of the impulse and corresponding separation velocity. In Smith's model, the intuitive meaning of the coefficient of restitution is clear. Energy dissipation is assured. The frictional impulse incorporates direction and magnitude information about the tangential components of both pre-collision and post-collision velocities, and satisfies the friction inequality.

Brach (1989) used two linear relations for changes in tangential velocity; these employed the kinematics coefficient of restitution at very small angles of incidence and a kinetic coefficient of restitution at larger angles. All of these approaches by Smith (1991) and Brach (1989) were designed to produce at large angles of incidence a ratio of tangential to normal impulse equal to the coefficient of friction; they represent Coulomb's law of friction only in the limit, as sliding becomes continuous in the initial direction.

Routh (1905) presented an analysis using graphic guidance of the tangential and normal impulse between two colliding bodies, assuming no tangential compliance. Routh's analysis deals with two phases of the contact, a "compression" phase in which the normal velocity difference passes from $\boldsymbol{v}_n$ to 0 and a "restitution" phase in which the normal velocity difference passes from 0 to $-\boldsymbol{w}_n$. In this analysis, Routh defines the coefficient of restitution, c, as the ratio of normal impulse during restitution, $\boldsymbol{g}_{nr}$, and normal impulse during compression, $\boldsymbol{g}_{nc}$, i.e., $c = \boldsymbol{g}_{nr} / \boldsymbol{g}_{nc}$. An assumption implicit in Routh's analysis is that the tangential velocities are as given by rigid body kinematics, i.e.,

sliding or the lack of sliding is unaffected by deformations. Routh indicates that motion following cessation of slip depends on the coefficient of friction μ and the limiting ratio μ', a geometric parameter that depends on the distribution of mass in the colliding bodies. If the coefficient of friction μ is larger than the limiting ratio μ', the colliding body will stop slipping and simply roll. If the coefficient of friction μ is less than the limiting ratio μ' then reverse slip occurs after slip stops or gross slip occurs throughout the collision. Although this analysis has constituted a contribution to realistic solution for rebounds, it indicates that, under some circumstances, reverse slip occurs immediately after initial slip stops and the tangential force is subject to discontinuous changes as the sliding reverse direction. However, in practice, sudden changes in tangential force implied by ignoring tangential deformations of colliding bodies are unlikely to occur. Consequently, it has been evident that even the relatively small elastic deformations that occur during impacts have served to introduce effects that must be taken into account in the analysis of the elastic collisions. Smith and Liu (1992) compared the graphs of Routh's analysis with those resulting from a detailed finite element analysis of forces and deformations during contact.

Impact phenomena should be dealt with as dynamic problem since vibrations are caused by impact. A basis for this analysis is the theory of local contact deformation developed by Hertz, which has found wide use in spite of the static elastic nature of its derivation. This analysis accounts for the fact, that the contact occurs over a surface and has small duration. For elastic bodies, the Hertzian theory of impact indicates that the contact area is proportional to $p^{2/3}$, where p is the impact force. The Hertzian theory of impact follows directly from his static theory of contact between frictionless elastic bodies where the deformation is assumed to be restricted to the vicinity of the contact area.

Although wave propagation in the bodies is ignored, this restricted theory has been shown (Hunter, 1957) to lead to acceptable results for sufficiently low velocity.

Extensions of the Hertz contact collision model to frictional collisions have been proposed. These models assume that the contacting bodies have locally spherical surfaces, where the contact behavior follows the approximate solution given by Mindlin (1949) and Deresiewicz (1953). Mindlin examined tangential compliance for the contact between two elastic spheres under the action of friction, keeping the normal force constant. He showed that, for small relative tangential loads, an annulus of micro-slip is generated at the boundary of the contact area. As tangential load increases, the inner radius of this annulus progressively reduces until, when the critical value of friction force is reached, the surface breaks away in gross slip. On the other hand, when the tangential force is subsequently decreased, this process would not simply reverse. A central circular region remains stuck while sliding or micro-slip occurs in the surrounding area. Hence, it is determined that the state of unloading is different from that of loading, and that the process is irreversible. The irreversibility implied by friction slip demonstrates that the final state of contact depends on the previous history of loading and not only on the final values of the normal and tangential forces. In addition, Mindlin and Deresiewicz (1953) have investigated changes in surface traction and compliance between spherical bodies in contact arising from various possible combinations of incremental changes of loads. Since the contact area is changed continuously, and neither the normal nor the tangential forces could be known previously, the interface conditions between the two bodies is more complex than might be expected.

Maw, Barber, and Fawcett (1976) use a numerical method to examine the oblique

impact of elastic spheres by trial and error. By using Hertzian theory, they postulated that where bodies respond to friction forces some of the work done in deflecting the bodies tangentially is stored as elastic strain energy in the solids and is recoverable under suitable circumstances. By assuming that the contact area comprises sticking and slipping regions and the coefficient of friction is constant in the slipping region, Maw developed a solution for the oblique impact of an elastic sphere on a fixed, perfectly rigid body. During collision, contact spreads from a point into a small region wherein tangential compliance influences the development of local slip. The tangential compliance of the contact surface under the action of Coulomb's friction have a significant effect on the rebound angle, if the local angle of incidence does not greatly exceed the angle of friction. Tangential elasticity exerts considerable influence at low angles of incidence. This analysis indicates that error will be incurred if the impact response is determined from some of the simpler rigid-body theories.

Liu (1991) used the ANSYS finite element code to evaluate the predictions made by simpler methods. During collision, the contact area grows from a point at the first contact to a maximum value at the end of the compression phase and vanishes when the bodies separate.

Aum (1992) modeled the collision process using tangential and normal springs and a friction element in conjunction with rigid-body impulse/velocity-change constants. In this model, the interface between two colliding bodies resembles the behavior of a pair of mutually perpendicular, non-linear springs which react independently against each of the bodies, with the exception that the normal compliance influences the stiffness of the tangential "spring". Tangential and normal vibrations are dependent on the initial

condition as well as the inertia of the colliding bodies. The stiffness of the springs is also effected by Poisson's ratio.

Stronge (1994) used a lumped parameter representation, different from Maw's elastic continuum approach, for compliance of the contact region. Stronge assumed the normal and tangential springs are independent and linear, and the tangential spring has no dissipation, while the normal spring has different linear loading and unloading rates. The energy dissipation in the normal spring becomes consistent with the definition of an "energetic" coefficient of restitution. The mass matrix of the equation of motion is a constant, which means the configuration changes negligibly during contact. The collision terminates when the force in the normal spring falls to zero. The analysis distinguishes between angles of incidence where the contact point initially sticks, slides before sticking, or slides throughout the contact period. The tangential compliance significantly alters friction; this affects changes in relative velocity unless the angle of incidence is so large that there is continuous sliding in the initial direction.

3. SIMPLIFIED PREDICTION OF PLANAR COLLISIONS

Assumptions based upon rigid body mechanics are discussed in this chapter. Analysis is done using generalized coordinates and generalized speeds of a dynamic system introduced by Kane and Levinson (1985). The background of the simplified prediction of planar collisions is focused on the generalized impulse-momentum relationship, which is used to formulate the inertia of the colliding system. This will later be supplemented by the modeling stiffness of local deformation of the contact area.

3.1 Generalized Impulse, Momentum and Kinetic Energy

Consider two rigid bodies B and B' colliding as the points P and P' on their respective surfaces move into coincidence, in Figure 3.1. (P and P' are points of B and B', respectively.)

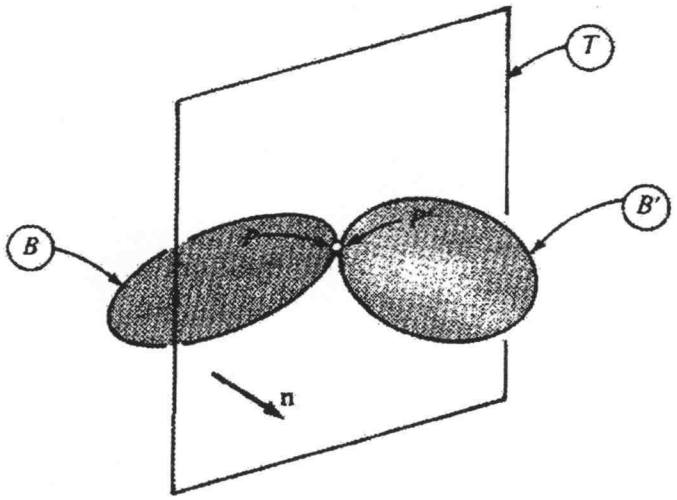

Figure 3.1 Two rigid bodies colliding with each other

If the system containing these bodies possesses n degrees of freedom, the velocities of the contact points P and P' can be written in terms of generalized speeds, u_r, as

$$\boldsymbol{v}^P = \sum_r \boldsymbol{v}_r^{\,P} u_r \,, \tag{3.1}$$

$$\boldsymbol{v}^{P'} = \sum_r \boldsymbol{v}_r^{\,P'} u_r \,, \tag{3.2}$$

where $\boldsymbol{v}_r^{\,P}$ and $\boldsymbol{v}_r^{\,P'}$ are the partial velocities. It is helpful to define the relative velocity $\boldsymbol{v}$ as,

$$\boldsymbol{v} = \boldsymbol{v}^P - \boldsymbol{v}^{P'} \,, \tag{3.3}$$

from which

$$\boldsymbol{v} = \sum_r \boldsymbol{v}_r u_r \,, \tag{3.4a}$$

where $\boldsymbol{v}_r = \boldsymbol{v}_r^{\,P} - \boldsymbol{v}_r^{\,P'}$. If the changes in configuration and contributions from forces other than the action-reaction at the contact point are neglected and the impulse of the force exerted on B and B' is denoted as $\boldsymbol{g}$, then the r^{th} component of generalized impulse can be expressed as

$$I_r = \boldsymbol{v}_r \cdot \boldsymbol{g} \,. \tag{3.5a}$$

Expressing the kinetic energy in terms of the selected generalized speeds, the inertia coefficients, m_{rs}, can be evaluated from

$$K = \frac{1}{2} \sum_r \sum_s m_{rs} u_r u_s \,. \tag{3.6}$$

According to the relationship

$$P_r = \frac{\partial K}{\partial u_r} \,, \tag{3.7}$$

this r[th] component of generalized momentum can be rewritten as

$$P_r = \sum_s m_{rs}\, u_s \,. \tag{3.8}$$

The impulse-momentum laws can then be expressed as

$$I_r = \Delta P_r = \sum_s m_{rs}\, \Delta u_s \ , \tag{3.9}$$

where Δu_s denotes the change in u_s during the contact.

If $\boldsymbol{v}$ and $\boldsymbol{w}$ are used to denote the relative velocity between the contact points P and P', at the beginning of contact and at the end of contact, then

$$\boldsymbol{w} = \boldsymbol{v} + \Delta \boldsymbol{v} \tag{3.10}$$

and

$$\Delta \boldsymbol{v} = \sum_r \boldsymbol{v}_r\, \Delta u_r \,. \tag{3.11a}$$

Now, let $\boldsymbol{e}_1$, $\boldsymbol{e}_2$ and $\boldsymbol{e}_3$ be a set of mutually perpendicular unit vectors, $l_{ri} = \boldsymbol{v}_r \cdot \boldsymbol{e}_i$ and $g_i = \boldsymbol{g} \cdot \boldsymbol{e}_i$. Then equation (3.4a), (3.5a) and (3.11a) can be written as

$$\begin{aligned} \boldsymbol{v} &= \boldsymbol{v}_1 u_1 + \boldsymbol{v}_2 u_2 + \cdots + \boldsymbol{v}_n u_n \\ &= (l_{11}\boldsymbol{e}_1 + l_{12}\boldsymbol{e}_2 + l_{13}\boldsymbol{e}_3)u_1 + \cdots + (l_{31}\boldsymbol{e}_1 + l_{32}\boldsymbol{e}_2 + l_{33}\boldsymbol{e}_3)u_3 \\ &= \left(\sum_r l_{r1} u_r\right)\boldsymbol{e}_1 + \left(\sum_r l_{r2} u_r\right)\boldsymbol{e}_2 + \left(\sum_r l_{r3} u_r\right)\boldsymbol{e}_3 \end{aligned} \tag{3.4b}$$

$$I_r = l_{r1} g_1 + l_{r2} g_2 + l_{r3} g_3 \tag{3.5b}$$

and

$$\Delta \boldsymbol{v} = \left(\sum_r l_{r1} \Delta u_r\right)\boldsymbol{e}_1 + \left(\sum_r l_{r2} \Delta u_r\right)\boldsymbol{e}_2 + \left(\sum_r l_{r3} \Delta u_r\right)\boldsymbol{e}_3 \,. \tag{3.11b}$$

So, the following matrix forms according to equation (3.4b), (3.5b), (3.6), (3.9) and (3.11b) become

$$\boldsymbol{v} = \boldsymbol{l}^T \boldsymbol{u} \,, \tag{3.12}$$

$$\boldsymbol{I} = \boldsymbol{l}\,\boldsymbol{g}\,, \tag{3.13}$$

$$K = \frac{1}{2}\boldsymbol{u}^T\boldsymbol{m}\,\boldsymbol{u}\,, \tag{3.14}$$

$$\boldsymbol{I} = \boldsymbol{m}\,\Delta\boldsymbol{u}\,, \tag{3.15}$$

and

$$\Delta\boldsymbol{v} = \boldsymbol{l}^T\Delta\boldsymbol{u}\,, \tag{3.16}$$

where $\boldsymbol{I}$, $\boldsymbol{u}$ and $\Delta\boldsymbol{u}$ are $(n\times 1)$ matrices, $\boldsymbol{g}$, $\boldsymbol{v}$ and $\Delta\boldsymbol{v}$ are (3×1) matrices, $\boldsymbol{l}$ is $(n\times 3)$ matrix, and $\boldsymbol{m}$ is $(n\times n)$ symmetric matrix for inertia. From equations (3.13) and (3.15),

$$\Delta\boldsymbol{u} = \boldsymbol{m}^{-1}\boldsymbol{l}\,\boldsymbol{g}\ , \tag{3.17}$$

and, substituting equation (3.17) into (3.16),

$$\Delta\boldsymbol{v} = \left(\boldsymbol{l}^T\boldsymbol{m}^{-1}\boldsymbol{l}\right)\boldsymbol{g} = \boldsymbol{N}\,\boldsymbol{g} \tag{3.18}$$

or

$$\boldsymbol{g} = \left(\boldsymbol{l}^T\boldsymbol{m}^{-1}\,\boldsymbol{l}\right)^{-1}\Delta\boldsymbol{v} = \boldsymbol{M}\,\Delta\boldsymbol{v}\ , \tag{3.19}$$

where

$$\boldsymbol{N} = \left(\boldsymbol{l}^T\boldsymbol{m}^{-1}\,\boldsymbol{l}\right) = \boldsymbol{M}^{-1}\,. \tag{3.20}$$

Both $\boldsymbol{N}$ and $\boldsymbol{M}$ are (3×3) symmetric matrices and depend on the configuration of the system at initial contact, but not on the motion. Also, if the configuration does not change significantly during impact, the small dynamic deformations during contact, and consequently $\boldsymbol{g}$, may be expected to depend on $\boldsymbol{v}$, but not on the particular set of generalized speeds that contribute to $\boldsymbol{v}$. Therefore, all pre-contact motions having the approach velocity $\boldsymbol{v}$ and the same configuration at the initial contact will result in the same impulse and corresponding separation velocity $\boldsymbol{w}$. Once $\Delta\boldsymbol{v}$ has been determined, changes in the generalized speeds can be evaluated from equation (3.17), where

$$\Delta \boldsymbol{u} = \boldsymbol{m}^{-1}\, \boldsymbol{l}\, \boldsymbol{M}\, \Delta \boldsymbol{v} \ , \tag{3.21}$$

and corresponding changes in velocities and angular velocities of interest can be evaluated using the appropriate partial velocities and partial angular velocities. Thus, from any set of generalized speeds, impulse and momentum relationships in equation (3.19) for the general configuration of the colliding system may be formulated in three dimensions.

The change in kinetic energy induced by the impulse is given by

$$\Delta K = \frac{1}{2}(\boldsymbol{u} + \Delta \boldsymbol{u})^T \cdot \boldsymbol{m} \cdot (\boldsymbol{u} + \Delta \boldsymbol{u}) - \frac{1}{2}\boldsymbol{u}^T \cdot \boldsymbol{m} \cdot \boldsymbol{u} \tag{3.22}$$

and through the relationship of generalized impulse and momentum described in this section, can also be expressed as:

$$\Delta K = \boldsymbol{g}^T \cdot \boldsymbol{v} + \frac{1}{2}\boldsymbol{g}^T \cdot \boldsymbol{M}^{-1} \cdot \boldsymbol{g}\,, \tag{3.23}$$

$$\Delta K = \boldsymbol{g}^T \cdot \frac{\boldsymbol{v} + \boldsymbol{w}}{2}, \tag{3.24}$$

and

$$\Delta K = \frac{1}{2}\left(\boldsymbol{w}^T \cdot \boldsymbol{M} \cdot \boldsymbol{w} - \boldsymbol{v}^T \cdot \boldsymbol{M} \cdot \boldsymbol{v}\right). \tag{3.25}$$

Along with the equation (3.25), the Cauchy quadric surface associated with $\boldsymbol{M}$ provides a convenient means for visualizing the constraint that the predicted change in kinetic energy should be non-positive, discussed in Smith (1991). Because $\boldsymbol{x} \cdot \boldsymbol{M} \cdot \boldsymbol{x}$ is a positive definite function of $\boldsymbol{x}$, Equation (3.25) indicates that the greatest possible loss of kinetic energy during contact would occur if $\boldsymbol{w} = 0$ (i.e., if the points P and P' have the same velocity) at the instant the reaction $\dot{\boldsymbol{g}} = 0$.

3.2 Kinematics of Planar Collisions

To simplify formulation of a contact law for planar collisions, as shown in Figure 3.2, a set of basis vectors $\boldsymbol{t}$ - $\boldsymbol{n}$ - $\boldsymbol{t}_1$ is introduced, substituting for $\boldsymbol{e}_1$ - $\boldsymbol{e}_2$ - $\boldsymbol{e}_3$. The vector, $\boldsymbol{n}$, is a unit-vector perpendicular to the common tangent to the surfaces at P and P' and directed from B' into B. The vector, $\boldsymbol{t}$, has the same direction as $\boldsymbol{n} \times (\boldsymbol{v} \times \boldsymbol{n})$, where $\boldsymbol{v}$ is the relative velocity between two contact points, and $\boldsymbol{t}_1 = \boldsymbol{t} \times \boldsymbol{n}$. The approach velocity can then be expressed as

$$\boldsymbol{v} = v_t \boldsymbol{t} + v_n \boldsymbol{n} . \tag{3.26}$$

Subject to an appropriate coordinate transformation, all of the matrices developed in previous section can be evaluated in terms of the unit vectors $\boldsymbol{t} - \boldsymbol{n}$ - $\boldsymbol{t}_1$. From equation (3.18), if there is no coupling of $\boldsymbol{N}$ between $\boldsymbol{t}_1$ and other directions, the relative velocity $\boldsymbol{w}$ and the impulse $\boldsymbol{g}$ could be expressed in terms of normal and tangential components as

$$\boldsymbol{w} = w_t \boldsymbol{t} + w_n \boldsymbol{n} \tag{3.27}$$

and

$$\boldsymbol{g} = g_t \boldsymbol{t} + g_n \boldsymbol{n} . \tag{3.28}$$

Thus, equation (3.18) can be rewritten as

$$\begin{Bmatrix} \Delta v_t \\ \Delta v_n \end{Bmatrix} = \begin{bmatrix} N_{tt} & N_{tn} \\ N_{nt} & N_{nn} \end{bmatrix} \begin{Bmatrix} g_t \\ g_n \end{Bmatrix} \tag{3.29}$$

It will be helpful to express $\boldsymbol{N}$ in terms of its principal values and the angle between $\boldsymbol{n}$ and one of the principal directions of $\boldsymbol{N}$. The principal values are

$$N_{1,2} = \frac{N_{tt} + N_{nn}}{2} \pm \sqrt{\left(\frac{N_{tt} - N_{nn}}{2} \right)^2 + N_{tn}^{\ 2}} , \tag{3.30}$$

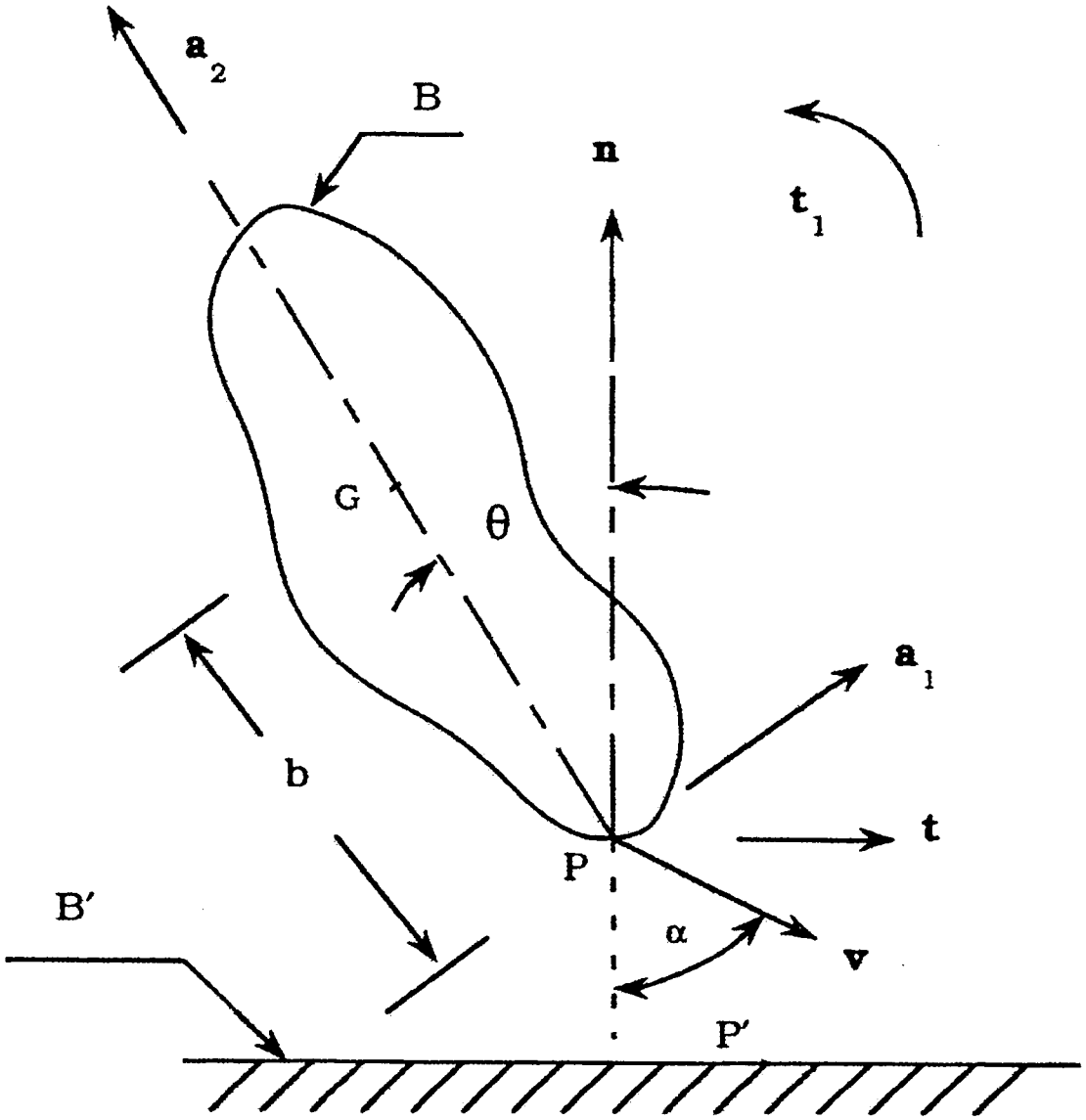

Figure 3.2 Planar collision between a rod and a flat plane

wherein N_1 is defined to be the larger of two. It follows that the expressions for the components of $\boldsymbol{N}$ are

$$N_{tt,nn} = \frac{N_1 + N_2}{2} \pm \left(\frac{N_1 - N_2}{2} \right) \cos 2\theta \tag{3.31}$$

and

$$N_{tn} = \left(\frac{N_1 - N_2}{2} \right) \sin 2\theta \tag{3.32}$$

where θ is the angle between $\boldsymbol{n}$ and the principal direction corresponding to N_1 and

$$\tan 2\theta = \frac{2N_{tn}}{N_{tt} - N_{nn}}. \tag{3.33}$$

Thus, in terms of principal values, $\boldsymbol{N}$ can be expressed as

$$\boldsymbol{N} = \begin{bmatrix} N_{tt} & N_{tn} \\ N_{nt} & N_{nn} \end{bmatrix} = \frac{1}{m} \begin{bmatrix} 1 + \lambda \cos 2\theta & \lambda \sin 2\theta \\ \lambda \sin 2\theta & 1 - \lambda \cos 2\theta \end{bmatrix}, \tag{3.34}$$

where

$$m = \frac{2}{N_1 + N_2} = \frac{2}{N_{tt} + N_{nn}} \tag{3.35}$$

and

$$\lambda = \frac{N_1 - N_2}{N_1 + N_2} = \frac{\sqrt{(N_{tt} - N_{nn})^2 + 4N_{tn}^2}}{N_{tt} + N_{nn}}, \tag{3.36}$$

where m and λ are dependent upon the system configuration.

The relationship between $\boldsymbol{M}$ and $\boldsymbol{N}$ and the physical meanings of λ are illustrated as follows. Consider a rod, which collides with an immobile body at the point P, as shown in Figure 3.2. The mass of the rod is denoted as m_B, the point G is the center of mass and the angle between the line PG and the normal vector of the contact surface is

denoted as θ. One set of basis vectors shown in Figure 3.2, in which vector $\boldsymbol{a}_2$ is parallel to PG and $\boldsymbol{a}_1 = \boldsymbol{a}_2 \times \boldsymbol{t}_1$. Generalized speeds are chosen such that

$$\boldsymbol{v}^G = u_1 \boldsymbol{t} + u_2 \boldsymbol{n} \tag{3.37}$$

and

$$\boldsymbol{\omega}^B = u_3 \boldsymbol{t} \times \boldsymbol{n}. \tag{3.38}$$

Let

$$\boldsymbol{r}_{GP} = b \sin\theta \boldsymbol{t} - b \cos\theta \boldsymbol{n} \tag{3.39}$$

and express the velocity of the contact point P as

$$\begin{aligned} \boldsymbol{v}^P &= \boldsymbol{v}^G + \boldsymbol{\omega}^B \times \boldsymbol{r}_{GP} \\ &= u_1 \boldsymbol{t} + u_2 \boldsymbol{n} + u_3 (b \cos\theta \boldsymbol{t} + b \sin\theta \boldsymbol{n}) \end{aligned} \tag{3.40}$$

The partial velocities for the relative velocity v become

$$\boldsymbol{v}_1 = \boldsymbol{t}, \tag{3.41}$$

$$\boldsymbol{v}_2 = \boldsymbol{n}, \tag{3.42}$$

$$\boldsymbol{v}_3 = b \cos\theta \ \boldsymbol{t} + b \sin\theta \ \boldsymbol{n} \ , \tag{3.43}$$

and the matrix $\boldsymbol{l}$ becomes

$$\boldsymbol{l} = \begin{bmatrix} 1 & 0 \\ 0 & 1 \\ b\cos\theta & b\sin\theta \end{bmatrix}. \tag{3.44}$$

The kinetic energy may be expressed as

$$K = \frac{1}{2} m_B \boldsymbol{v}^G \cdot \boldsymbol{v}^G + \frac{1}{2} I_3 \boldsymbol{\omega}^B \cdot \boldsymbol{\omega}^B \tag{3.45}$$

where I_3 is the central moment of inertia of rod for $\boldsymbol{a}_3$. Denoting the central radius of gyration of rod as k_3, equation (3.45) may be rewritten as

$$K = \frac{1}{2} m_B \left(u_1^{\,2} + u_2^{\,2} + k_3^{\,2} u_3^{\,2} \right). \tag{3.46}$$

From equation (3.20), hence, $\boldsymbol{m}^{-1}$ becomes

$$\boldsymbol{m}^{-1} = \frac{1}{m_B k_3^{\,2}} \begin{bmatrix} k_3^{\,2} & 0 & 0 \\ 0 & k_3^{\,2} & 0 \\ 0 & 0 & 1 \end{bmatrix} \tag{3.47}$$

and the matrix $\boldsymbol{M}$ becomes

$$\boldsymbol{M} = \frac{m_B}{k_3^{\,2} + b^2} \begin{bmatrix} k_3^{\,2} + b^2 \sin^2\theta & -b^2 \cos\theta \sin\theta \\ -b^2 \cos\theta \sin\theta & k_3^{\,2} + b^2 \cos^2\theta \end{bmatrix}. \tag{3.48}$$

The two eigenvectors $\boldsymbol{a}_1$ and $\boldsymbol{a}_2$ of this operator are shown in Figure 3.2 and are related to the tangential and normal base vectors by

$$\boldsymbol{a}_1 = \cos\theta\, \boldsymbol{t} + \sin\theta\, \boldsymbol{n}, \tag{3.49}$$

$$\boldsymbol{a}_2 = -\sin\theta\, \boldsymbol{t} + \cos\theta\, \boldsymbol{n}, \tag{3.50}$$

and corresponding eigenvalues are

$$M_1 = \frac{I_3'}{I_3} m_B = \frac{k_3^{\,2}}{k_3^{\,2} + b^2} m_B, \tag{3.51}$$

$$M_2 = m_B\ , \tag{3.52}$$

where I_3' is the moment of the inertia of rod about the axis through P' and perpendicular to the plane of motion.

Since $\boldsymbol{N} = \boldsymbol{M}^1$ from equation (3.20), the eigenvalues of $\boldsymbol{N}$ are the reciprocals of those of $\boldsymbol{M}$:

$$N_1 = \frac{I_3'}{I_3} = \frac{k_3^{\,2} + b^2}{k_3^{\,2} m_B}, \tag{3.53}$$

$$N_2 = \frac{I}{m_B}. \tag{3.54}$$

From equations (3.35) and (3.36), the values of m and λ become

$$m = \frac{2 I_3 m_B}{I_3' + I_3} = \frac{2 k_3^2 m_B}{2 k_3^2 + b^2} \tag{3.55}$$

and

$$\lambda = \frac{I_3' - I_3}{I_3' + I_3} = \frac{b^2}{2 k_3^2 + b^2} \tag{3.56}$$

From equation (3.36) and (3.56), λ can be seen to lie between zero to one and larger values of λ reflect more pronounced inertia coupling.

For contact between an end of an unconstrained, slender rod and an immobile body, λ=0.6, while the value of λ for the double pendulum discussed in Smith (1991) is 0.964 in the configuration considered there.

Another parameter that affects the collision is the angle α between $-\boldsymbol{n}$ and $\boldsymbol{v}$ shown in Figure 3.2. The initial velocity $\boldsymbol{v}$ can be expressed in terms of incident angle α.

$$\boldsymbol{v} = v(\sin\alpha\, \boldsymbol{t} - \cos\alpha\, \boldsymbol{n}) \tag{3.57}$$

so that this incident angle α is given by

$$\tan\alpha = \frac{v_t}{-v_n} \tag{3.58}$$

Observe that a redundancy in results would occur if the sign of both the angles θ and α were reversed; in the following, this redundancy is avoided by restricting α to the range $(0, \pi/2)$ and considering values of θ throughout the range $(-\pi/2, \pi/2)$.

4. CONTACT MECHANICS OF ELASTIC BODY

For evaluation of the impulse and changes in velocities, additional relationships between force and relative motion in the region of contact are required. The analysis of the interactions among deformations, surface tractions, and sliding with friction is helpful for the purpose at hand to produce an acceptably accurate prediction. The contact mechanics of elastic body in both normal and tangential direction will be discussed in the following. Some suitable simplifying assumptions can be obtained from the analysis of the contact mechanics.

4.1 Geometry of Smooth Non-Conforming Surfaces in Contact

When two non-conforming solids are brought into contact, they touch initially at a single point or along a line. Under the action of the slightest load they deform in the vicinity of their point of first contact so that they touch over an area, which is finite though small compared with the dimensions of the two bodies. A theory of contact is required to predict the shape of this contact area and how it grows in size with increasing load, the magnitude and distributions of surface traction, normal and possibly tangential, transmitted across the interface. Finally it should enable the components of deformation and stress in both bodies to be calculated in the vicinity of the contact region.

Before the problem in elasticity can be formulated, a description of the geometry of the contacting surfaces is necessary. We assume that at the point of contact these bodies have spherical surfaces with the radii R_1 and R_2, shown as Figure 4.1.

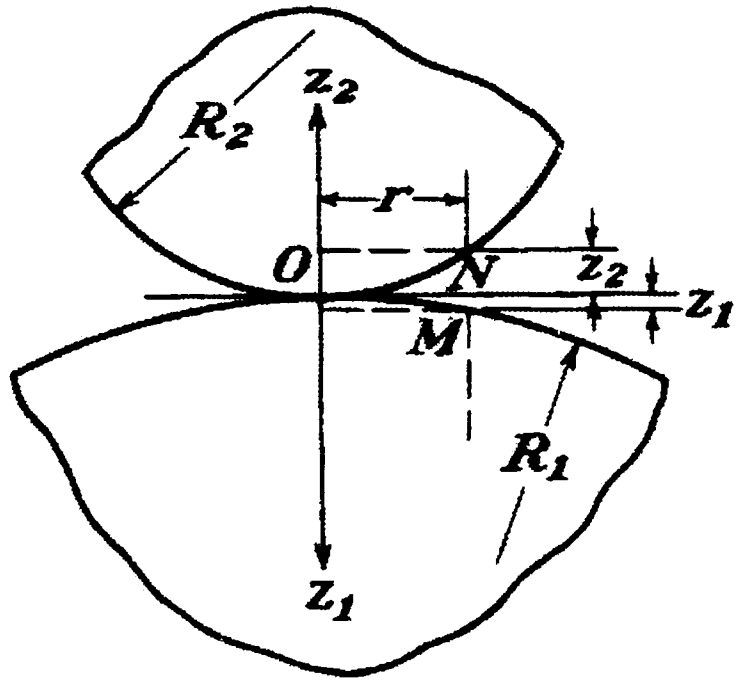

Figure 4.1 The geometry of two contacting surfaces

If there is no pressure between the bodies, we have contact at one point O. The distances from the plane tangent at O to points such as M and N on the spheres at a very small distance r from the axes z_1 and z_2 are distances z_1 and z_2. The distance r is much small in comparison with R_1 and R_2. From Figure 4.1, we have

$$\tan\theta = \frac{z_1}{r}, \quad \tan(90^0 - \theta) = \frac{r}{z_1}.$$

Let $\overline{OM} = x$, $\quad \tan(90^0 - \theta) = \dfrac{R_1}{\left(\dfrac{x}{2}\right)}$,

therefore,

$$\frac{R_1}{\left(\dfrac{x}{2}\right)} = \frac{r}{z_1}, \quad x = \frac{2z_1R_1}{r}.$$

Since $x^2 = r^2 + z_1^2$, we will have

$$\frac{4z_1^2 R_1^2}{r^2} = r^2 + z_1^2 \tag{4.1}$$

and

$$z_1 = \frac{r^2}{\sqrt{4R_1^2 - r^2}}. \tag{4.2}$$

Because $R_1 >> r$, and $\sqrt{4R_1^2 - r^2} \doteq \sqrt{4R_1^2} = 2R_1$,

$$\therefore \quad z_1 = \frac{r^2}{2R_1}. \tag{4.3}$$

Using the same procedure, we have

$$z_2 = \frac{r^2}{2R_2}. \tag{4.4}$$

The mutual distance between these points M and N is

$$z_1 + z_2 = r^2\left(\frac{1}{2R_1} + \frac{1}{2R_2}\right) = \frac{r^2(R_1 + R_2)}{2R_1R_2}. \tag{4.5}$$

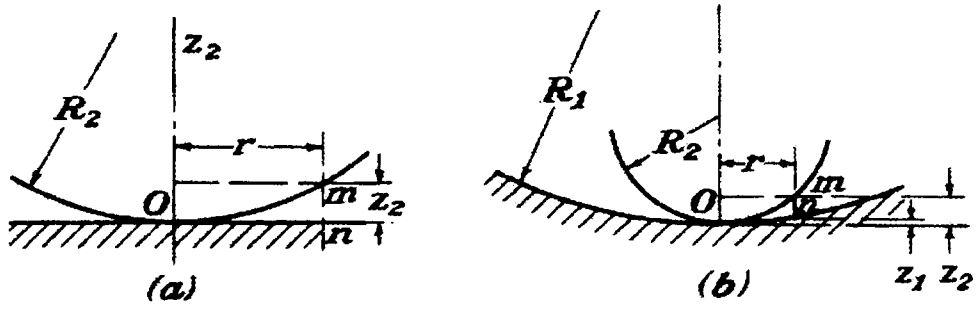

Figure 4.2 The contact between (*a*) a sphere and a plane (*b*) a ball and a spherical seat

In the particular case of contact between a sphere and a plane, as Figure 4.2 (*a*), $\frac{1}{R_1}$ is zero and the equation for $z_1 + z_2$, the distance between points *M* and *N*, gives

$$z_1 + z_2 = \frac{r^2}{2R_2}. \tag{4.6}$$

In the case of contact between a ball and a spherical seat, as shown in Figure 4.2 (*b*), R_1 is negative. The equation for the distance between points *M* and *N* is

$$z_1 - z_2 = \frac{r^2(R_1 - R_2)}{2R_1R_2}. \tag{4.7}$$

Now, consider the contact between two surfaces with a more general profile. Let's take the point of first contact as the origin of a rectangular coordinate system in which the ***x*-*y*** plane is the common tangent plane to the two surfaces and the ***z***-axis lies along the common normal directed positively into the lower solid, as shown in Figure 4.3. Each surface is considered to be smooth on both micro and macro scale. On the micro scale this implies the absence or disregard of small surface irregularities which would lead to discontinuous contact or highly local variations in contact pressure. On the macro scale the profiles of the surfaces are continuous up to their second derivative in the contact region. Thus we may express the profile of each surface in the region close to the origin approximately by an expression of the form

$$z_1 = A_1x^2 + B_1y^2 + C_1xy + \cdots, \tag{4.8}$$

where higher order terms in *x* and *y* are neglected.

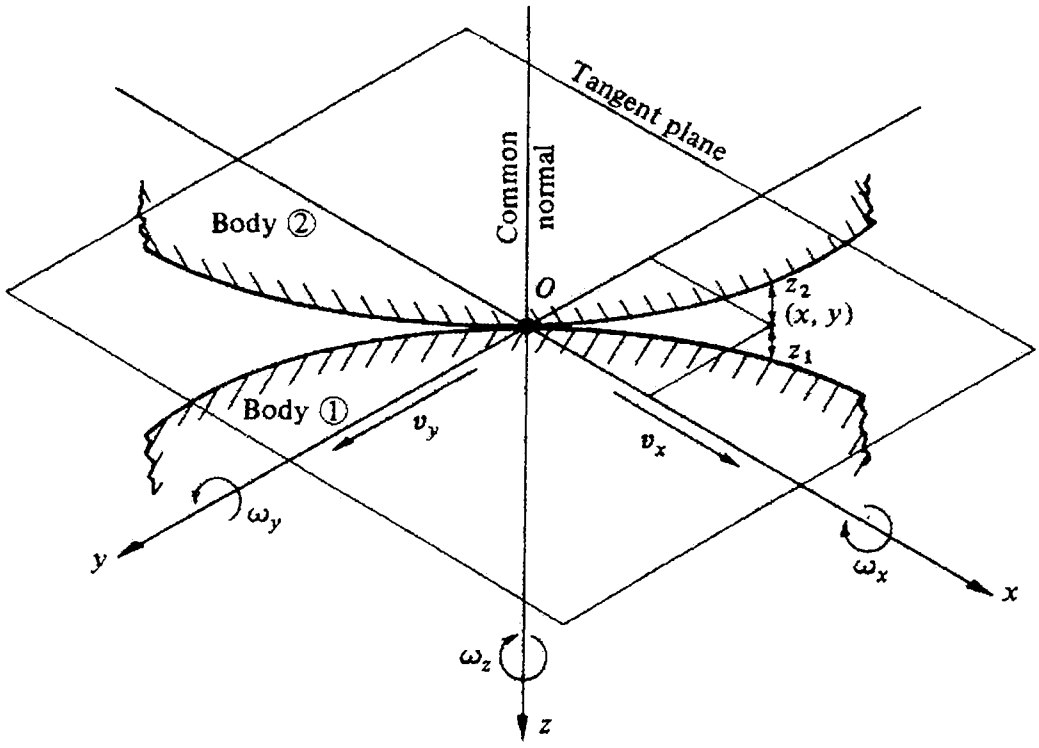

Figure 4.3 Non-conforming surfaces in contact at O

By choosing the orientation of the x and y axes, x_1 and y_1, so that the terms in xy vanishes. We will have

$$z_1 = \frac{1}{2R_1'} x_1^2 + \frac{1}{2R_1''} y_1^2, \tag{4.9}$$

where R_1' and R_1'' are the maximum and minimum values of the principal radius of curvature of all possible cross sections of the profile. A similar expression may be written for the second surface,

$$z_2 = -\left(\frac{1}{2R_2'} x_2^2 + \frac{1}{2R_2''} y_2^2 \right). \tag{4.10}$$

Now, let θ be the angle by which the axes of principal curvature of each surface are inclined to each other, as shown in Figure 4.4. We now transform the coordinates to a common set of axes (x, y) inclined at angle α to x_1 and angle β to x_2 as shown. We will have

$$\begin{aligned} x_1 &= \cos\alpha\, x - \sin\alpha\, y, \quad y_1 = \cos\alpha\, y + \sin\alpha\, x \\ x_2 &= \cos\beta\, x + \sin\beta\, y, \quad y_2 = \cos\beta\, y - \sin\beta\, x \end{aligned} \tag{4.11}$$

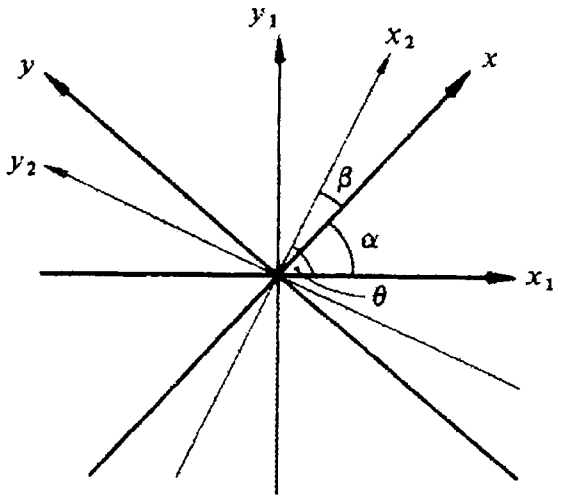

Figure 4.4 The inclined axes at an arbitrary angle

The separation between the two surfaces is then given by $h = z_1 - z_2$. We now transpose equation (4.8) and its counterpart to a common set of axes x and y, where by

$$
\begin{aligned}
h = z_1 - z_2 &= \frac{1}{2R_1'} x_1^2 + \frac{1}{2R_1''} y_1^2 + \frac{1}{2R_2'} x_2^2 + \frac{1}{2R_2''} y_2^2 \\
&= \frac{1}{2R_1'}\left(\cos^2\alpha\, x^2 - 2\cos\alpha\sin\alpha\, xy + \sin^2\alpha\, y^2\right) \\
&+ \frac{1}{2R_1''}\left(\cos^2\alpha\, y^2 + 2\cos\alpha\sin\alpha\, xy + \sin^2\alpha\, x^2\right) \\
&+ \frac{1}{2R_2'}\left(\cos^2\beta\, x^2 + 2\cos\alpha\sin\alpha\, xy + \sin^2\beta\, y^2\right) \\
&+ \frac{1}{2R_2''}\left(\cos^2\beta\, y^2 - 2\cos\beta\sin\beta\, xy + \sin^2\beta\, x^2\right) \\
&= A x^2 + B y^2 + C xy
\end{aligned}
\tag{4.12}
$$

in which

$$
C = \frac{1}{2}\left(\frac{1}{R_2'} - \frac{1}{R_2''}\right)\sin 2\beta - \frac{1}{2}\left(\frac{1}{R_1'} - \frac{1}{R_1''}\right)\sin 2\alpha\,. \tag{4.13}
$$

We now choose α to satisfy $\dfrac{\sin 2\alpha}{\sin 2\beta} = \dfrac{\frac{1}{2}\left(\frac{1}{R_2'} - \frac{1}{R_2''}\right)}{\frac{1}{2}\left(\frac{1}{R_1'} - \frac{1}{R_1''}\right)}$ (4.14)

so that C vanishes and

$$
A = \frac{1}{2R_1'}\cos^2\alpha + \frac{1}{2R_1''}\sin^2\alpha + \frac{1}{2R_2'}\cos^2\beta + \frac{1}{2R_2''}\sin^2\beta = \frac{1}{2R'} \tag{4.15}
$$

$$
B = \frac{1}{2R_1'}\sin^2\alpha + \frac{1}{2R_1''}\cos^2\alpha + \frac{1}{2R_2'}\sin^2\beta + \frac{1}{2R_2''}\cos^2\beta = \frac{1}{2R''} \tag{4.16}
$$

where A and B are positive constant and R', R'' are defined as the principal relative radius of curvature. Finally,

$$
A + B = \frac{1}{2}\left(\frac{1}{R_1'} + \frac{1}{R_1''} + \frac{1}{R_2'} + \frac{1}{R_2''}\right) = \frac{1}{2}\left(\frac{1}{R'} + \frac{1}{R''}\right) \tag{4.17}
$$

$$
\begin{aligned}
A-B &= \frac{1}{2R_1'}\cos^2\alpha + \frac{1}{2R_1''}\sin^2\alpha + \frac{1}{2R_2'}\cos^2\beta + \frac{1}{2R_2''}\sin^2\beta \\
&\quad - \frac{1}{2R_1'}\sin^2\alpha - \frac{1}{2R_1''}\cos^2\alpha - \frac{1}{2R_2'}\sin^2\beta - \frac{1}{2R_2''}\cos^2\beta \\
&= \frac{1}{2R_1'}\cos 2\alpha - \frac{1}{2R_1''}\cos 2\alpha + \frac{1}{2R_2'}\cos 2\beta - \frac{1}{2R_2''}\cos 2\beta \\
&= \frac{1}{2}\left(\frac{1}{R_1'} - \frac{1}{R_1''}\right)\cos 2\alpha + \frac{1}{2}\left(\frac{1}{R_2'} - \frac{1}{R_2''}\right)\cos 2\beta
\end{aligned}
\tag{4.18}
$$

Since

$$
\begin{aligned}
h &= Ax^2 + By^2 = \frac{1}{2R'}x^2 + \frac{1}{2R''}y^2 \\
&= \frac{x^2}{\left(\frac{1}{\sqrt{A}}\right)^2} + \frac{y^2}{\left(\frac{1}{\sqrt{B}}\right)^2} = \frac{x^2}{\left(\sqrt{2R'}\right)^2} + \frac{y^2}{\left(\sqrt{2R''}\right)^2},
\end{aligned}
\tag{4.19}
$$

it is evident that contours of constant gap h between the undeformed surfaces are ellipses, the length of whose axes are in the ratio $(B/A)^{1/2} = (R'/R'')^{1/2}$.

A normal compressive load is now applied to the two solids and the point of contact spreads into an area. If the two bodies are solids of revolution, then $R_1'=R_1''=R_1$, and $R_2'=R_2''=R_2$, where upon

$$
A = B = \frac{1}{2}\left(\frac{1}{R_1} + \frac{1}{R_2}\right). \tag{4.20}
$$

$$
\text{Then } h = Ax^2 + By^2 = \frac{1}{2}\left(\frac{1}{R_1} + \frac{1}{R_2}\right)\left(x^2 + y^2\right), \tag{4.21}
$$

for $r^2 = x^2 + y^2$, the separation will be

$$
h = \frac{1}{2}\left(\frac{1}{R_1} + \frac{1}{R_2}\right)r^2 = \frac{r^2\left(R_1 + R_2\right)}{2R_1R_2}. \tag{4.22}
$$

This equation agrees with equation (4.5) derived for the spherical surfaces in Figure 4.1.

4.2 Normal Contact Mechanics

We shall now consider the deformation when a normal load P is applied. In Figure 4.5, two solids of general shape are shown in cross-section after deformation. Before deformation, the separation between two corresponding surface points $S_1(x, y, z_1)$, $S_2(x, y, z_2)$ is given by the equation,

$$h = \frac{1}{2R'}x^2 + \frac{1}{2R''}y^2. \tag{4.23}$$

During compression, distant points in the two bodies T_1 and T_2 move towards the contact point O, parallel to the z-axis, by displacements δ_1 and δ_2 respectively. Due to the contact pressure the surface of each body is displaced parallel to the z-axis by an amount $\bar{u}_{z1}$ and $\bar{u}_{z2}$ (measured positive into each body) relative to the distant points T_1 and T_2. If the points S_1 and S_2 are coincident within the contact surface then

$$\bar{u}_{z1} + \bar{u}_{z2} + h = \delta_1 + \delta_2. \tag{4.24}$$

Writing $\delta = \delta_1 + \delta_2$ and $h = Ax^2 + By^2$, the elastic displacement is

$$\bar{u}_{z1} + \bar{u}_{z2} = \delta - Ax^2 - By^2, \tag{4.25}$$

where x and y are the common coordinates of S_1 and S_2 projected onto the x-y plane.

If S_1 and S_2 lie outside the contact area so that they do not touch, it follows that

$$\bar{u}_{z1} + \bar{u}_{z2} > \delta - Ax^2 - By^2. \tag{4.26}$$

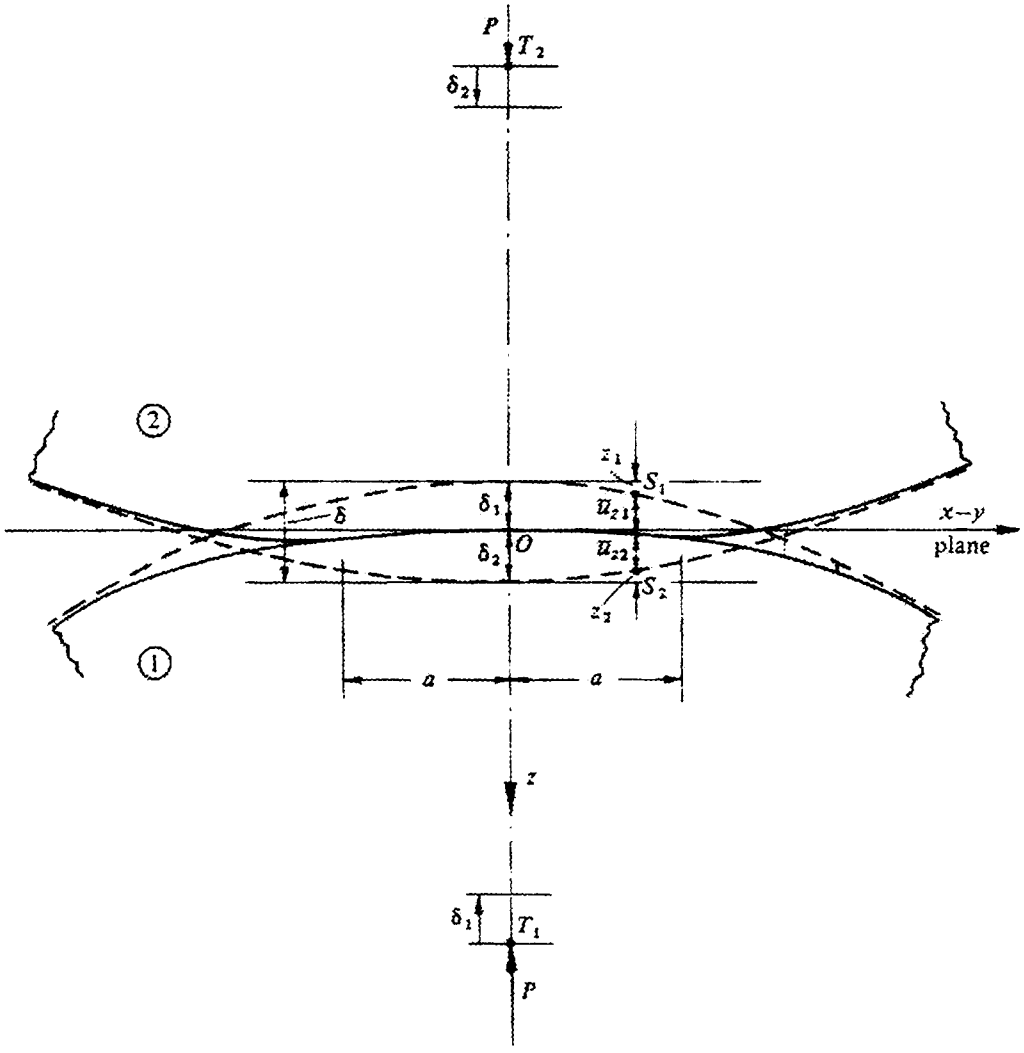

Figure 4.5 The geometry of the deformation of two colliding bodies

For simplicity, we shall restrict the discussion to solids of revolution in which the contact area is a circle of radius a. From Figure 4.5,

$$\delta_1 = \bar{u}_{z1}(0), \quad \delta_2 = \bar{u}_{z2}(0), \tag{4.27}$$

so that the separation can be written as

$$\bar{u}_{z1}(0)-\bar{u}_{z1}(x)+\bar{u}_{z2}(0)-\bar{u}_{z2}(x)=h=\frac{1}{2}\left(\frac{1}{R_1}+\frac{1}{R_2}\right)x^2, \tag{4.28}$$

and in non-dimensional form

$$\left[\frac{\bar{u}_{z1}(0)}{a}-\frac{\bar{u}_{z1}(x)}{a}\right]+\left[\frac{\bar{u}_{z2}(0)}{a}-\frac{\bar{u}_{z2}(x)}{a}\right]=\frac{1}{2}\left(\frac{1}{R_1}+\frac{1}{R_2}\right)\left(\frac{x^2}{a}\right). \tag{4.29}$$

Let

$$x=a,\quad \bar{u}_z(0)-\bar{u}_z(a)=d \tag{4.30}$$

the deformation within the contact area becomes

$$\frac{d_1}{a}+\frac{d_2}{a}=\frac{a}{2}\left(\frac{1}{R_1}+\frac{1}{R_2}\right). \tag{4.31}$$

Provided that the deformation is small, i.e., d ≪ a, the state of strain in each solid is characterized by the ratio d/a. The magnitude of the strain will be proportional to the contact pressure divided by the elastic modulus. If p_m is the average contact pressure acting mutually on each solid, we have

$$\frac{p_m}{E_1}+\frac{p_m}{E_2}\propto a\left(\frac{1}{R_1}+\frac{1}{R_2}\right),\ \text{i.e.,}\ p_m\propto\frac{a\left(\frac{1}{R_1}+\frac{1}{R_2}\right)}{\frac{1}{E_1}+\frac{1}{E_2}}. \tag{4.32}$$

In the contact of spheres, or other solids of revolution, the compressive load $p=\pi a^2 p_m$; hence from the equation above,

$$a\propto\left[\frac{p\left(\frac{1}{E_1}+\frac{1}{E_2}\right)}{\frac{1}{R_1}+\frac{1}{R_2}}\right]^{\frac{1}{3}} \tag{4.33}$$

and

$$p_m \propto \left[\frac{p\left(\frac{1}{R_1}+\frac{1}{R_2}\right)^2}{\left(\frac{1}{E_1}+\frac{1}{E_2}\right)^2} \right]^{\frac{1}{3}}. \tag{4.34}$$

Thus, the radius of the contact circle and the contact pressure increase as the cube root of the load. In the case of three-dimensional contact, the compressions of each solid δ_1 and δ_2 are proportional to the local indentations d_1 and d_2. From Equation (4.25),

$$\delta_1 = \bar{u}_{z1}(0), \quad \delta_2 = \bar{u}_{z2}(0) \tag{4.35}$$

and

$$\begin{aligned} \bar{u}_{z1}(0) - \bar{u}_{z1}(a) &= d_1 = \delta_1 - \bar{u}_{z1}(a) \\ \bar{u}_{z2}(0) - \bar{u}_{z2}(a) &= d_2 = \delta_2 - \bar{u}_{z2}(a) \end{aligned} \tag{4.36}$$

$$\delta_1 + \delta_2 - \left[\bar{u}_{z1}(a) + \bar{u}_{z2}(a)\right] = d_1 + d_2 \tag{4.37}$$

hence the approach of distant points is given by

$$\delta = \delta_1 + \delta_2 \propto d_1 + d_2 \propto \left[p^2 \left(\frac{1}{E_1}+\frac{1}{E_2}\right)^2 \left(\frac{1}{R_1}+\frac{1}{R_2}\right) \right]^{\frac{1}{3}}. \tag{4.38}$$

Therefore we can conclude that the approach of two bodies due to elastic compression in the contact region is proportional to (load)$^{2/3}$. By simple dimensional reasoning, the contact area, stress and deformation are expected to grow with increasing load. But, to obtain the exact values of these quantities, we must turn to the theory of elasticity.

4.3 Hertz Theory of Elastic Contact

The first satisfactory analysis of the stresses at the contact of two elastic solids is due to Hertz. For the purpose of calculating the local deformations, he pointed out that

each body can be regarded as an elastic half-space loaded over a small elliptical region of its plane surface.

Denoting the significant dimension of the contact area by a, the relative radius of curvature by R, the significant radii of each body by R_1 and R_2 and the significant dimensions of the bodies both laterally and in depth by l, we may summarize the assumptions made in the Hertz theory as follows:

i. The surfaces are continuous and non-conforming: $a \ll R$;

The surface just outside the contact region behaves approximately as a surface of a half-space.

ii. The strains are small: $a \ll R$;

That the significant dimensions of the contact area must be small compared with the relative radii of curvature of the surfaces is a necessary condition to ensure that the strains in the contact region are sufficiently small to lie within the scope of the linear theory of elasticity.

iii. Each solid can be considered as an elastic half-space: $a \ll R_{1,2}$, $a \ll l$;

For the purpose of calculating the local deformations, each body can be regarded as an elastic half-space loaded over a small elliptical region of its plane surface. The significant dimensions of the contact area must be small compared with the dimensions of each body. Therefore, the well-developed methods for solving boundary-value problems for the elastic half-space are available for the solution of contact problems.

iv. The surfaces are frictionless: $q_x = q_y = 0$.

The surfaces are assumed to be frictionless so that only a normal pressure is transmitted between them.

Considering the simpler case of solids of revolution, $R_1' = R_1'' = R_1$, $R_2' = R_2'' = R_2$, the contact area will be a circular of radius a. Inside the contact surface,

$$\bar{u}_{z1} + \bar{u}_{z2} = \delta - Ax^2 - By^2, \tag{4.39}$$

$$A = B = \frac{1}{2}\left(\frac{1}{R_1} + \frac{1}{R_2}\right) = \frac{1}{2R'}, \tag{4.40}$$

and

$$x^2 + y^2 = r^2, \tag{4.41}$$

therefore,

$$\bar{u}_{z1} + \bar{u}_{z2} = \delta - \frac{1}{2R}\left(x^2 + y^2\right) = \delta - \frac{1}{2R}r^2, \tag{4.42}$$

where $\frac{1}{R} = \frac{1}{R_1} + \frac{1}{R_2}$ is the relative curvature.

The pressure given by Hertz theory, which is exerted between two frictionless elastic solids of revolution in contact, is given by

$$p = p_0\left[1 - \left(\frac{r}{a}\right)^2\right]^{\frac{1}{2}}. \tag{4.43}$$

The total load compressing the solids is related to the pressure by

$$p = \int_0^a p(r)2\pi r\, dr = \frac{2}{3}p_0\pi a^2. \tag{4.44}$$

Hence the maximum pressure p_0 is 3/2 times the mean pressure p_m. The vertical displacement at the boundary plane (z = 0) is

$$\bar{u}_{z\,z=0} = \frac{p(1-\nu^2)}{\pi E r}. \tag{4.45}$$

A circular region of radius a is shown in Figure 4.6. It is required to find the displacement at a surface point B due to pressure distributed over the circular region. Solution in closed form can be found for axi-symmetrical pressure distribution of the form, given by equation (4.43). Therefore, regarding the pressure p at C, acting on a surface element of area $sdsd\phi$, as concentrated force $psdsd\phi$, the normal displacement at B is given by,

$$\bar{u}_z = \frac{(1-\nu^2)psdsd\phi}{\pi E s} = \frac{(1-\nu^2)}{\pi E} pdsd\phi. \tag{4.46}$$

The total deflection is now obtained by double integration.

$$\bar{u}_z = \frac{(1-\nu^2)}{\pi E} \iint_S d\phi\, ds. \tag{4.47}$$

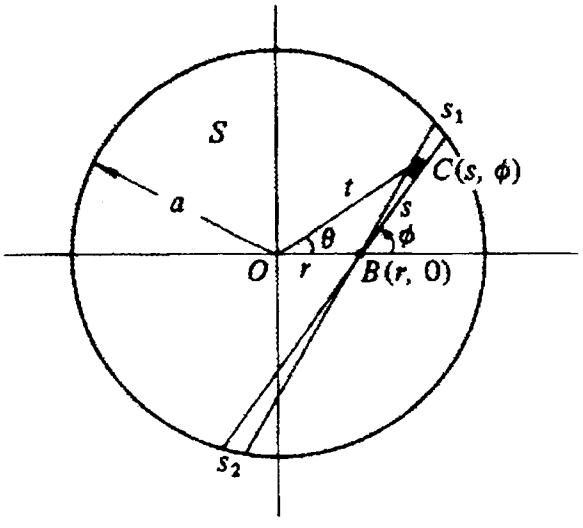

Figure 4.6 Pressure applied to a circular region at an internal point C

From Figure 4.6, we have $t^2 = r^2 + s^2 + 2rs\cos\phi$. (4.48)

Let

$$\alpha^2 = a^2 - r^2, \quad \beta = r\cos\phi, \tag{4.49}$$

$$\begin{aligned} p(r) &= \frac{p_0}{a}\sqrt{a^2 - r^2} = p(s,\phi) = \frac{p_0}{a}\sqrt{a^2 - t^2} \\ &= \frac{p_0}{a}\sqrt{a^2 - r^2 - s^2 - 2rs\cos\phi} = \frac{p_0}{a}\sqrt{\alpha^2 - 2\beta s - s^2}, \\ &= \frac{p_0}{a}\left(\alpha^2 - 2\beta s - s^2\right)^{\frac{1}{2}} \end{aligned} \tag{4.50}$$

$$\int_s\int_\phi p(s,\phi)\,d\phi\,ds = \frac{p_0}{a}\int_s\int_\phi (\alpha^2 - 2\beta s - s^2)^{\frac{1}{2}}\,d\phi\,ds, \tag{4.51}$$

$$\int_0^{s_1} (\alpha^2 - 2\beta s - s^2)^{\frac{1}{2}}\,ds = -\frac{1}{2}\alpha\beta + \frac{1}{2}(\alpha^2 + \beta^2)\left[\frac{\pi}{2} - \tan^{-1}\left(\frac{\beta}{\alpha}\right)\right]. \tag{4.52}$$

The terms $\alpha\beta$ and $\tan^{-1}(\alpha/\beta)$ vanish when integrated with respect to ϕ between the limits 0 and 2π, so that equation (4.47) becomes

$$\bar{u}_z(r) = \frac{(1-\nu^2)}{\pi E a}\int_0^{2\pi}\frac{\pi}{4}\left(a^2 - r^2 + r^2\cos^2\phi\right)d\phi = \frac{(1-\nu^2)\pi p_0}{4Ea}(2a^2 - r^2). \tag{4.53}$$

The pressure acting on the second body is equal to that on the first, so that by writing

$$\frac{1}{E^*} = \frac{1-\nu_1^{\,2}}{E_1} + \frac{1-\nu_2^{\,2}}{E_2}, \tag{4.54}$$

$$\bar{u}_{z_1} = \frac{1-\nu_1^{\,2}}{E_1}\frac{\pi p_0}{4a}(2a^2 - r^2), \tag{4.55}$$

$$\bar{u}_{z_2} = \frac{1-\nu_2^{\,2}}{E_2}\frac{\pi p_0}{4a}(2a^2 - r^2), \tag{4.56}$$

$$\bar{u}_{z_1} + \bar{u}_{z_2} = \frac{1}{E^*}\frac{\pi p_0}{4a}(2a^2 - r^2) = \delta - \left(\frac{1}{2R}\right)r^2, \tag{4.57}$$

Therefore,

$$\frac{\pi p_0}{4aE^*} = \frac{1}{2R}, \tag{4.58}$$

$$a = \frac{2p_0 R\pi}{4E^*} = \frac{\pi p_0 a}{2E^*}, \tag{4.59}$$

$$\delta = \frac{\pi p_0 a}{2E^*}. \tag{4.60}$$

The total load compressing the solid is

$$p = \int_0^a p(r)2\pi r\,dr = \frac{2}{3}p_0\pi a^2. \tag{4.61}$$

In a practical problem, it is usually the total load which is specified, so that it is convenient to express a, δ, p_0 in terms of the total load. The radius of the contact surface is

$$a = \frac{\pi p_0 R}{2E^*} = \frac{\pi R}{2E^*}\frac{3P}{2\pi a^2}, \tag{4.62}$$

$$\text{therefore, } a = \left(\frac{3PR}{4E^*}\right)^{\frac{1}{3}}. \tag{4.63}$$

The compression displacement is

$$\delta = \frac{\pi p_0 a}{2E^*} = \frac{\pi a}{2E^*}\frac{3P}{2\pi a^2} = \frac{3P}{4E^*\left(\frac{3PR}{4E^*}\right)^{\frac{1}{3}}} = \left(\frac{9P^2}{16RE^{*2}}\right)^{\frac{1}{3}}. \tag{4.64}$$

The maximum pressure is

$$p_0 = \frac{3P}{2\pi a^2} = \left(\frac{27P^3}{8\pi^3}\frac{16E^{*2}}{9P^2R^2}\right)^{\frac{1}{3}} = \left(\frac{6PE^{*2}}{\pi^3R^2}\right)^{\frac{1}{3}}. \tag{4.65}$$

These equations have the same form as Equations (4.33), (4.38) and (4.34), which were obtained by dimensional reasoning. However they also provide specific values for the contact size, compression and maximum pressure.

The equation of normal compression demonstrates a nonlinear force-displacement relationship in the normal direction. It is most meaningful to compare the rates of change of displacement with load. For bodies having the same elastic constants, differentiating equation with the normal load gives a normal compliance.

$$\frac{d\delta_z}{dP} = \frac{d}{dP}\left(\frac{9P^2}{16RE^{*2}}\right)^{\frac{1}{3}} = \frac{d}{dP}\left(\frac{3P}{4\sqrt{R}E^*}\right)^{\frac{2}{3}} \tag{4.66}$$

where

$$\frac{1}{E^*} = \frac{1-\nu_1^{\,2}}{E_1} + \frac{1-\nu_2^{\,2}}{E_2} = \frac{2(1-\nu^2)}{E} \tag{4.67}$$

$$\frac{1}{4E^{*2}} = \left(\frac{1-\nu^2}{E^2}\right)^2 \tag{4.68}$$

The normal compliance C_n is

$$\begin{aligned} C_n = \frac{d\delta_z}{dP} &= \frac{2}{3}\left(\frac{3P}{4\sqrt{R}E}\right)^{-\frac{1}{3}}\left(\frac{3}{4\sqrt{R}E}\right) = \frac{1}{2E^*}\left(\frac{4E^*}{3PR}\right)^{\frac{1}{3}} \\ &= \frac{2(1+\nu)}{E}\frac{(1-\nu)}{2}a^{-1} = \frac{1-\nu}{2Ga} \end{aligned} \tag{4.69}$$

where

$$G = \frac{E}{2(1+\nu)} \tag{4.70}$$

4.4 Tangential Loading

In this analysis, we exclude rolling and the discussion of the contact mechanics in tangential direction is restricted to the contact stresses in simple rectilinear sliding. Shown in Figure 4.7, the system has a slider with a curved profile moving from right to left over a flat surface. We regard the point of initial contact as a fixed origin and imagine the material of the lower surface moving through the contact region from left to right with a steady velocity V. For convenience we choose the x-axis parallel to the direction of sliding.

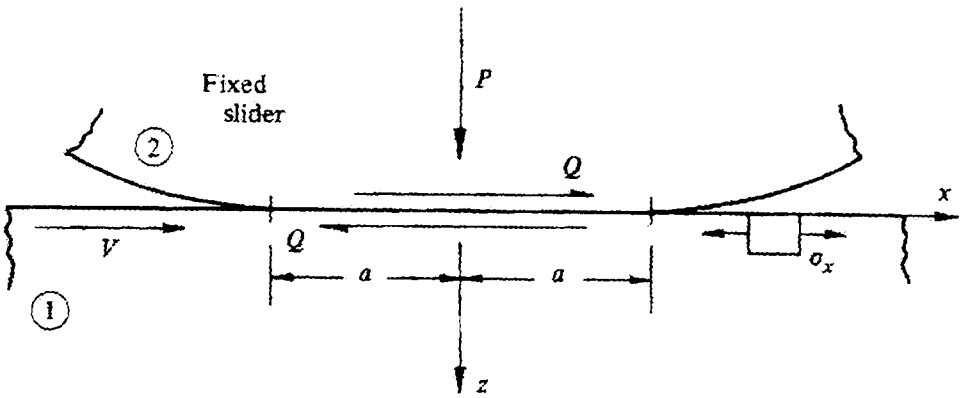

Figure 4.7 Sliding contact

A normal force P pressing the bodies together gives rise to an area of contact which, in the absence of friction forces, would have dimensions given by the Hertz theory. Thus in a frictionless contact the contact stresses would be unaffected by sliding, whereas real surfaces introduce a tangential force of friction Q, acting on each surface, in

a direction which opposes the motion. The force Q represents the force of "kinetic friction" between the surfaces if we imagine the bodies have a steady sliding motion. The force Q arises from "static friction"; it may take any value which does not exceed the force of "limiting friction" when sliding is incipient. We now investigate the situation of two bodies, nominally with no relative velocity but subjected to a tangential force tending to cause them to slide. The influence of tangential traction upon the normal pressure and the contact area is generally small, particularly when the coefficient of limiting friction is appreciably less than unity. In our analysis of problems involving tangential traction, therefore, we shall neglect this interaction and assume that the stresses and deformation due to the normal pressure and the tangential traction are independent of each other, and that they can be superposed to find the resultant stress.

A tangential force, whose magnitude is less than the force of limiting friction, when applied to two bodies pressed into contact, will not give rise to a sliding motion but, nevertheless, will induce frictional traction at the contact surface. We shall examine the tangential surface traction, which arises from a combination of normal and tangential forces, which does not cause the bodies to slide relative to each other.

The problem is illustrated in Figure 4.8. The normal force P gives rise to a contact area and pressure distribution, which we assume to be given by the Hertz theory. The effect of the tangential force Q is to cause the bodies to deform in shear, as indicated by the distorted central line in Figure 4.8. Points on the contact surface will undergo tangential displacement u_x and u_y relative to distant points T_1 and T_2 in the undeformed region of each body. It will be shown that the effect of a tangential force less than the limiting friction force ($Q < \mu P$) is to cause a small relative motion, referred to as "slip" or

"micro-slip", over part of the interface. The remainder of the interface deforms without relative motion and in such regions the surfaces are said to adhere or to "stick".

In Figure 4.8, A_1 and A_2 denote two points on the interface which were coincident before the application of the tangential force. Under the action of the force, points in the body such as T_1 and T_2, distant from the interface, move through effectively rigid displacements δ_{x1}, δ_{y1} and δ_{x2}, δ_{y2} while A_1 and A_2 experience tangential elastic displacements u_{x1}, u_{y1} and u_{x2}, u_{y2} relative to T_1 and T_2. If the absolute displacements of A_1 and A_2 (i.e., relative to O) are denoted by s_{x1}, s_{y1} and s_{x2}, s_{y2}, the components of slip between A_1 and A_2 may be written

$$\begin{aligned} s_x &\equiv s_{x1} - s_{x2} = \left(\bar{u}_{x1} - \delta_{x1}\right) - \left(\bar{u}_{x2} - \delta_{x2}\right) \\ &= \left(\bar{u}_{x1} - \bar{u}_{x2}\right) - \left(\delta_{x1} - \delta_{x2}\right) \end{aligned} \tag{4.71}$$

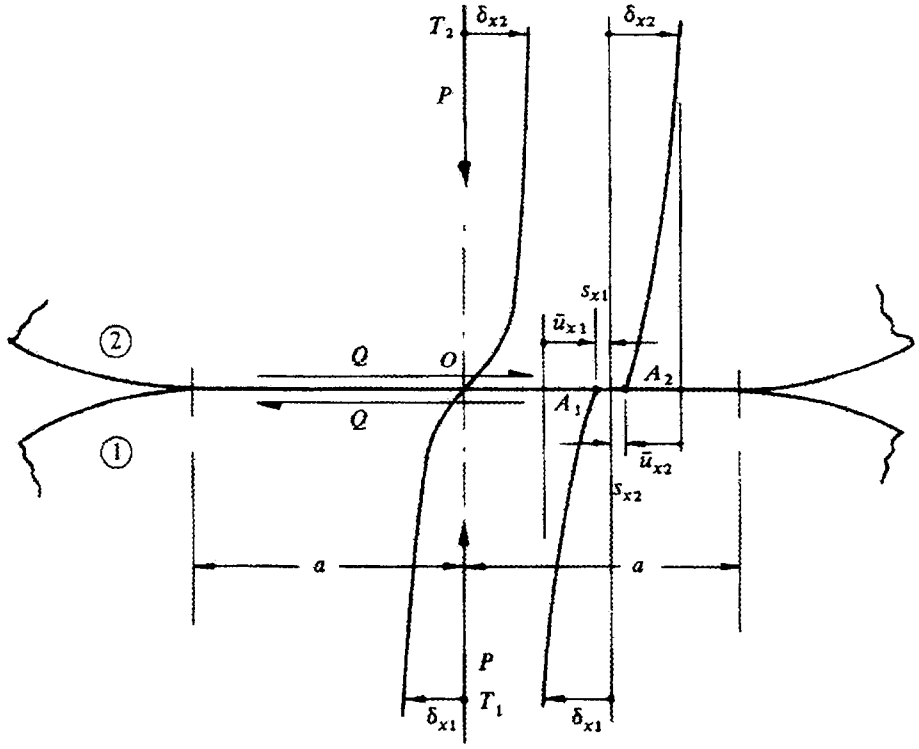

Figure 4.8 The two contact bodies under the action of the force

A similar relation governs the tangential displacements in the y-direction. If the points A_1 and A_2 are located in a 'stick' region the slip s_x and s_y will be zero, so that

$$\bar{u}_{x1} - \bar{u}_{x2} = \delta_{x1} - \delta_{x2} \equiv \delta_x \tag{4.72}$$

$$\bar{u}_{y1} - \bar{u}_{y2} = \delta_{y1} - \delta_{y2} \equiv \delta_y \tag{4.73}$$

Within the 'stick' region, δ_x and δ_y are constants, independent of the position A_1 and A_2. Further, if the two bodies have the same elastic modulus, all surface points within a 'stick' region will undergo the same tangential displacement. At points within a stick region, the resultant tangential traction cannot exceed its limiting value, i.e.,

$$|g(x,y)| \le \mu |p(x,y)| . \tag{4.74}$$

In a region where the surfaces slip, the tangential and normal traction are related by

$$|g(x,y)| = \mu |p(x,y)| . \tag{4.75}$$

In addition, the direction of the frictional traction q must oppose the direction of slip,

$$\frac{q(x,y)}{|q(x,y)|} = -\frac{s(x,y)}{|s(x,y)|} . \tag{4.76}$$

Equations (4.73) to (4.77) provide boundary conditions which must be satisfied by the surface traction and surface displacements at the contact interface. Equations (4.73), (4.74) and (4.75) apply in a stick region and Equations (4.76) and (4.77) apply in a slip region.

4.5 Contact of Spheres – No Slip

Consider the case of two spherical bodies pressed by a normal force P into a circular area of contact with the radius,

$$a = \left(\frac{3PR}{4E^*}\right)^{\frac{1}{3}}, \tag{4.77}$$

and an ellipsoidal pressure distribution given

$$p(r) = p_0\left(1 - \frac{r^2}{a^2}\right)^{\frac{1}{2}}. \tag{4.78}$$

If a tangential force $\boldsymbol{Q}$, applied subsequently, causes elastic deformation without slip at the interface, then it follows that the tangential displacement of all points in the contact area is the same. The distribution of tangential traction which produces a uniform tangential displacement of a circular region on the surface of an elastic half-space is

$$q_x(x,y) = q_0\left(1 - \frac{r^2}{a^2}\right)^{-\frac{1}{2}}. \tag{4.79}$$

The traction is radially symmetrical in magnitude and everywhere parallel to the x-axis, where $q_0 = \frac{Q_x}{2\pi a^2}$. The corresponding displacement is given by:

$$\bar{u}_x = \frac{\pi(2-\nu)}{4G} q_0 a. \tag{4.80}$$

Substituting into Equation (4.73) gives the relative tangential displacement between distant points T_1 and T_2 in the two bodies,

$$\delta_x = \bar{u}_{x1} - \bar{u}_{x2} = \frac{Q_x}{8a}\left(\frac{2-\nu_1}{G_1} + \frac{2-\nu_2}{G_2}\right). \tag{4.81}$$

Therefore, we have

$$\frac{2Q_x}{\mu p}\left(\frac{2-\nu_1}{G_1} + \frac{2-\nu_2}{G_2}\right) = \frac{16a\delta_x}{\mu p}. \tag{4.82}$$

The tangential displacement δ_x is directly proportional to the tangential force Q_x. The relationship is shown by the broken line A of Figure 4.9. The tangential traction necessary for no slip rises to a theoretically infinite value at the periphery of the contact circle so that some micro-slip is inevitable at the edge of contact.

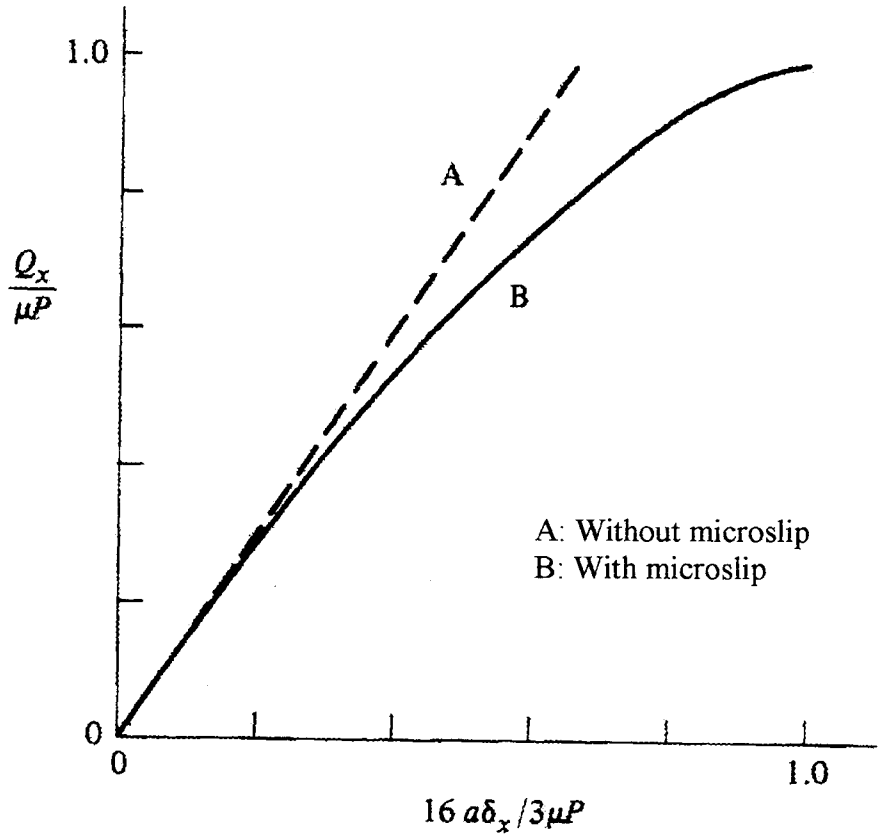

Figure 4.9 Tangential displacement δ_x of a circular contact by a tangential force Q_x; (A) with no slip, (B) with slip at the periphery of the contact

4.6 Contact of Spheres – Partial Slip

If the tangential force Q is increased to its limiting value μP, so that the bodies are on the point of sliding and only the two points in contact at the origin are 'stick', the tangential traction is given by

$$q'(x,y) = \mu\, p(x,y) = \mu\, p_0 \left(1 - \frac{r^2}{a^2}\right)^{\frac{1}{2}} \tag{4.83}$$

where $p_0 = \dfrac{3P}{2\pi a^2}$. (4.84)

The tangential displacements within the contact circle, $r \le a$. due to the traction can be found as:

$$\bar{u}_x' = \frac{\pi \mu p_0}{32 G a}\left[4(2-\nu)a^2 + (4-\nu)x^2 + (4-3\nu)y^2\right] \tag{4.85}$$

$$\bar{u}_y' = \frac{\pi \mu p_0}{32 G a} 2\nu\, x\, y\,. \tag{4.86}$$

The surface displacements are distributed parabolically within the contact circle. At the origin only,

$$\bar{u}_{x1} - \bar{u}_{x2} = \text{constant} = \delta_x\,, \tag{4.87}$$

elsewhere in the contact region the surfaces must slip.

We now consider an additional distribution of traction given by

$$q''(x,y) = -\frac{c}{a} p_0 \left(1 - \frac{r^2}{c^2}\right)^{\frac{1}{2}} \tag{4.88}$$

acting over the circular area $r \le c$.

The tangential displacements produced by this traction within that circle are

$$\bar{u}_x'' = -\frac{c}{a}\frac{\pi \mu p_0}{32 G c}\left[4(2-\nu)c^2 + (4-\nu)x^2 + (4-3\nu)y^2\right] \tag{4.89}$$

$$\bar{u}_y'' = -\frac{c}{a}\frac{\pi \mu p_0}{32 G c} 2\nu\, x\, y\,. \tag{4.90}$$

If we now superpose the two tractions q' and q'', the resultant displacement in the circle, $r \le c$, are given:

$$\bar{u}_x = \bar{u}_x' + \bar{u}_x'' = \frac{\pi \mu p_0}{8Ga}(2-\nu)(a^2 - c^2) \tag{4.91}$$

$$\bar{u}_y = 0. \tag{4.92}$$

We see that these displacements satisfy the condition for no slip within the circle $r \le c$, with the result that

$$\begin{aligned} \bar{u}_{x1} - \bar{u}_{x2} &= (\delta_{x1} - \delta_{x2}) = \delta_x \\ &= \frac{\pi \mu p_0}{8G_1 a}(2-\nu_1)(a^2 - c^2) + \frac{\pi \mu p_0}{8G_2 a}(2-\nu_2)(a^2 - c^2). \\ &= \frac{\pi \mu p_0}{8a}\left(\frac{2-\nu_1}{G_1} + \frac{2-\nu_2}{G_2}\right)(a^2 - c^2) \end{aligned} \tag{4.93}$$

Since $p_0 = \dfrac{3p}{2\pi a^2}$, therefore, (4.94)

$$\delta_x = \frac{3\mu p}{16}\left(\frac{2-\nu_1}{G_1} + \frac{2-\nu_2}{G_2}\right)\frac{a^2 - c^2}{a^3}. \tag{4.95}$$

Thus the stick region is the circle of radius c whose value can be found from the magnitude of the tangential force.

$$Q_x = \int_0^a 2\pi q' r\, dr - \int_0^c 2\pi q'' r\, dr = \mu p\left(1 - \frac{c^3}{a^3}\right) \tag{4.96}$$

whence $\dfrac{c}{a} = \left(1 - \dfrac{Q_x}{\mu p}\right)^{\frac{1}{3}}$. (4.97)

The tangential traction acts parallel to the x-axis at all points; it is given by q' in the annulus $c \le r \le a$ and by the resultant of q' and q'' in the central circle $r \le c$. The relative tangential displacement of the two bodies is found by substituting equation (4.97) into (4.95),

$$\delta_x = \frac{3\mu p}{16a}\left(\frac{2-\nu_1}{G_1}+\frac{2-\nu_2}{G_2}\right)\left[1-\left(1-\frac{Q_x}{\mu p}\right)^{\frac{2}{3}}\right] \tag{4.98}$$

This nonlinear expression is plotted in the line B of Figure 4.9.

It is instructive to compare the compliance of two spherical bodies to tangential force with the compliance to normal force found from the Hertz theory. Since the normal displacement δ_z is non-linear with load, it is most meaningful to compare the rates of change of displacement with load. For bodies having the same elastic constants, differentiating Equation (4.64) gives a normal compliance,

$$\frac{d\delta_z}{dp} = \frac{2}{3}\left[\frac{9}{4}\left(\frac{1-\nu^2}{E}\right)^2\left(\frac{1}{R_1}+\frac{1}{R_2}\right)\frac{1}{p}\right]^{\frac{1}{3}} = \frac{1-\nu}{2Ga}. \tag{4.99}$$

The tangential compliance for small values of Q_x is given by equation (4.81):

$$\frac{d\delta_x}{dQ_x} = \frac{2-\nu}{4Ga}. \tag{4.100}$$

So that the ratio of the tangential compliance, C_t, to normal compliance, C_n, is $2-\nu/2(1-\nu)$, which varies from 1.17 to 1.5 as Poisson's ratio varies from 0.25 to 0.5 and is independent of the normal load. Thus the tangential and normal compliance are roughly similar in magnitude.

5. SIMPLIFIED CONTACT MODEL

The influence of tangential traction upon normal pressure in the contact area is generally small, particularly when the coefficient of limiting friction is less than unity. Therefore, for the analysis of collisions involving tangential traction, it is assumed that the stress and deformation due to normal and tangential forces are independent of each other, but that they could be superposed to evaluate the resultant stress and deformation. In this chapter, a simplified model with coupled, non-linear and conservative springs in the normal and tangential direction is presented, based upon the contact mechanics discussed in the previous chapter. The basic assumptions and equations of tangential and normal motion will be discussed.

5.1 Model Description

In order to focus on the effects of normal and tangential compliance during collision, consider a body that collides against a half-space as shown in Figure 5.1(*a*). At the contact point, the body and the half-space have a common tangent plane. Let unit vectors $\boldsymbol{t}$ and $\boldsymbol{n}$ be oriented in directions tangent and normal to this plane respectively. The displacement of $\boldsymbol{P}$ relative to $\boldsymbol{B}'$ is defined as $(u_t\,\boldsymbol{t} + u_n\,\boldsymbol{n})$ and the displacement of $\boldsymbol{Q}$ relative to $\boldsymbol{B}'$ is defined as $(s\,\boldsymbol{t} + u_n\,\boldsymbol{n})$, where $s(t)$ is the extension of the springs in the tangential direction. The contact point $\boldsymbol{P}$ is defined as the point of $\boldsymbol{B}$ coincident with $\boldsymbol{Q}$ when $s = u_n = 0$. The interaction forces, $\boldsymbol{f}(t)$, between two bodies are shown in Figure 5.1(*b*). Let $\boldsymbol{v}$ be a given initial approach velocity at the incident angle α between $\boldsymbol{v}$ and -

$\boldsymbol{n}$, $\bar{v}(t)$ the velocity of the contact point at any instant time during impact, and $\boldsymbol{w}$ the value of $\bar{v}$ at the end of contact.

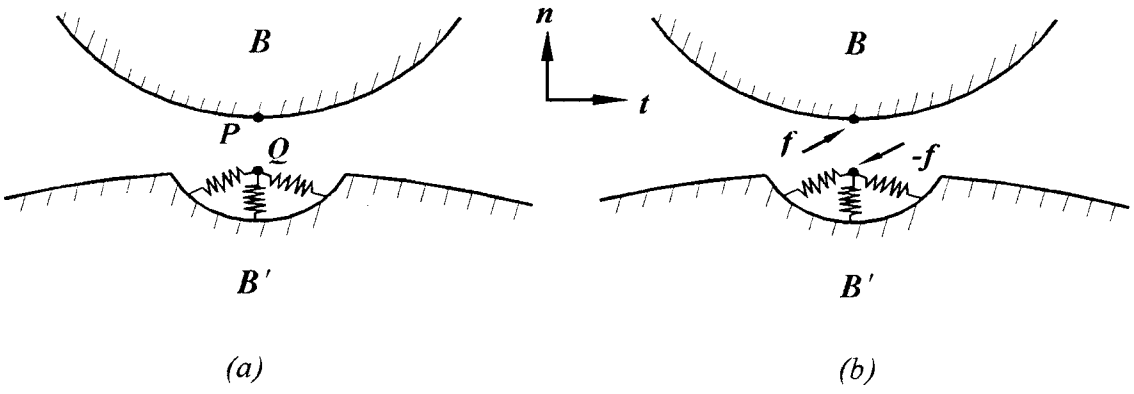

Figure 5.1 (*a*) The contact area of two colliding bodies (*b*) The interaction force of the contact area

In order to get the tangential force-displacement equation, the non-linear force-displacement relationship in the normal direction from Hertz theory as shown in the preceding chapter can be used,

$$f_n = \frac{4}{3}\sqrt{R}E(-u_n)^{\frac{3}{2}} \tag{5.1}$$

in which $R = \dfrac{1}{\dfrac{1}{R_1}+\dfrac{1}{R_2}}$ and $E = \dfrac{1}{\dfrac{1-\nu_1^{\,2}}{E_1}+\dfrac{1-\nu_2^{\,2}}{E_2}}$.

After a normal force presses two elastic bodies to contact, a tangential force applied subsequently causes the elastic deformation without slip throughout the contact area. The relative displacement in the tangential direction for two elastic bodies, as discussed in previous chapter, is given

$$u_t = u_{t_1} - u_{t_2} = \frac{f_t}{8a}\left(\frac{2-\nu_1}{G_1} + \frac{2-\nu_2}{G_2}\right). \tag{5.2}$$

Since from Hertz theory, the normal displacement,

$$u_n = \left(\frac{9F_n^{\,2}}{16RE^2}\right)^{\frac{1}{3}} = \frac{a^2}{R}, \tag{5.3}$$

then, substituting $a = \sqrt{(-u_n)R}$ into equation (5.2), we will have the displacement of the tangential spring which becomes coupled with the displacement of the normal spring,

$$s = \frac{-f_t}{8\sqrt{R(-u_n)}}\left(\frac{2-\nu_1}{G_1} + \frac{2-\nu_2}{G_2}\right). \tag{5.4}$$

Therefore, the tangential force can be expressed as

$$f_t = -8G\sqrt{R}\,s(-u_n)^{\frac{1}{2}} \tag{5.5}$$

where $G = \dfrac{1}{\dfrac{2-\nu_1}{G_1} + \dfrac{2-\nu_2}{G_2}}$. (5.6)

For the special case in which the two spheres are composed of the same material,

$$\nu_1 = \nu_2 = \nu\ , \tag{5.7}$$

$$E_1 = E_2 = E^*, \tag{5.8}$$

and $$\frac{1}{E} = \frac{1-\nu_1^{\,2}}{E_1} + \frac{1-\nu_2^{\,2}}{E_2} = \frac{2(1-\nu^2)}{E^*}, \tag{5.9}$$

then $$G = \frac{(1-\nu)E}{2(2-\nu)}. \tag{5.10}$$

The tangential and normal forces of this simplified-coupled model may be expressed as

$$f_n = \frac{4}{3}\sqrt{R}\,E\,(-u_n)^{\frac{3}{2}}, \tag{5.11}$$

$$f_t = -\frac{4(1-\nu)}{2-\nu}\sqrt{R}\,E\,s(-u_n)^{\frac{1}{2}}. \tag{5.12}$$

We can express the applied force $\boldsymbol{f}$ in both normal and tangential directions and both are functions of the displacement of the normal spring, u_n and the displacement of the tangential spring, s, where the displacement $\boldsymbol{u} = u_n \boldsymbol{e}_n + s\boldsymbol{e}_t$,

$$\boldsymbol{f} = f_n \boldsymbol{e}_n + f_t \boldsymbol{e}_t \tag{5.13}$$

where $f_n = f_n(u_n, s)$, (5.14)

$$f_t = f_t(u_n, s). \tag{5.15}$$

The increment of work of this force is,

$$dW = f_n\, du_n + f_t\, ds, \tag{5.16}$$

so that the work along some path will be

$$W = \int \boldsymbol{f} \cdot d\boldsymbol{u} = \int f_n\, du_n + \int f_t\, ds. \tag{5.17}$$

If the expressions are to represent an elastic, energy-conservative system, there must exist a potential $V(u_n, s)$ such that $dW = dV$.

Since $dV = \frac{\partial V}{\partial u_n} du_n + \frac{\partial V}{\partial s} ds$, (5.18)

by equating energy expressions of dV, Equations (5.16) and (5.18), we will have

$$f_n = \frac{\partial V}{\partial u_n}, \quad f_t = \frac{\partial V}{\partial s}, \tag{5.19}$$

and

$$\frac{\partial f_n}{\partial s} = \frac{\partial}{\partial s}\frac{\partial V}{\partial u_n}, \quad \frac{\partial f_t}{\partial u_n} = \frac{\partial}{\partial u_n}\frac{\partial V}{\partial s}. \tag{5.20}$$

For the existence of the elastic potential energy, the two equations above must be equal, i.e.,

$$\frac{\partial f_n}{\partial s} = \frac{\partial f_t}{\partial u_n} = \frac{2(1-\nu)}{2-\nu}\sqrt{R}E\left(\frac{s}{\sqrt{-u_n}}\right). \tag{5.21}$$

Therefore, the normal force is expressed as follows with one more function of u_n, $\Phi(u_n)$, added,

$$\begin{aligned} f_n &= \frac{1-\nu}{2-\nu}\sqrt{R}E\frac{s^2}{\sqrt{-u_n}} + \Phi(u_n) \\ &= \frac{1-\nu}{2-\nu}\sqrt{R}E\frac{s^2}{\sqrt{-u_n}} + \frac{4}{3}\sqrt{R}E(-u_n)^{\frac{3}{2}} \\ &= \sqrt{R}E(-u_n)^{\frac{3}{2}}\left[\frac{4}{3} + \frac{1-\nu}{2-\nu}\frac{s^2}{(-u_n)^2}\right] \end{aligned} \tag{5.22}$$

The complete normal and tangential forces of the non-linear coupled-conservative model can be expressed as

$$f_n = \sqrt{R}E(-u_n)^{\frac{3}{2}}\left[\frac{4}{3} + \frac{1-\nu}{2-\nu}\frac{s^2}{(-u_n)^2}\right] \tag{5.23}$$

$$f_t = -\frac{4(1-\nu)}{2-\nu}\sqrt{R}Es(-u_n)^{\frac{1}{2}}, \tag{5.24}$$

When the contact area is subject to sticking, which, from the Coulomb friction law, occurs when the tangential force is less than the limiting friction force, the tangential velocity of colliding bodies is equal to the extension rate of the tangential spring; that is,

$$\dot{s} = \bar{v}_t = \dot{u}_t, \text{ for } |f_t| < \mu f_n. \tag{5.25}$$

If the tangential force reaches the limiting friction force and the colliding bodies begin to slip, the tangential force satisfies

$$f_t = -\mu \frac{\bar{v}_t - \dot{s}}{|\bar{v}_t - \dot{s}|} f_n, \tag{5.26}$$

and this relationship must replace equation (5.25).

Upon substitution of equations (5.11) and (5.12), the condition for sticking, $|f_t| < \mu f_n$, becomes

$$\left(\frac{|s|}{-u_n}\right)^2 - \frac{4}{\mu}\frac{|s|}{(-u_n)} + 4\kappa > 0 \tag{5.27}$$

in which the dimensionless ratio κ is defined and limited by

$$\frac{2}{3} < \kappa \equiv \frac{2-\nu}{3(1-\nu)} < 1. \tag{5.28}$$

The left-hand member of equation (5.27) has roots at $\frac{|s|}{-u_n} = \frac{2}{\mu}\left(1 \pm \sqrt{1-\kappa\mu^2}\right)$ and has a minimum value of $-4\left(\frac{1}{\mu^2} - \kappa\right)$ at $\frac{|s|}{-u_n} = \frac{2}{\mu}$. This implies that, if $\mu > \frac{1}{\sqrt{\kappa}}$, there will always be sticking, and, if $\mu < \frac{1}{\sqrt{\kappa}}$, sliding will occur if

$$\frac{2}{\mu}\left(1 - \sqrt{1-\kappa\mu^2}\right) < \frac{|s|}{-u_n} < \frac{2}{\mu}\left(1 + \sqrt{1-\kappa\mu^2}\right). \tag{5.29}$$

Now, when the quadratic term in equation (5.23), which was appended to insure that equations (5.23) and (5.24) imply a conservative elastic system, becomes significant compared with $\frac{4}{3}$, the validity of equation (5.23) becomes doubtful. Therefore, values of $\frac{|s|}{-u_n}$ greater than approximately $\frac{2}{\mu}$ will not be considered in this investigation, so that

the upper limit $\frac{2}{\mu}\left(1+\sqrt{1-\kappa\mu^2}\right)$ in equation (5.29) will be outside the limits of this study. Denoting the lower limit as

$$C=\frac{2}{\mu}\left(1-\sqrt{1-\kappa\mu^2}\right), \tag{5.30}$$

we may write the conditions for sticking at the contact point as $\mu > \frac{1}{\sqrt{\kappa}}$ or,

$$-C < \frac{s}{-u_n} < C. \tag{5.31}$$

When these conditions are met, the system must satisfy

$$\dot{s} = \dot{u}_t \tag{5.25}$$

which will continue to govern until contact is lost or until $\frac{s}{-u_n} = \pm C$, at which equation (5.25) must be replaced with

$$\dot{s} = -\frac{s}{|s|} C\, \dot{u}_n \tag{5.32}$$

The factor $\frac{s}{|s|}$ assures that the direction of the friction force is consistent with the direction of tangential elastic deformation. Equation (5.32) will continue to govern until contact is lost or $\dot{s} = \dot{u}_t$, at which time equation (5.32) must be replaced with equation (5.25). Initial stick or slip will be determined by the criteria

$$\tan\alpha = \frac{\dot{u}_t(0)}{\dot{u}_n(0)} \quad \begin{cases} < C & \text{stick} \\ > C & \text{slip} \end{cases} \tag{5.33}$$

Remaining governing equations are the kinetic relationships discussed earlier:

$$\begin{Bmatrix} \bar{v}_t - v_t \\ \bar{v}_n - v_n \end{Bmatrix} = \begin{bmatrix} N_{tt} & N_{tn} \\ N_{nt} & N_{nn} \end{bmatrix} \begin{bmatrix} g_t \\ g_n \end{bmatrix}. \tag{5.34}$$

By substituting $v_i = \dot{u}_i$, $v_t = v \sin\alpha$, and $v_n = v \cos\alpha$ into these equations, and $f_i = \dot{g}_i$ into equations (5.23) and (5.24), the system governing contact may be written and summarized as follows:

$$\dot{g}_t = -\frac{4(1-\nu)}{2-\nu} \sqrt{R}\, E\, s \sqrt{-u_n}\,, \tag{5.35}$$

$$\dot{g}_n = \sqrt{R}\, E (-u_n)^{\frac{3}{2}} \left(\frac{4}{3} + \frac{1-\nu}{2-\nu} \frac{s^2}{u_n^{\,2}} \right), \tag{5.36}$$

$$\dot{u}_t = v \sin\alpha + N_{tt}\, g_t + N_{tn}\, g_n, \tag{5.37}$$

$$\dot{u}_n = -v \cos\alpha + N_{nt}\, g_t + N_{nn}\, g_n, \tag{5.38}$$

$$\dot{s} = \begin{cases} \dot{u}_t & \text{whenever} \quad \dfrac{|s|}{-u_n} < C \\ -\dfrac{s}{|s|} C\, \dot{u}_n & \text{whenever} \quad \dfrac{|s|}{-u_n} = C \end{cases} \tag{5.39}$$

Non-dimensional quantities may be introduced in terms of the length

$$\eta = \left(\frac{m^2 v^4}{E^2 R} \right)^{\frac{1}{5}} \tag{5.40}$$

Impulse, displacement of the contact point and the tangential spring, and duration of impact are expressed in terms of non-dimensional quantities as follows:

$$g_i = m v \gamma_i \tag{5.41}$$

$$u_i = \eta \delta_i \tag{5.42}$$

$$s = \eta \varepsilon \tag{5.43}$$

$$t = \frac{\eta}{v}\tau \tag{5.44}$$

where the subscript i represents the normal and tangential directions, $\boldsymbol{t}$ and $\boldsymbol{n}$, respectively. By following chain rule for the differentiating with respect to time,

$$\dot{\phi} = \frac{d\tau}{dt}\frac{d\phi}{d\tau} = \frac{v}{\eta}\phi', \tag{5.45}$$

the equations governing non-dimensional force and displacement of the contact point are given as follows:

$$\gamma_t' = -\frac{4(1-\nu)}{2-\nu}\varepsilon\sqrt{-\delta_n} = -\frac{4}{3\kappa}\varepsilon\sqrt{-\delta_n} \tag{5.46}$$

$$\gamma_n' = (-\delta_n)^{\frac{3}{2}}\frac{1}{3}\left(4 + \frac{\varepsilon^2}{\kappa\delta_n{}^2}\right) \tag{5.47}$$

$$\delta_t' = \sin\alpha + (1 + \lambda\cos 2\theta)\gamma_t + \lambda\sin 2\theta\,\gamma_n \tag{5.48}$$

$$\delta_n' = -\cos\alpha + \lambda\sin 2\theta\,\gamma_t + (1 - \lambda\cos 2\theta)\gamma_n\,. \tag{5.49}$$

$$\varepsilon' = \delta_t' \qquad \text{whenever } \frac{|\varepsilon|}{(-\delta_n)} < \frac{2}{\mu}\left(1 - \sqrt{1-\kappa\mu^2}\right) \text{ (stick)} \tag{5.50}$$

$$\varepsilon' = -\frac{2}{\mu}\left(1 - \sqrt{1-\kappa\mu^2}\right)\frac{\varepsilon}{|\varepsilon|}\delta_n' \quad \text{whenever } \frac{|\varepsilon|}{(-\delta_n)} = \frac{2}{\mu}\left(1 - \sqrt{1-\kappa\mu^2}\right) \text{ (slip)} \tag{5.51}$$

The initial conditions, at $\tau = 0$, are

$$\delta_t(0) = 0\,, \tag{5.52}$$

$$\delta_n(0) = 0\,, \tag{5.53}$$

$$\gamma_t(0) = 0,, \tag{5.54}$$

and

$$\gamma_n(0) = 0\,. \tag{5.55}$$

The condition for judging initial stick or slip is to be decided by the incident angle α, where

$$\tan\alpha = \frac{\delta_t'(0)}{\delta_n'(0)}. \tag{5.56}$$

If

$$-\frac{2}{\mu}\left(1-\sqrt{1-\kappa\mu^2}\right) < \tan\alpha < \frac{2}{\mu}\left(1-\sqrt{1-\kappa\mu^2}\right), \tag{5.57}$$

the bodies stick at the beginning of impact and the velocity of the tangential spring is as determined by equation (5.50);

$$\varepsilon'(0) = \delta_t'(0), \tag{5.58}$$

otherwise, slide occurs at the beginning of impact and equation (5.51) is used for representation of the velocity of the tangential spring

$$\varepsilon'(0) = -\frac{2}{\mu}\left(1-\sqrt{1-\kappa\mu^2}\right)\delta_n'(0). \tag{5.59}$$

Sliding (or sticking) may give way to sticking (or sliding) at some point during the impact. Such behavior will be seen in the examples presented later.

The following was used to judge whether the slip continues or stick occurs during the numerical integration.

$$\frac{\varepsilon(i)}{|\varepsilon(i)|}\left[\delta_t'(i)-\varepsilon_t'(i)\right] > 0. \tag{5.60}$$

If the inequality is true, then slip stops and stick occurs. Otherwise, slip continues throughout the impact.

The motion resulting from these coupled, nonlinear, conservative springs on the oblique impact of elastic sphere are discussed in the following. Although this model does

not account for all of the complexity of a real collision process, it provides the ability to greatly simplify the prediction of the rebound. Comparisons with more accurate and complex analyses in the following indicate that it provides acceptable accuracy.

5.2 Oblique Impact of Elastic Spheres

In this section, the oblique impact of elastic spheres is investigated, using the methods developed in the previous section. A sphere colliding with a massive flat surface is taken for example. As shown in Figure 5.2, the parameters of inertia coupling for the colliding system are $\lambda = 5/9$ and $\theta = 0$. From the non-dimensional system equations, it may be seen that only the incident velocity and the coefficient of friction characterize the motion of impact for a given value of Poisson's ratio.

Consider a sphere with the Poisson's ratio $\nu = 0.3$ and the coefficient of friction $\mu = 0.5$ striking on a flat surface. As shown in Figure 5.2, the angles are related to the velocity components as

$$\alpha_1 = \tan^{-1}\left(\frac{v_t}{-v_n}\right) \tag{5.61}$$

and

$$\alpha_2 = \tan^{-1}\left(\frac{w_t}{w_n}\right), \tag{5.62}$$

where v_t, v_n, w_t and w_n are the incident and reflecting velocities of the point P, respectively, in the tangential and. normal directions.

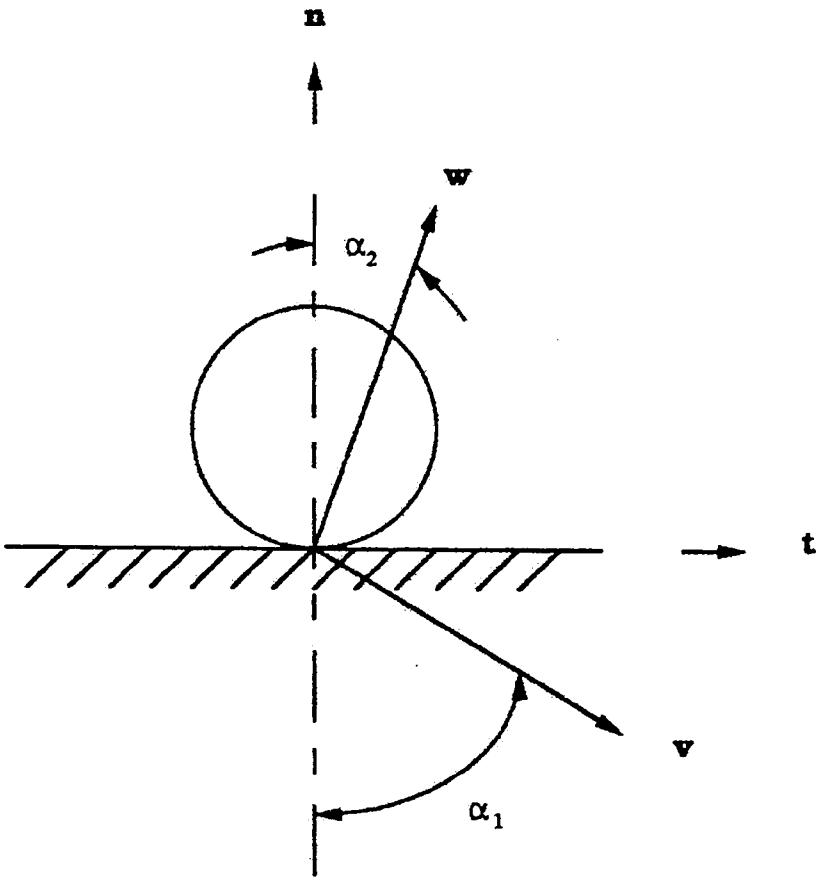

Figure 5.2 The definitions of the angle of incidence and the angle of reflection

Given the above material constants, Maw et al. (1976) introduced a non-dimensional quantity for incident velocity,

$$\Psi = \frac{2(1-\nu)}{\mu(2-\nu)}\tan\alpha\,, \tag{5.63}$$

where the values of Ψ and α that correspond to incidence will be denoted as Ψ_1 and α_1 and those that correspond to the reflection as Ψ_2 and α_2. Since Ψ is proportional to the ratio between $\tan\alpha$ and the coefficient of friction μ, Ψ_1 and Ψ_2 are referred to,

respectively, as the non-dimensional angle of incidence and the non-dimensional angle of reflection.

Results from the detailed and complex analysis of Maw, et. al., will be compared with those from integration of the dimensionless equations of the previous section, specialized for the case of the sphere. For this comparison, the computed values of w_t are used for the evaluation of the corresponding values of Ψ_2, and non-dimensional tangential force and time are defined, respectively, as

$$\Psi_2 = \frac{2(1-\nu)}{\mu(2-\nu)}\frac{w_t}{w_n}, \tag{5.64}$$

$$\Phi_t = \frac{F_t}{\mu F_{n,\max}}, \tag{5.65}$$

and

$$\tau = \frac{t}{T}, \tag{5.66}$$

where t is any instant time during the contact and T is the duration of contact. For the non-linear coupled-conservative model the plot of non-dimensional tangential force Φ_t with respect to the dimensionless time τ for different value of Ψ_1 is given in Figure 5.3. For Ψ_1 =1.2, the values for non-dimensional tangential and normal force, impulse, displacement, velocity are plotted from Figure 5.4 to Figure 5.11.

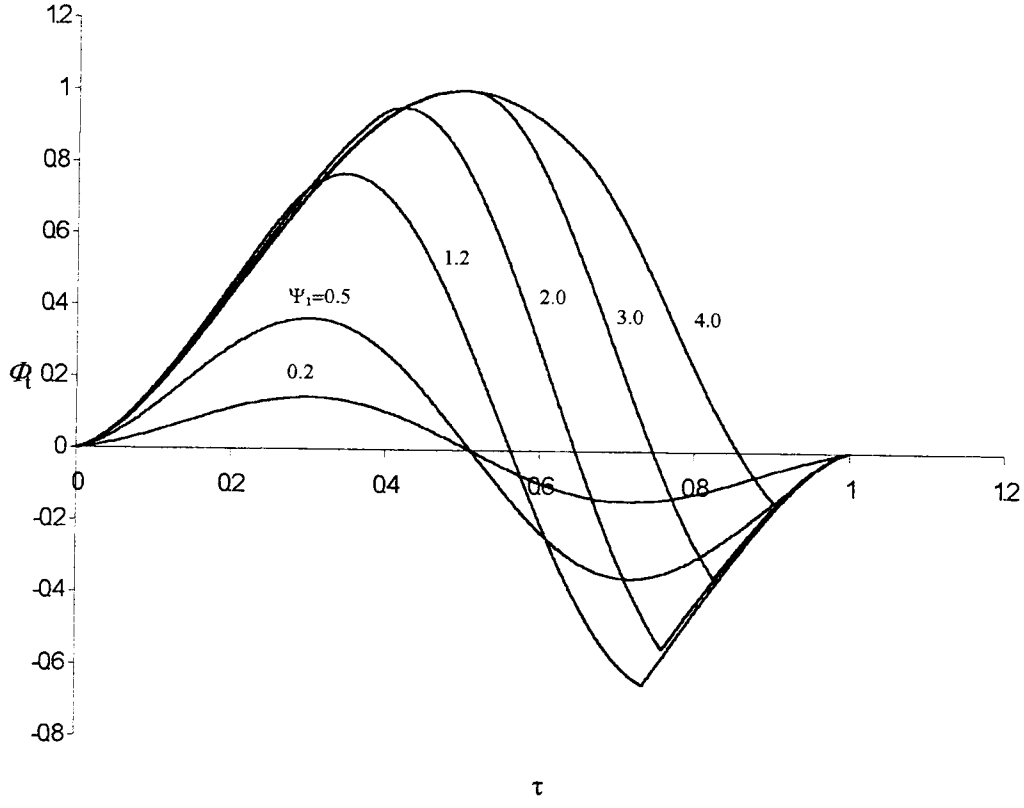

Figure 5.3 Non-dimensional tangential force during impact for various non-dimensional incident angle Ψ_1

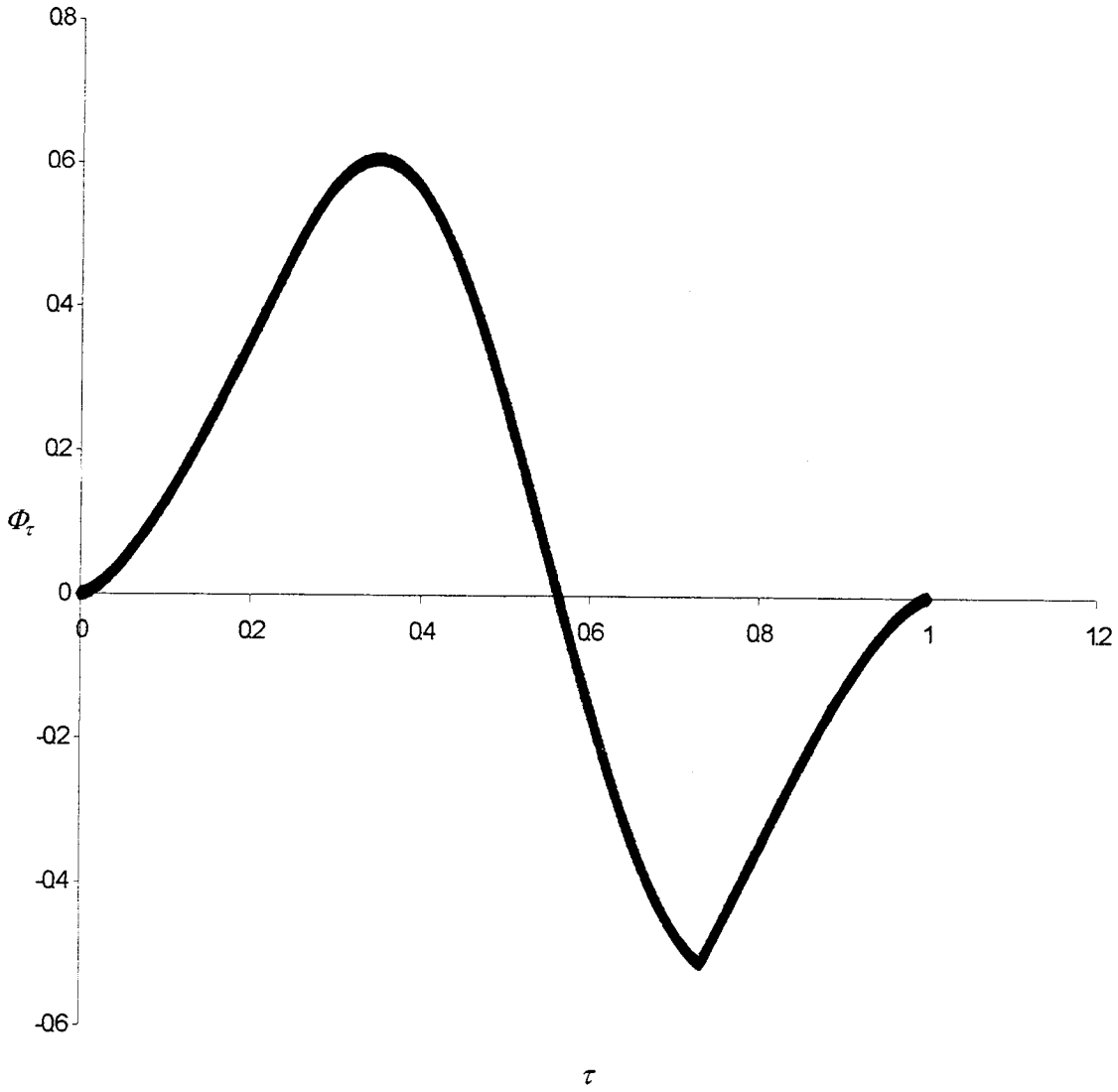

Figure 5.4 Non-dimensional tangential force during impact at Ψ_1=1.2

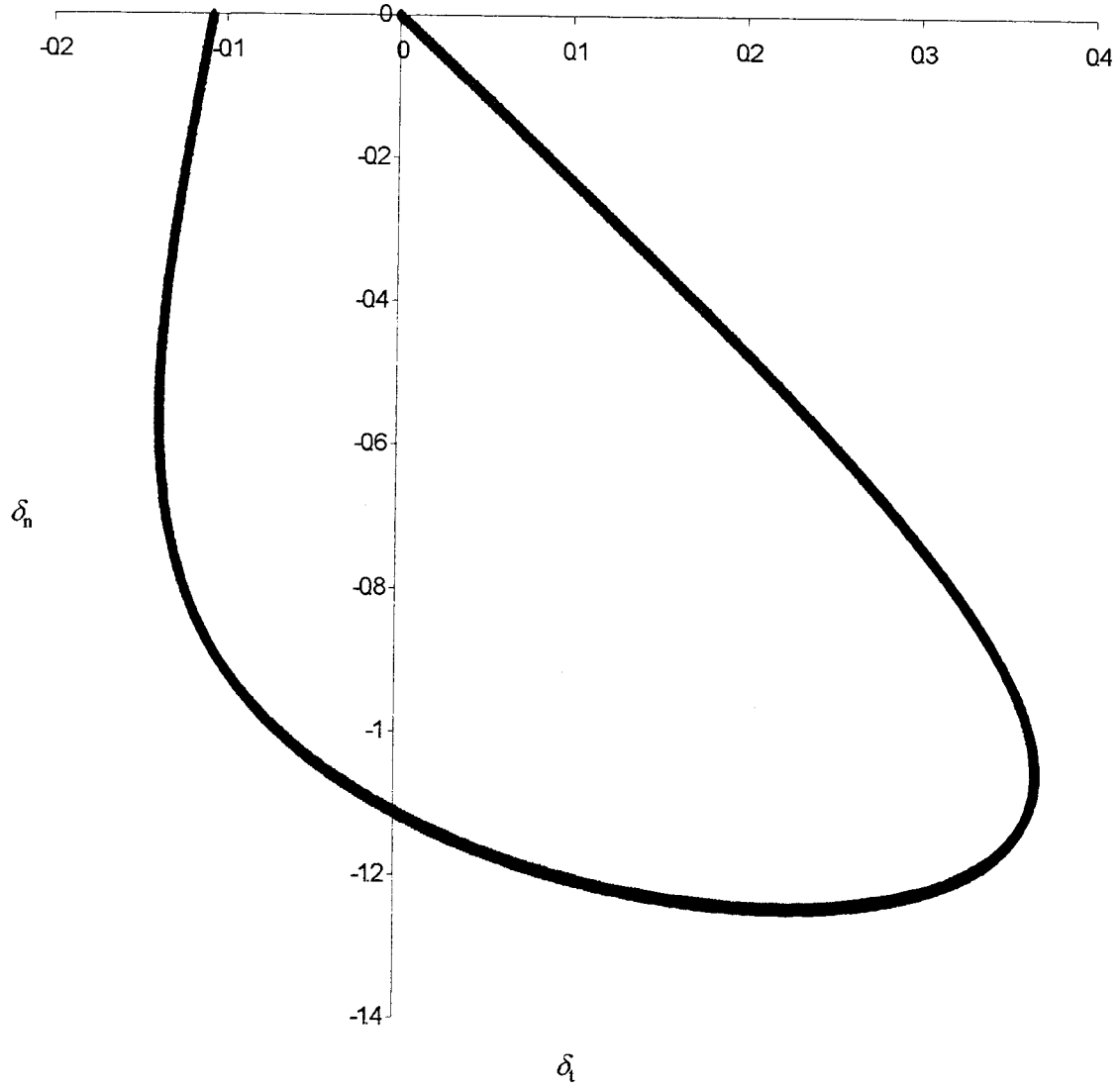

Figure 5.5 Non-dimensional normal and tangential displacement of contact point at Ψ_1=1.2

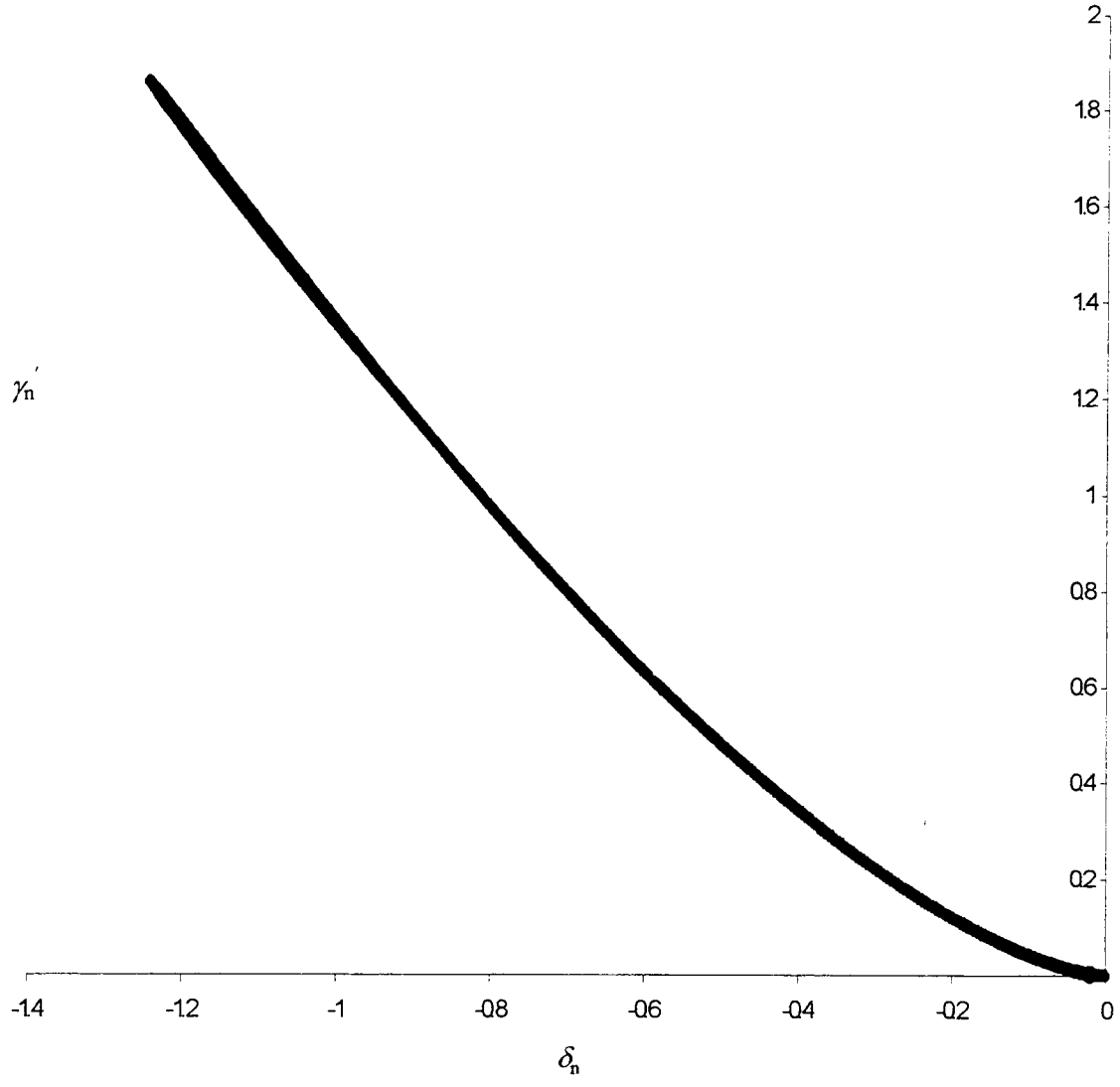

Figure 5.6 Non-dimensional normal displacement and normal force of contact point at Ψ_1=1.2

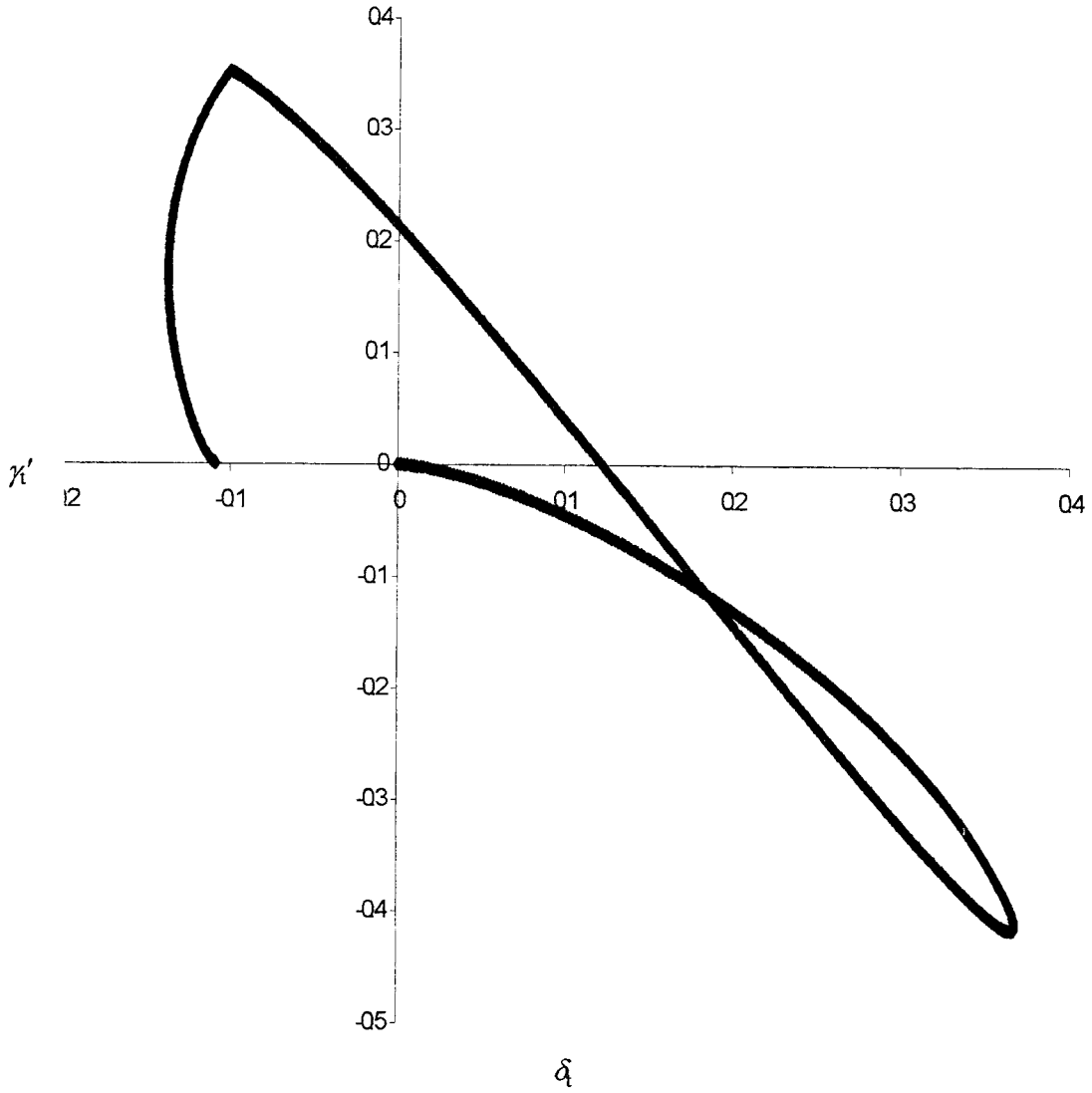

Figure 5.7 Non-dimensional tangential displacement and tangential force of contact point at Ψ_1=1.2.

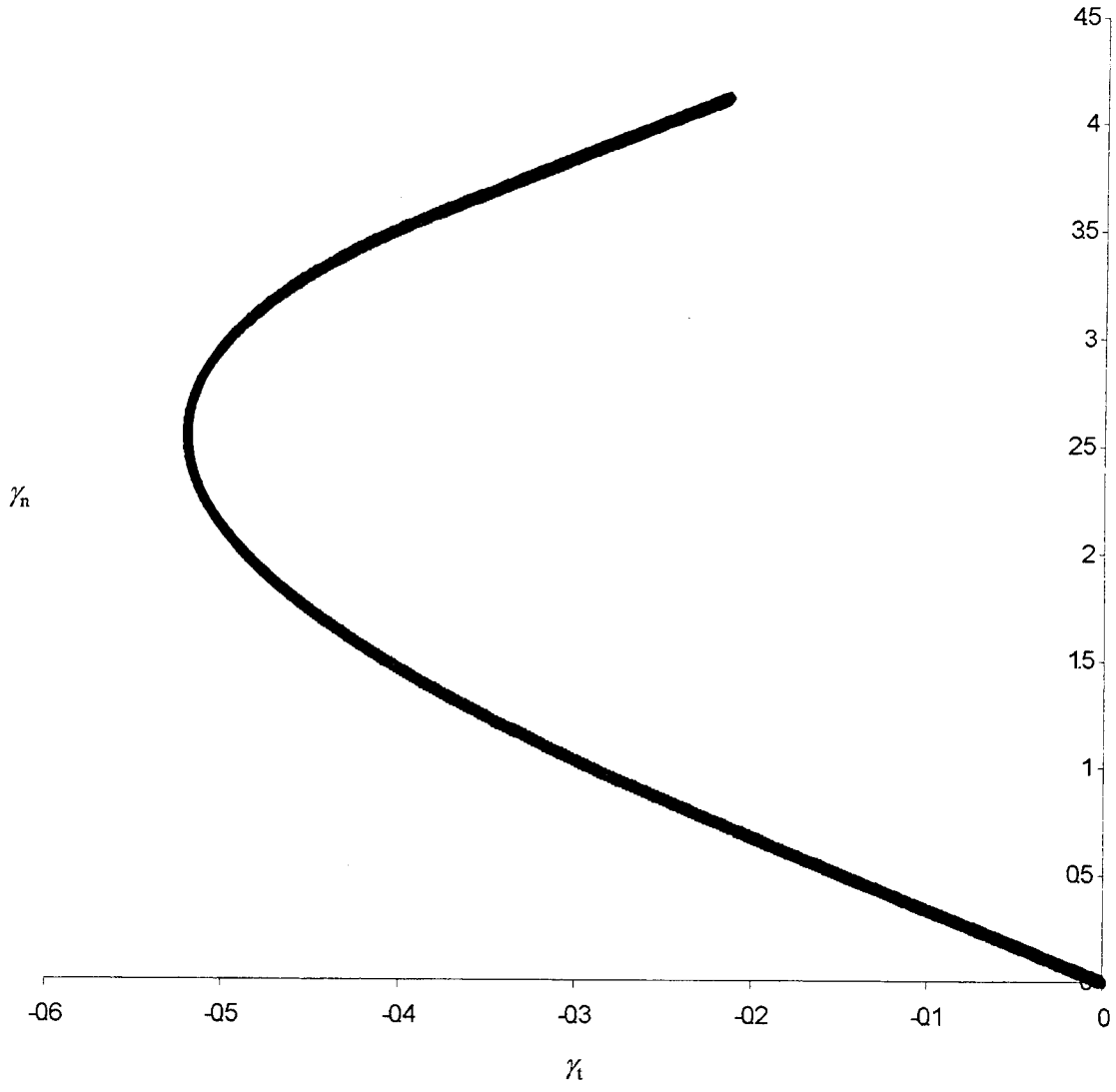

Figure 5.8 Non-dimensional normal and tangential impulse of contact point at Ψ_1=1.2.

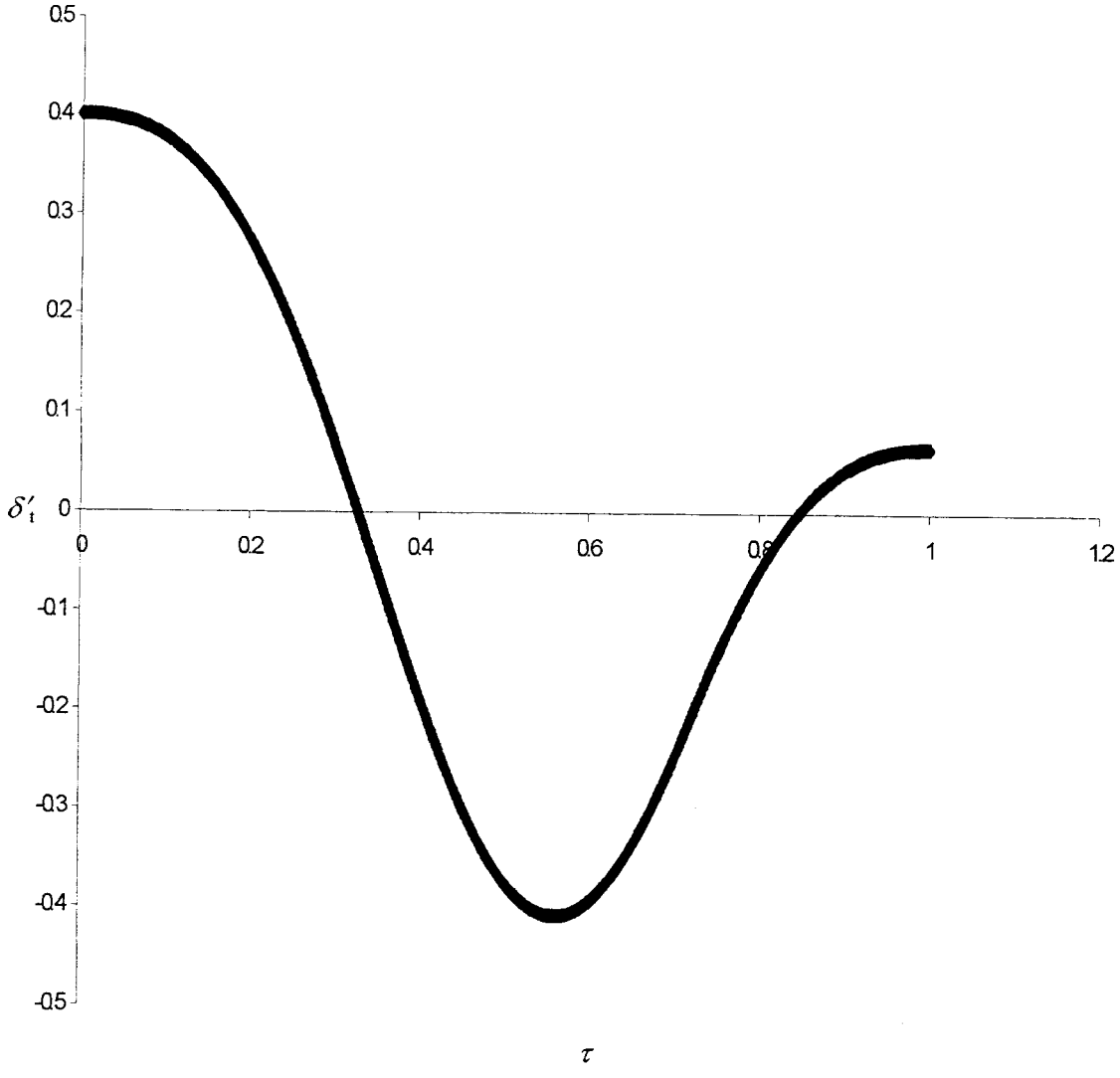

Figure 5.9 Non-dimensional tangential velocity of contact point at Ψ_1=1.2.

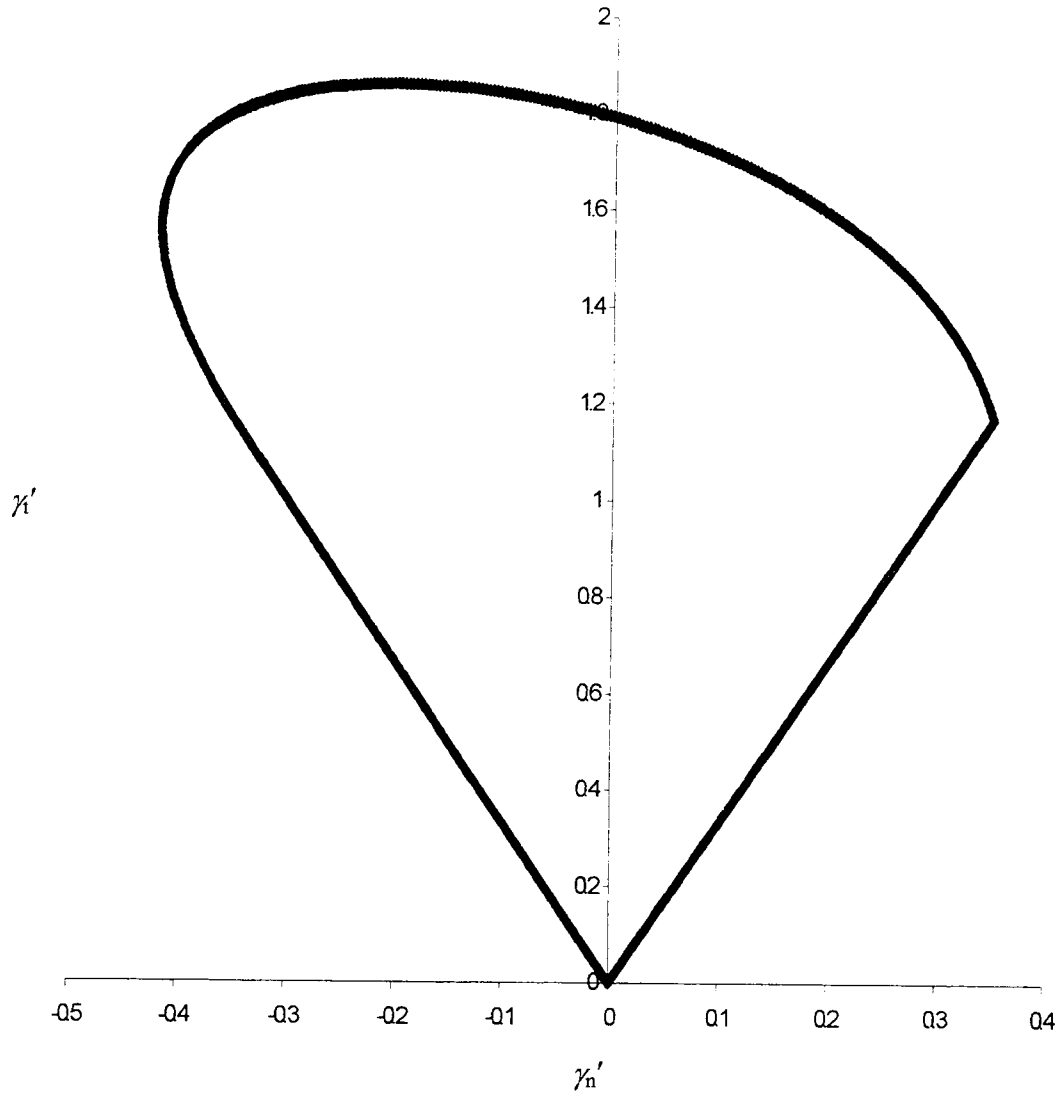

Figure 5.10 Non-dimensional tangential and normal force of contact point at Ψ_1=1.2.

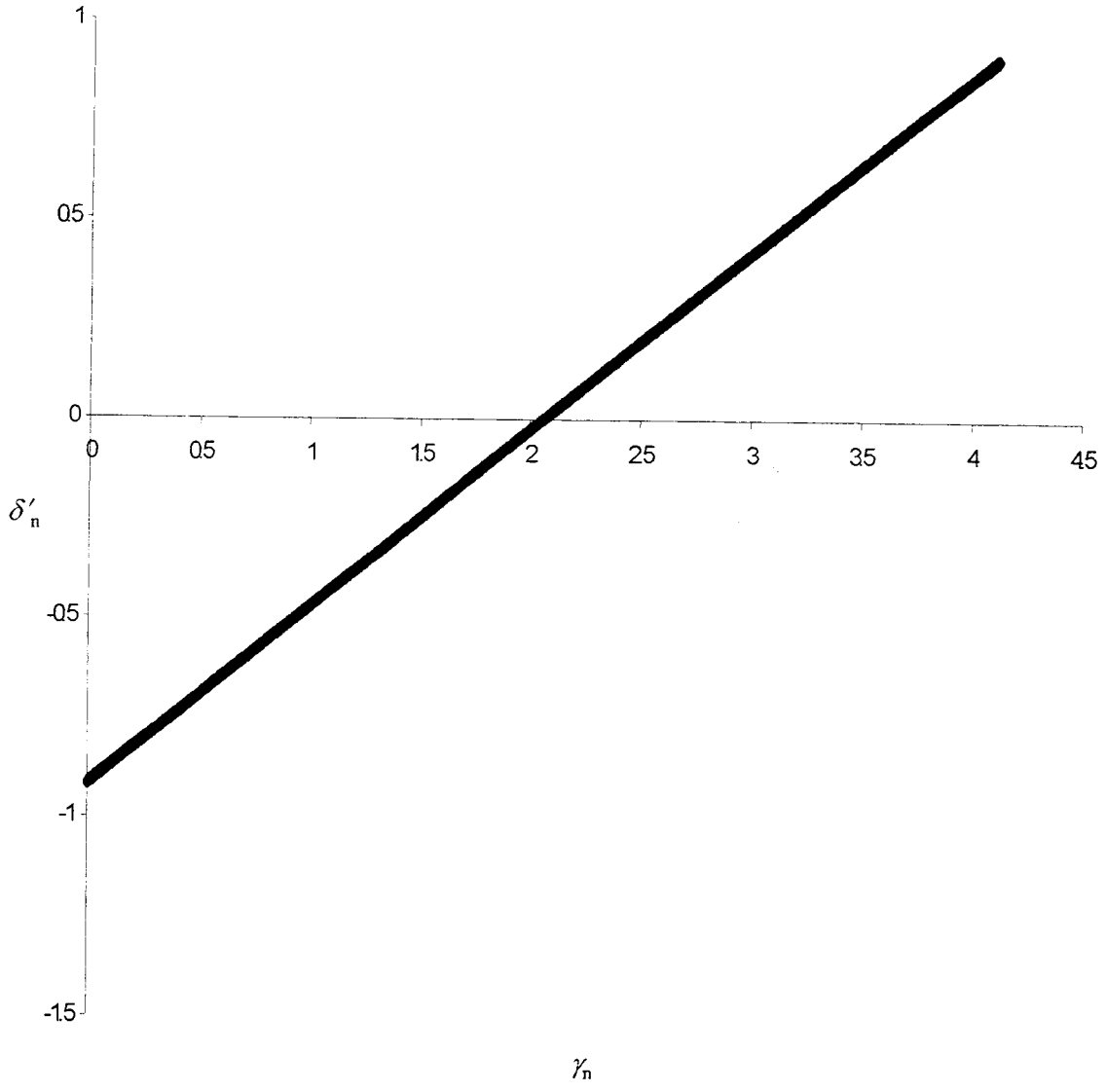

Figure 5.11 Non-dimensional normal velocity and normal impulse of contact point at Ψ_1=1.2.

5.3 The Effect of the Radius of Gyration

Once gross slip ceases, the tangential compliance and the inertia of the sphere act very much like a non-linear mass-spring system. Therefore the natural frequencies of this system may be expected to depend upon the radius of gyration of the sphere. Introduce another non-dimensional quantity,

$$\chi = \frac{(1-\nu)(1+\lambda)}{(2-\nu)(1-\lambda)}, \tag{5.67}$$

which is independent of the friction coefficient and a function of the Poisson ratio for a given value of λ. For a given Poisson ratio, as χ is increased, the radius of gyration is reduced. This prediction is confirmed by the results presented in Figure 5.12. As χ is increased, the number of reversals in tangential force during the cycle increases. The rebound prediction of the angle of reflection as a function of χ for solid sphere is shown in Figure 5.13. The rebound prediction for four different objects with different configuration parameter, the solid sphere, solid disc, shell and hoop, are examined here. For a given Poisson ratio, $\nu = 0.3$, the configuration parameter λ for each object are shown in Table 5.1. From Figure 5.14, Figure 5.15, Figure 5.16, Figure 5.17, we can see the angle of reflection is influenced by the configuration parameter λ, which is a function of the radius of gyration, i.e., $\lambda = \frac{b^2}{2k_3^{\,2} + b^2}$, as discussed in chapter 3.

	Solid Sphere	Solid Disc	Shell	Hoop
λ	0.556	0.5	0.429	0.333

Table 5.1 The configuration parameter of four different objects

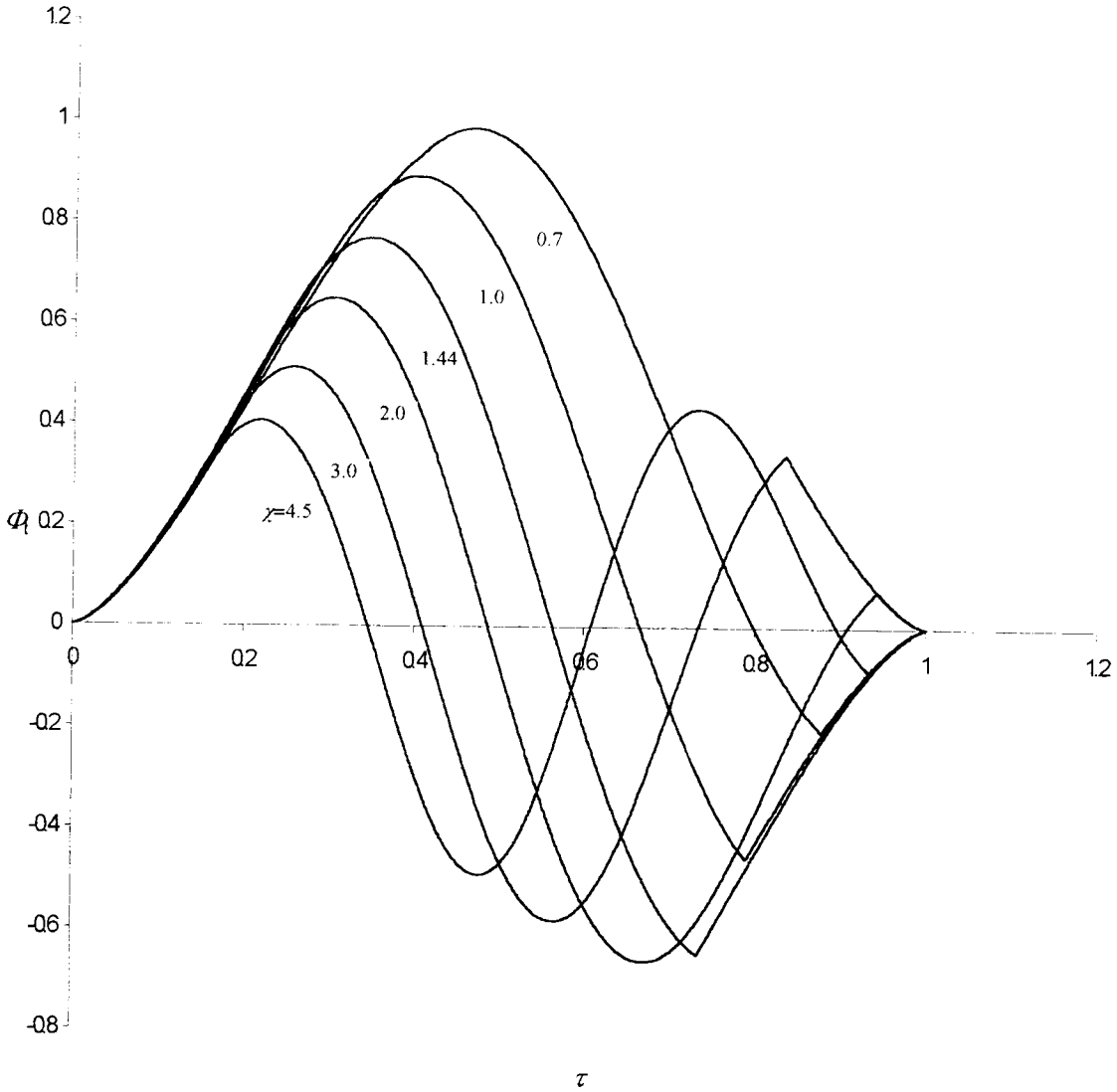

Figure 5.12 Non-dimensional tangential force during impact for various radii of gyration, χ, at Ψ_1=1.2

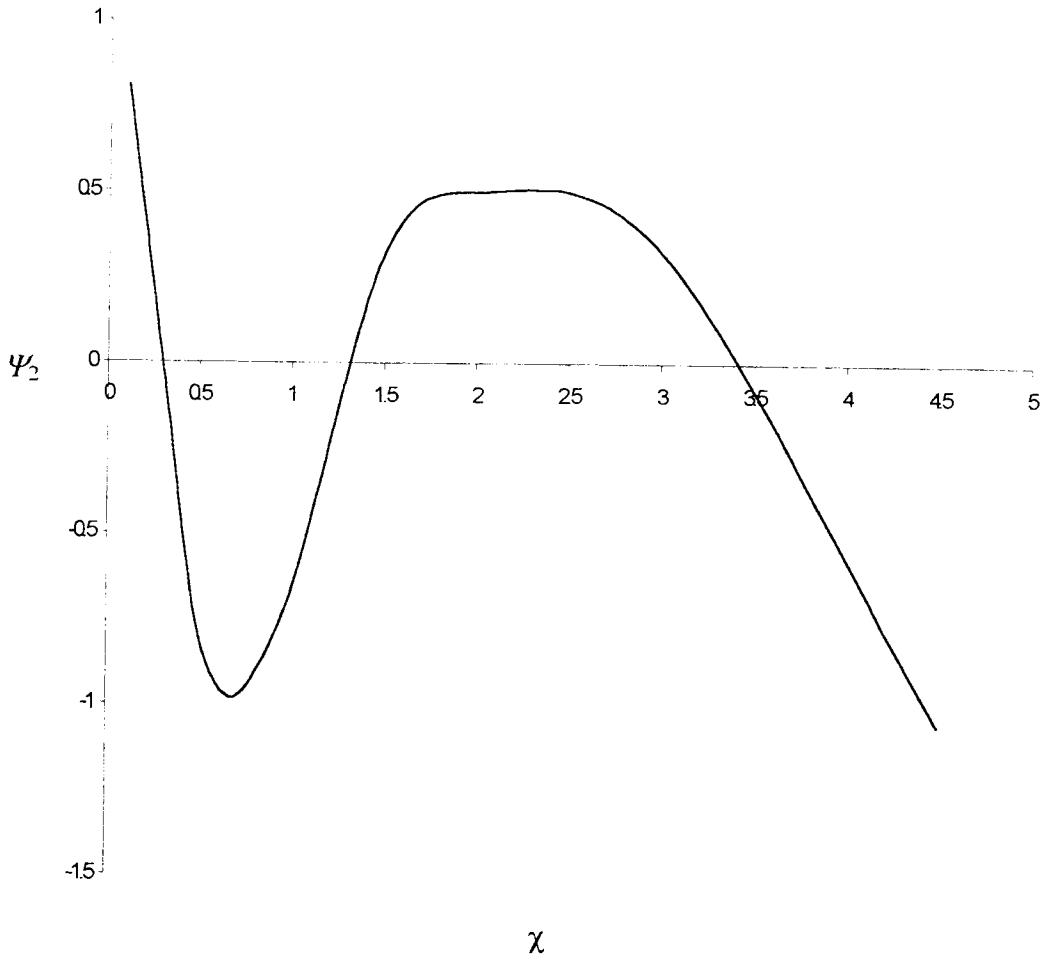

Figure 5.13 The local angle of reflection as a function of χ for a local angle of incidence Ψ_1=1.2

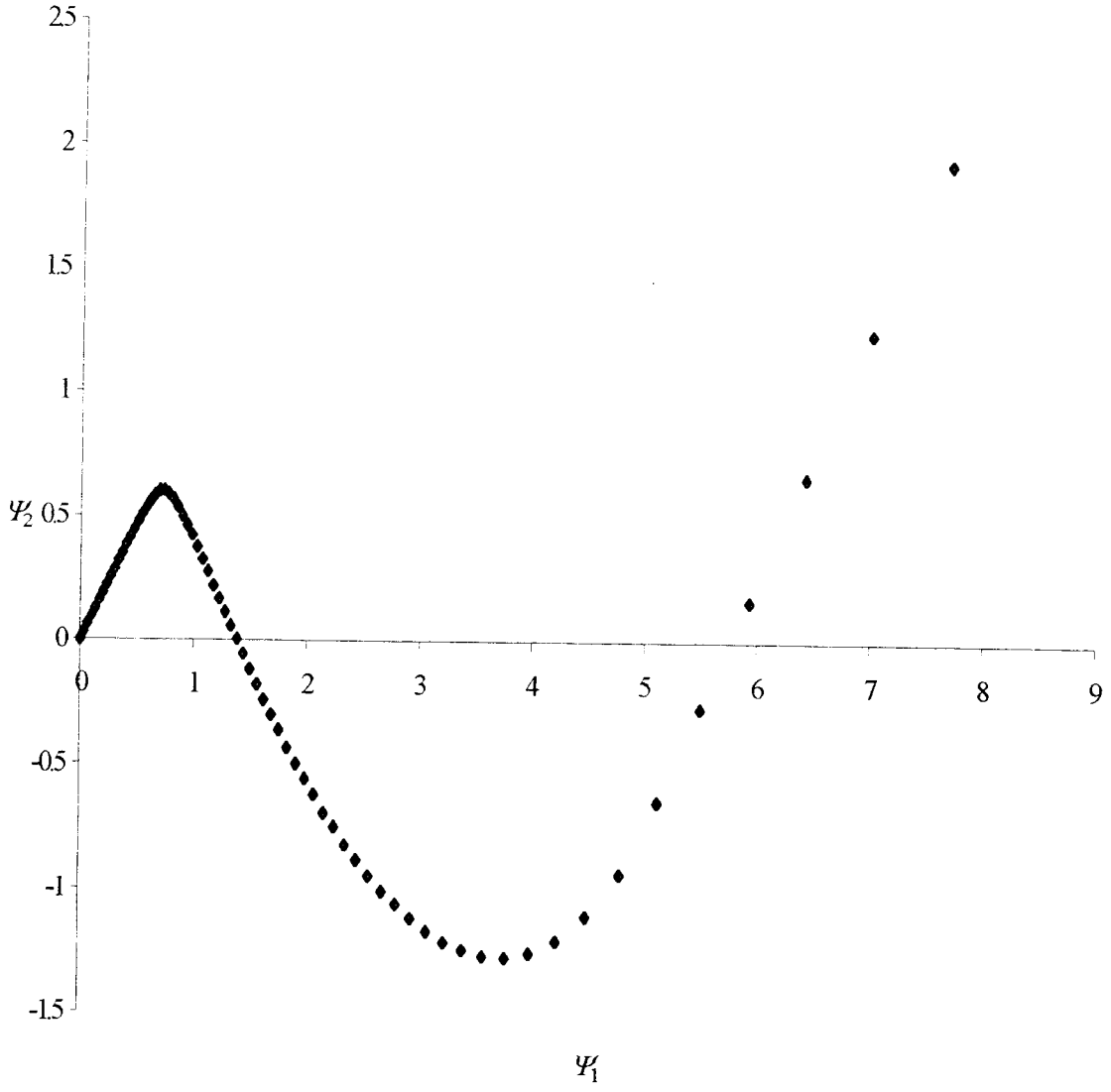

Figure 5.14 Non-dimensional angle of reflection Ψ_2 and angle of incidence Ψ_1 for the sphere with Poisson's ratio 0.3

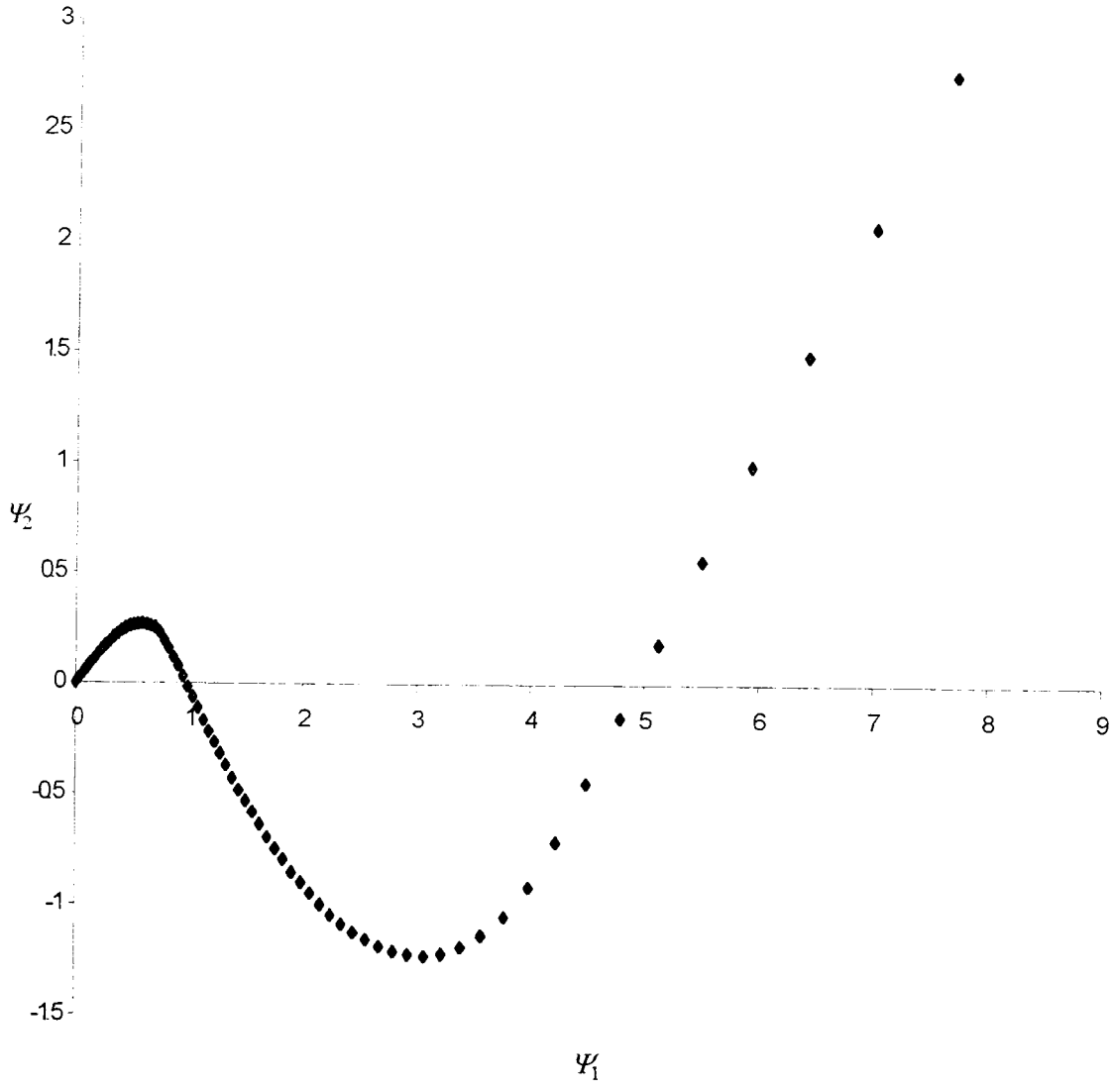

Figure 5.15 Rebound prediction for the solid disc

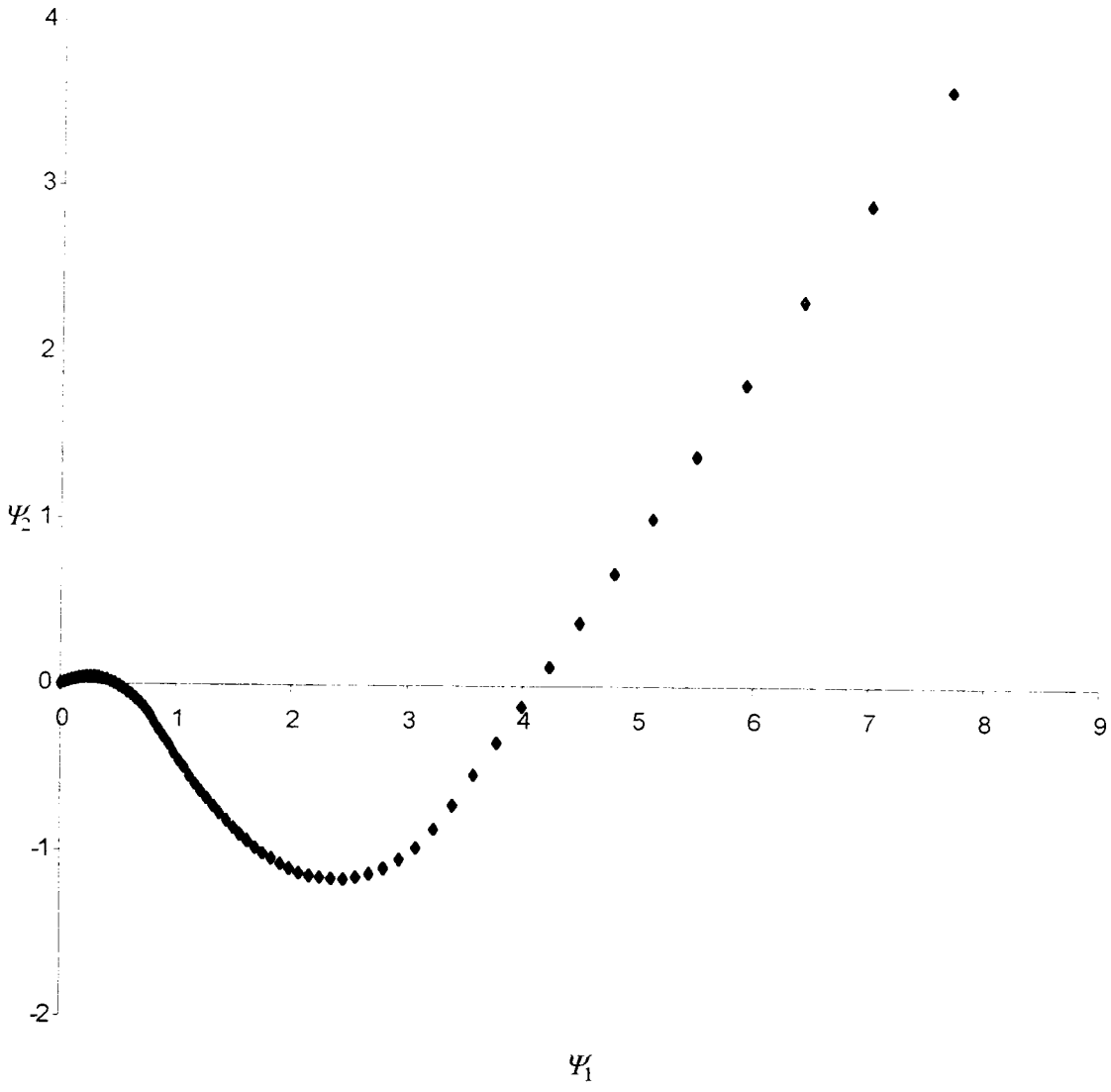

Figure 5.16 Rebound prediction for the shell

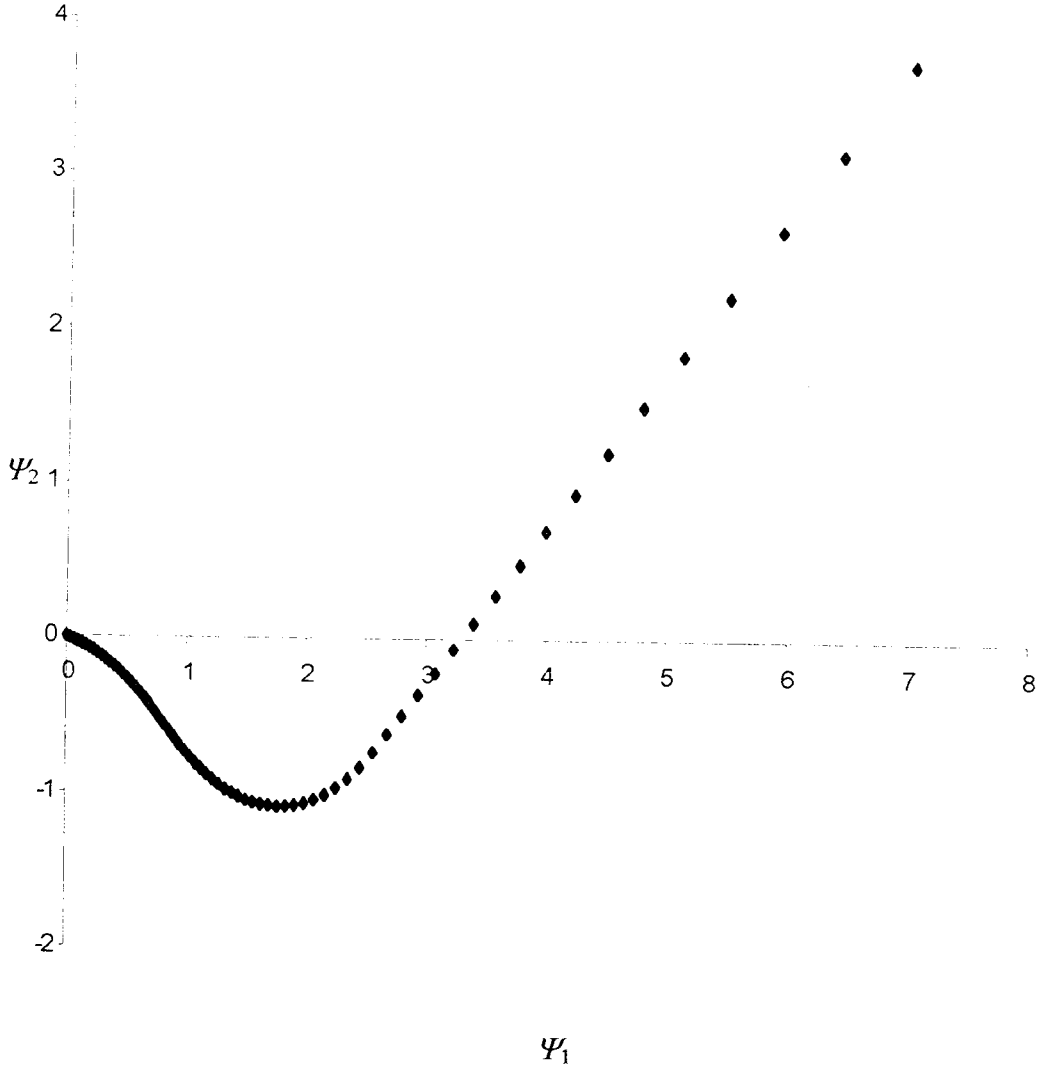

Figure 5.17 Rebound prediction for the hoop

5.4 Coefficient of Restitution and the Kinetic Energy Loss

The duration of impact is separated into a compression phase and a restitution phase. The duration from first contact to the instant at which the normal component of the relative velocity reaches zero is called the compression phase. The restitution phase follows the compression phase and terminates at the end of contact. In this definition, the motions of $\boldsymbol{P}$ and $\boldsymbol{P}'$ are understood to belong to rigid bodies $\boldsymbol{B}$ and $\boldsymbol{B}'$, even though it is recognized that deformation is necessary to preclude penetration. Thus, the instant that separates the compression and restitution phases is that at which maximum penetration (even in the rigid-body idealization) is reached. The three definitions for the coefficient of restitution are considered as follows:

The first definition is given as

$$c = \frac{g_{nr}}{g_{nc}}, \tag{5.68}$$

where g_{nc} is the normal component of impulse $\boldsymbol{g}$ accumulated during the compression phase and g_{nr} is that accumulated during the restitution phase,

The second definition is given as

$$e = \frac{\boldsymbol{n}\cdot\boldsymbol{w}}{-\boldsymbol{n}\cdot\boldsymbol{v}}, \tag{5.69}$$

where $\boldsymbol{v}$ and $\boldsymbol{w}$ are the relative velocities at the beginning of contact and at the end of contact, respectively.

The inertia operator $\boldsymbol{N}$ plays an important role in the work done by the contact force at $\boldsymbol{P}$ and $\boldsymbol{P}'$. The force exerted on $\boldsymbol{B}$ by $\boldsymbol{B}'$ at $\boldsymbol{P}$ denoted $\boldsymbol{f}$, the sum of the works of this force at any time may be expressed as

$$
\begin{aligned}
W &= \int \boldsymbol{f} \cdot d\boldsymbol{u} \\
&= \int \bar{\boldsymbol{v}} \cdot \boldsymbol{f}\, dt \\
&= \int \bar{\boldsymbol{v}} \cdot d\boldsymbol{g} \\
&= \int \left(\boldsymbol{v} + \boldsymbol{g} \cdot \boldsymbol{N}\right) \cdot d\boldsymbol{g} \\
&= \boldsymbol{v} \cdot \boldsymbol{g} + \frac{1}{2} \boldsymbol{g} \cdot \boldsymbol{N} \cdot \boldsymbol{g} \\
&= \left[\boldsymbol{v} + \frac{1}{2}\left(\bar{\boldsymbol{v}} - \boldsymbol{v}\right)\right] \cdot \boldsymbol{g} \\
&= \frac{\boldsymbol{v} + \bar{\boldsymbol{v}}}{2} \cdot \boldsymbol{g}
\end{aligned}
\tag{5.70}
$$

in agreement with equation (3.24). An alternative expression for the change in kinetic energy at any time is equation (3.25), which can be written with the help of equation (3.20) as

$$
\Delta K = \frac{1}{2}\left(\bar{\boldsymbol{v}} \cdot \boldsymbol{N}^{-1} \cdot \bar{\boldsymbol{v}} - \boldsymbol{v} \cdot \boldsymbol{N}^{-1} \cdot \boldsymbol{v}\right). \tag{5.71}
$$

Because $\boldsymbol{x} \cdot \boldsymbol{N}^{-1} \cdot \boldsymbol{x}$ is a positive definite function of $\boldsymbol{x}$, this indicates that the greatest possible loss of kinetic energy during contact would occur if $\bar{\boldsymbol{v}} = 0$ (i.e., if the point $\boldsymbol{P}$ and $\boldsymbol{P}'$ have the same velocity). For planar collisions the maximum possible loss in kinetic energy could be expressed in terms of the parameters as

$$
\left|\Delta K\right|_{\max} = \frac{1}{2} \boldsymbol{v} \cdot \boldsymbol{N}^{-1} \cdot \boldsymbol{v} \tag{5.72}
$$

and for planar collisions it can be expressed in terms of parameters.

$$
\left|\Delta K\right|_{\max} = \frac{\left[1 + \lambda \cos 2(\alpha - \theta)\right] m v^2}{2\left(1 - \lambda^2\right)} \tag{5.73}
$$

Recently, a third coefficient of restitution was introduced by Stronge (1990) as

$$
d = \sqrt{\frac{W_{nr}}{-W_{nc}}}, \tag{5.74}
$$

where W_{nc} and W_{nr} are the sums of the work done by the normal components of the reaction forces at the contact point during the compression phase and during the restitution phase, respectively. Displacements in the definition of work used here must be understood to be those of points of "rigid" bodies (which would imply and artificial penetration, as mentioned above).

From equation (5.70) the normal component of work done by the contact force then becomes

$$W_n = \int \bar{v}_n \cdot dg_n \tag{5.75}$$

during the compression and restitution phases, respectively.

Although the coefficient of the restitution, e, is often considered as a material property, from Figure 5.18, we can see the coefficient of restitution is affected by the angle of the incidence. From Figure 5.19, we can see the influence of the coefficient of friction on the coefficient of restitution. The larger the coefficient of friction is, the more the coefficient of restitution changes. From Figure 5.20, we can also see that both the angle of incidence and the coefficient of friction affect the kinetic energy loss of the oblique impact of a solid sphere. For a given angle of incidence, the larger the coefficient of friction, the more the kinetic energy loss.

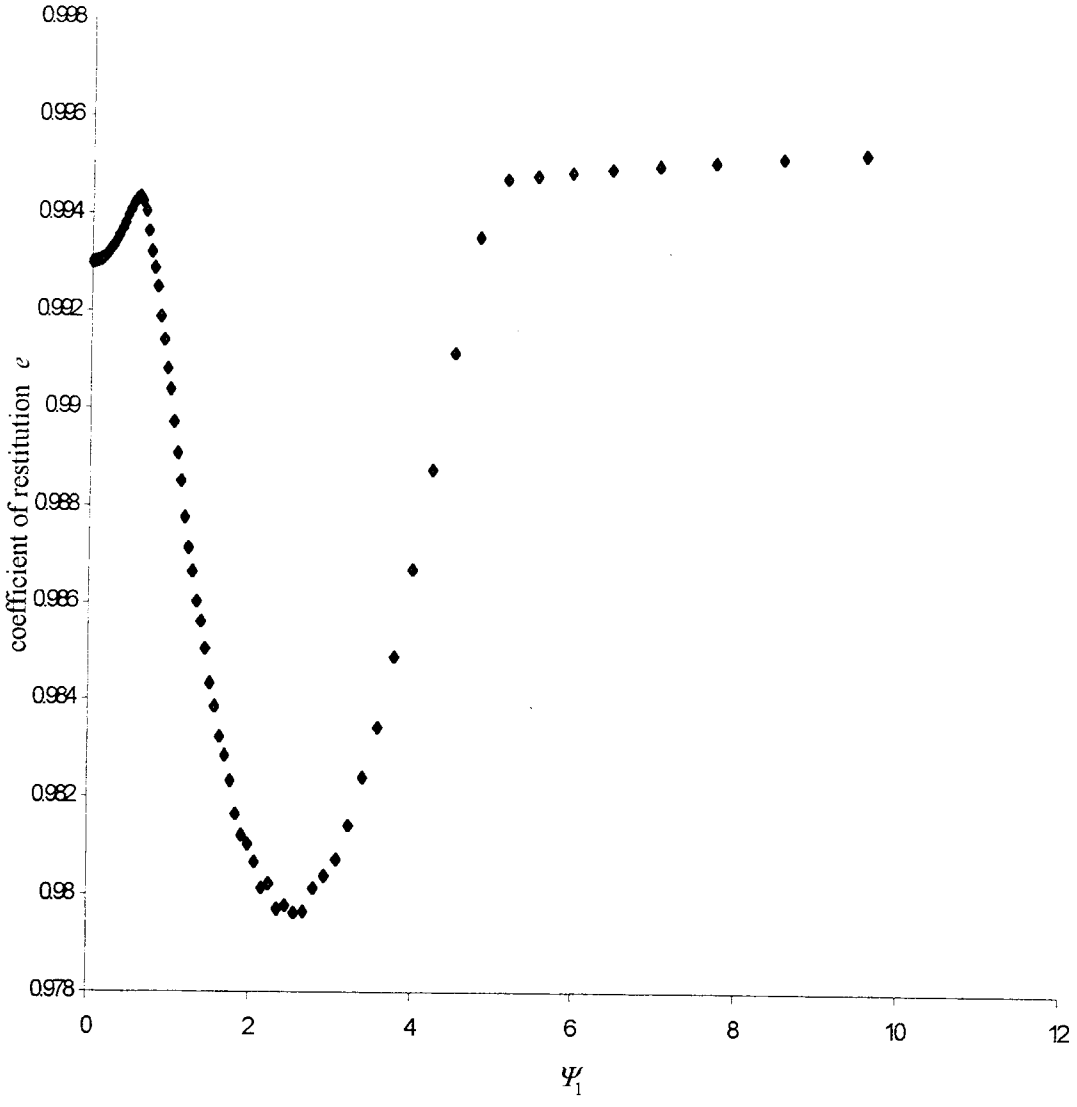

Figure 5.18 Coefficient of restitution for different angles of incidence

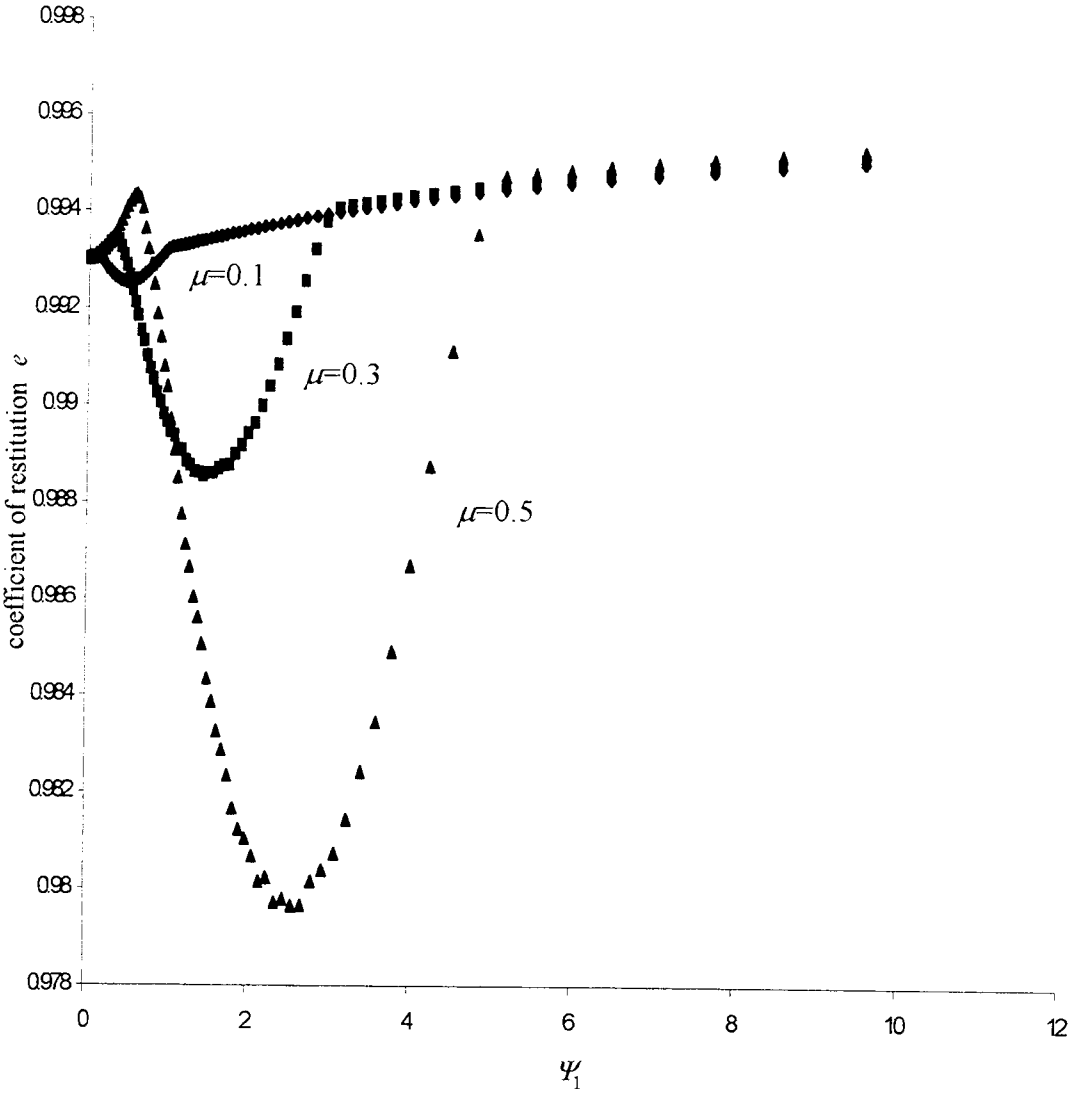

Figure 5.19 Coefficient of restitution with different coefficient of friction for different angles of incident

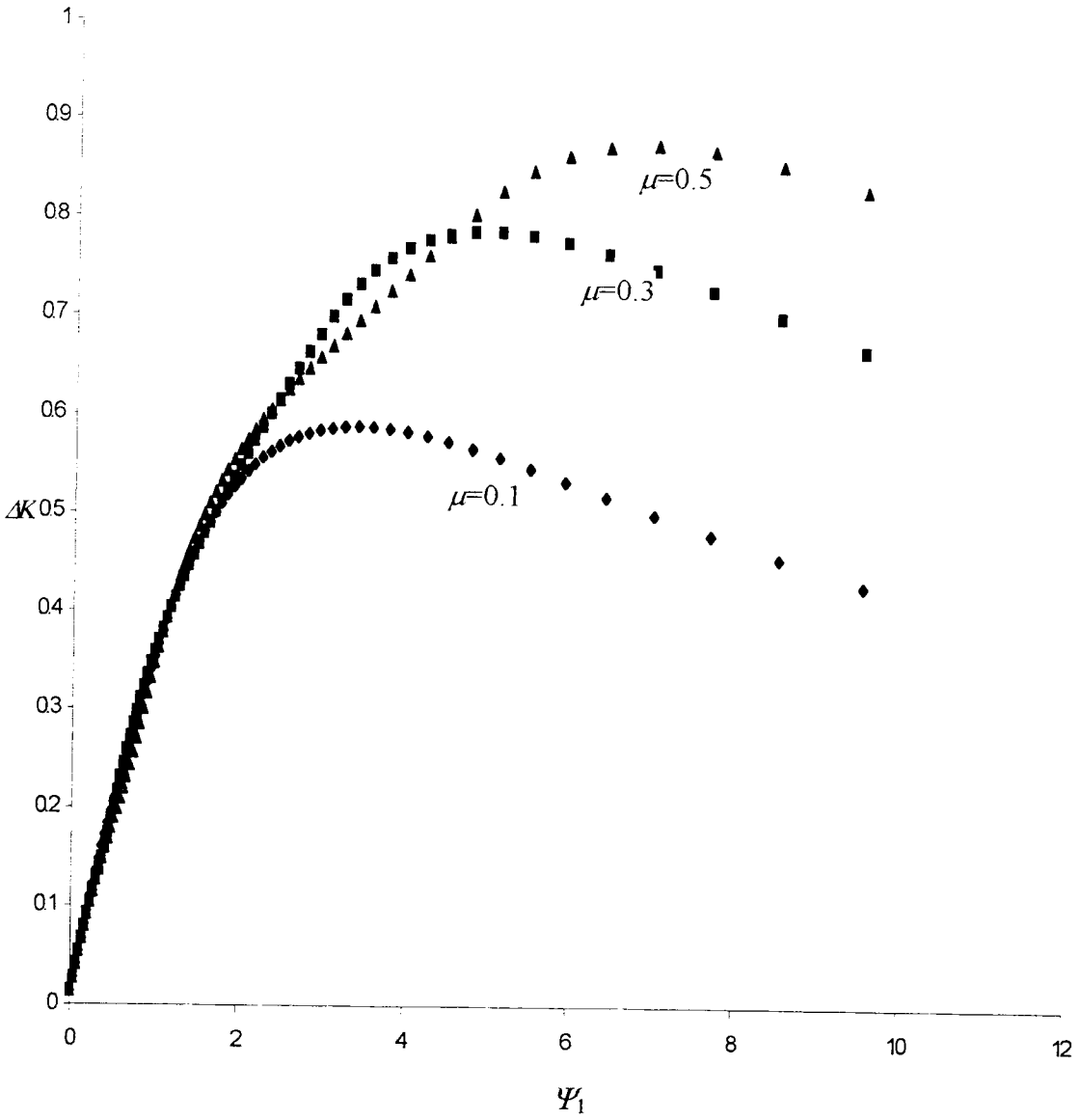

Figure 5.20 Kinetic energy loss with different coefficient of friction for different angles of incidence

5.5 Systems with Tangential-Normal Inertia Coupling

Considering a special case shown in Figure 5.21, the rod of uniform density has a circular cylindrical portion with hemispherical ends and collides against a flat plane. In terms of the dimensions given as the Figure 3.2, the quantities used here are

$$b^2 = \frac{L^2}{4} + LR\cos\phi + R^2 \tag{5.76}$$

$$k_3^{\,2} = \frac{\frac{8}{15}R^3 + \frac{3}{4}R^2L + \frac{1}{3}RL^2 + \frac{1}{12}L^3}{\frac{4}{3}R + L} \tag{5.77}$$

$$\phi = \theta + \sin^{-1}\left(\frac{R\sin\theta}{L/2}\right) \tag{5.78}$$

The above three equations show that the configuration parameter

$$\lambda = \left(1 + \frac{2k_3^{\,2}}{b^2}\right)^{-1} \tag{5.79}$$

is a function of L/R and ϕ. For comparison, all dimensions and material constant are taken to be the same as in the previous research of Liu (1991), where $L/R = 5.0$, and the Poisson's ratio ν= 0.28. Four cases are presented in Figure 5.22, Figure 5.26, Figure 5.30 and Figure 5.34 and the relative parameters for these cases are shown on Table 5.2.

case	a	b	c	d
μ	0.5	1.0	0.5	1.0
λ	0.63922	0.63252	0.61240	0.61573
θ	0.27018	0.38956	-0.62204	-0.59062
$\tan\alpha$	1.54900	9.53159	1.07757	1.35013

Table 5.2 The parameters used in the rod impact cases

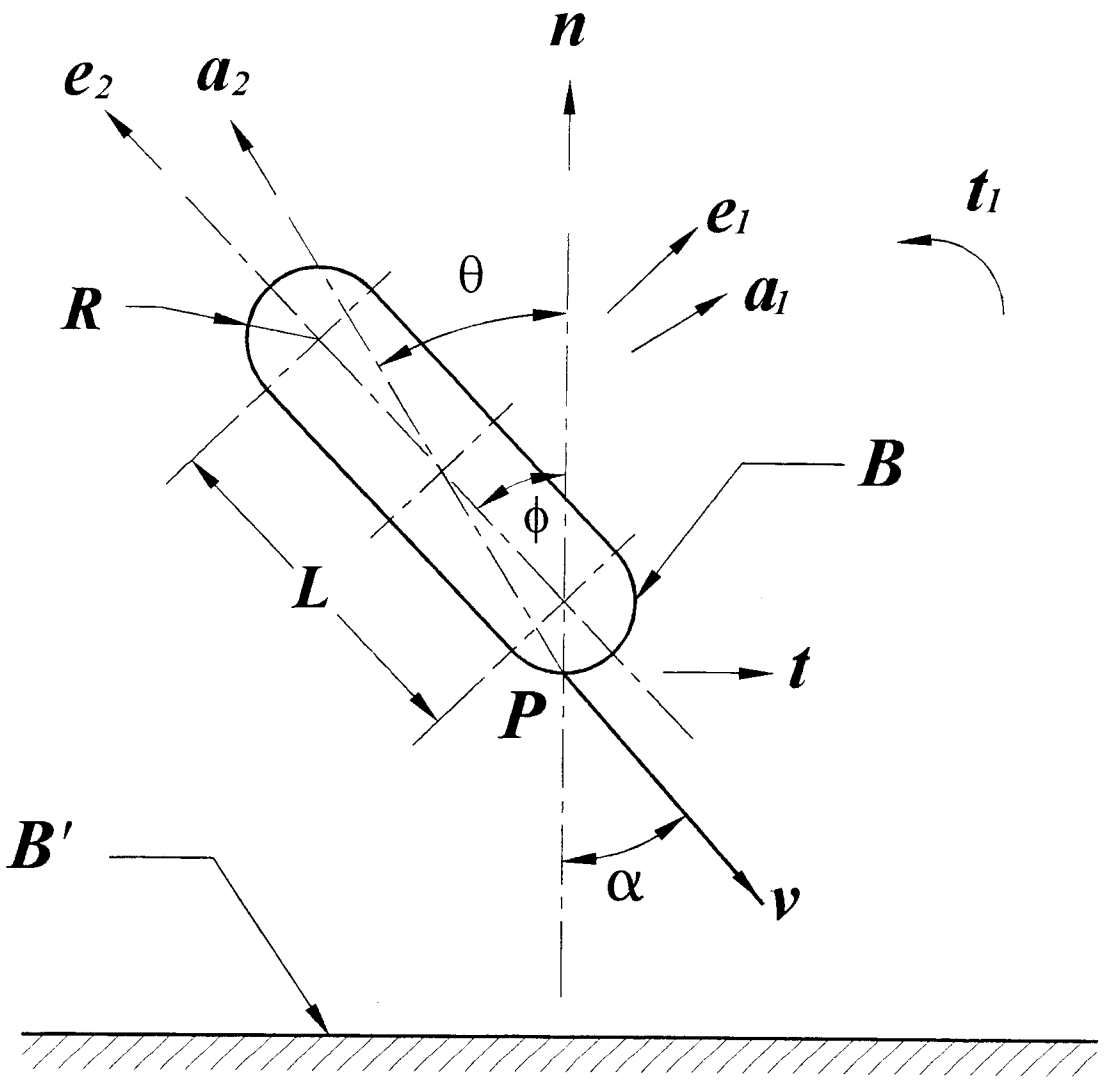

Figure 5.21 Collision between a cylindrical rod and a flat plane

In order to compare with previous research, the variation of the normal impulse and the tangential impulse for four cases are shown in Figure 5.23, Figure 5.27, Figure 5.31, and Figure 5.35, which are very close to the results of ANSYS finite element code by Liu (1991). In Figure 5.24, Figure 5.28, Figure 5.32 and Figure 5.36, the variation between the normal velocity and the normal impulse show quite linear. The relationship of the normal displacement and the tangential displacement are shown in Figure 5.25, Figure 5.29, Figure 5.33, and Figure 5.37, which are very close to previous research.

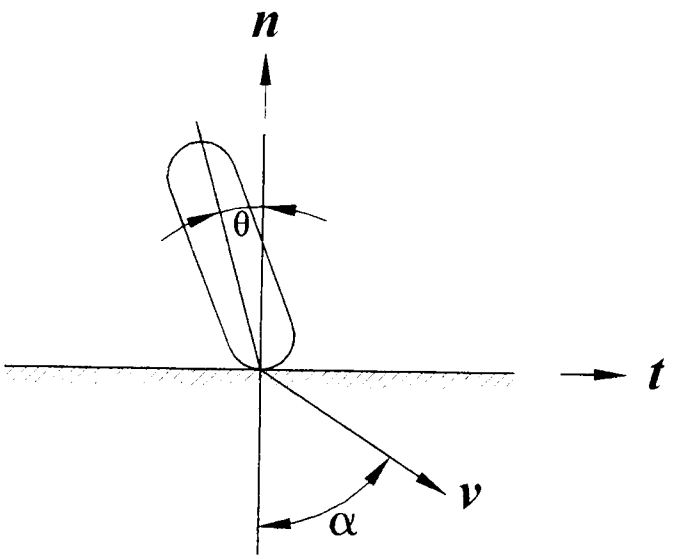

Figure 5.22 The rod impact of case a ($\theta = 0.27018$, $\tan\alpha = 1.549$)

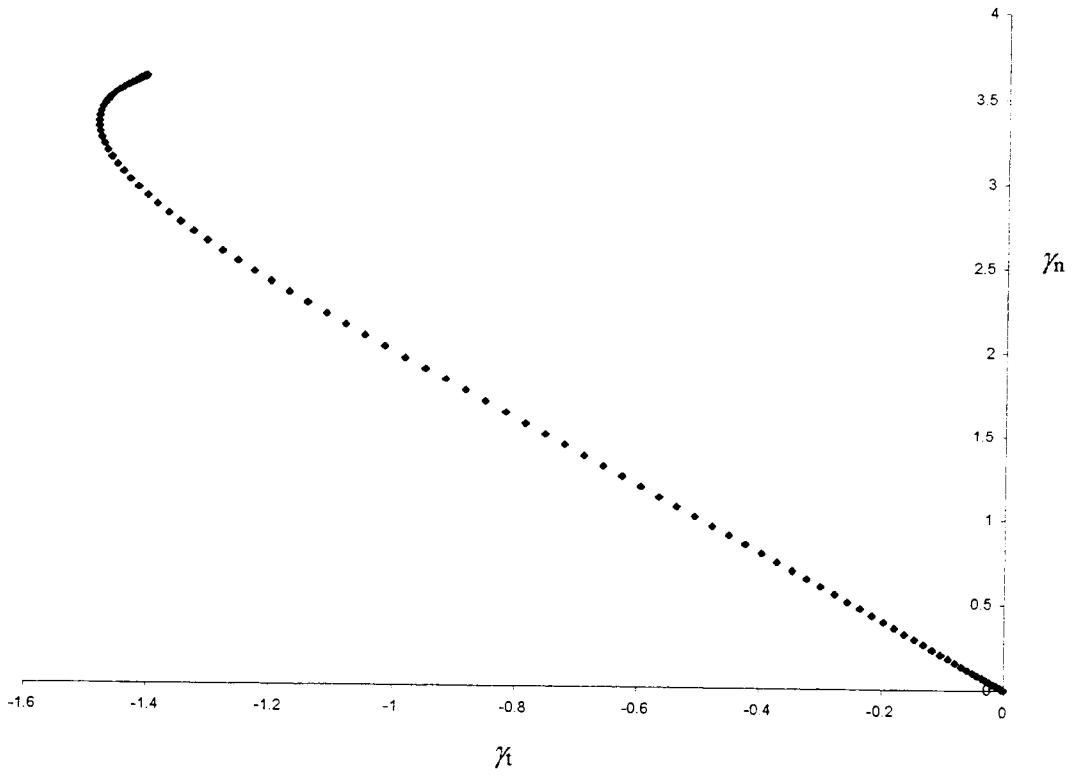

Figure 5.23 The normal impulse and the tangential impulse of the rod impact for case a

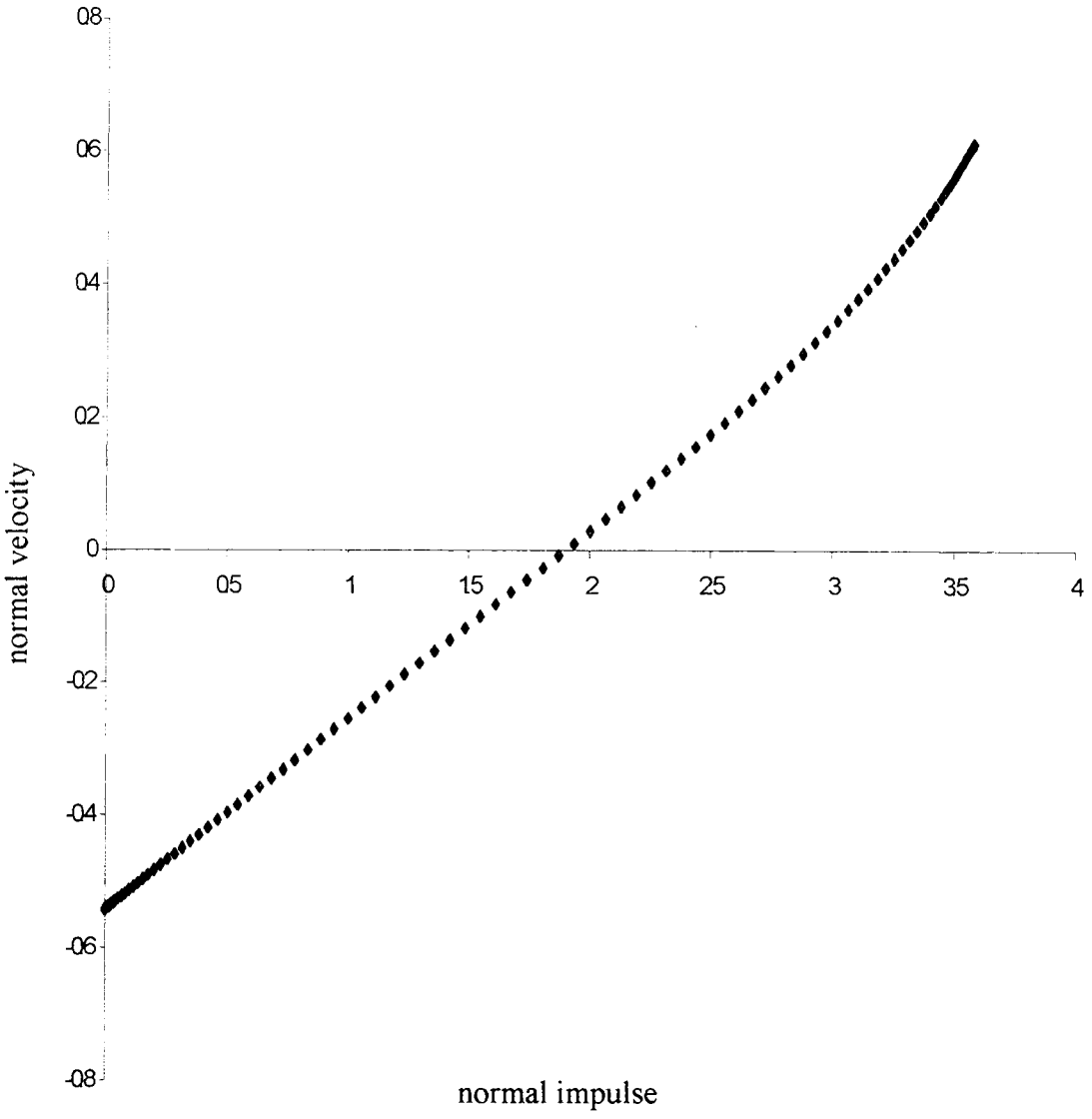

Figure 5.24 The normal velocity and the normal impulse of the rod impact for case a

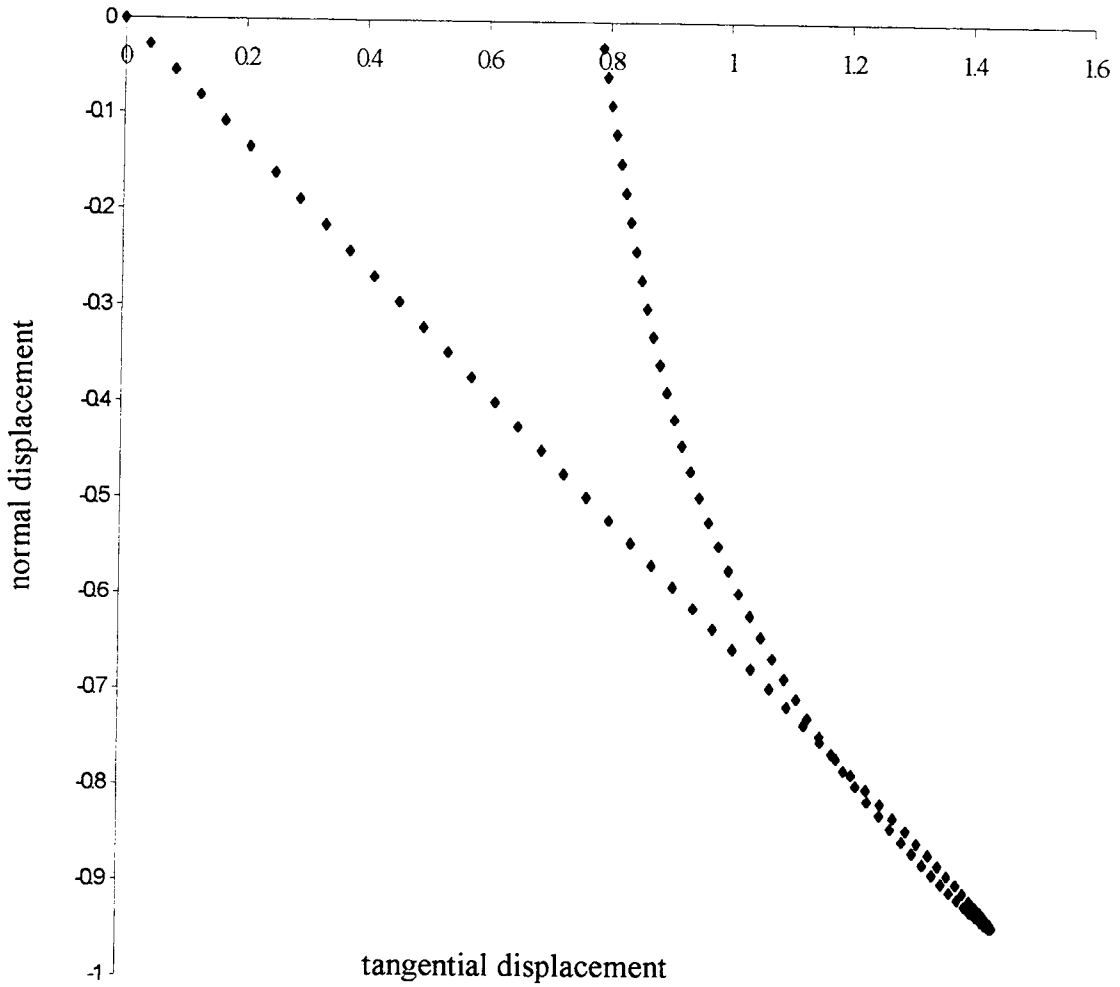

Figure 5.25 The normal displacement and the tangential displacement for case a

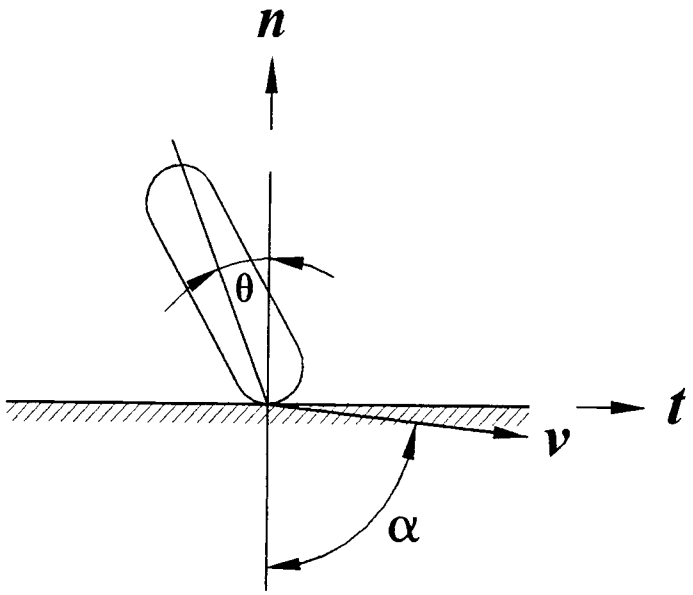

Figure 5.26 The rod impact of case b ($\theta = 0.38956$, $\tan\alpha = 9.53159$)

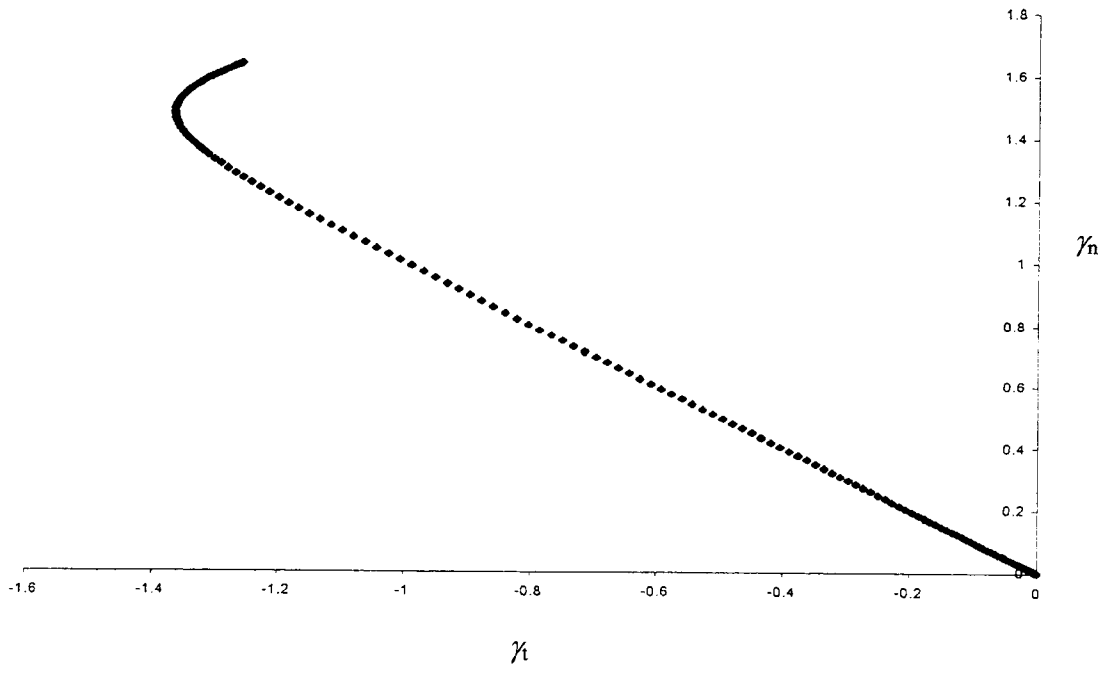

Figure 5.27 The normal impulse and the tangential impulse of the rod impact for case b

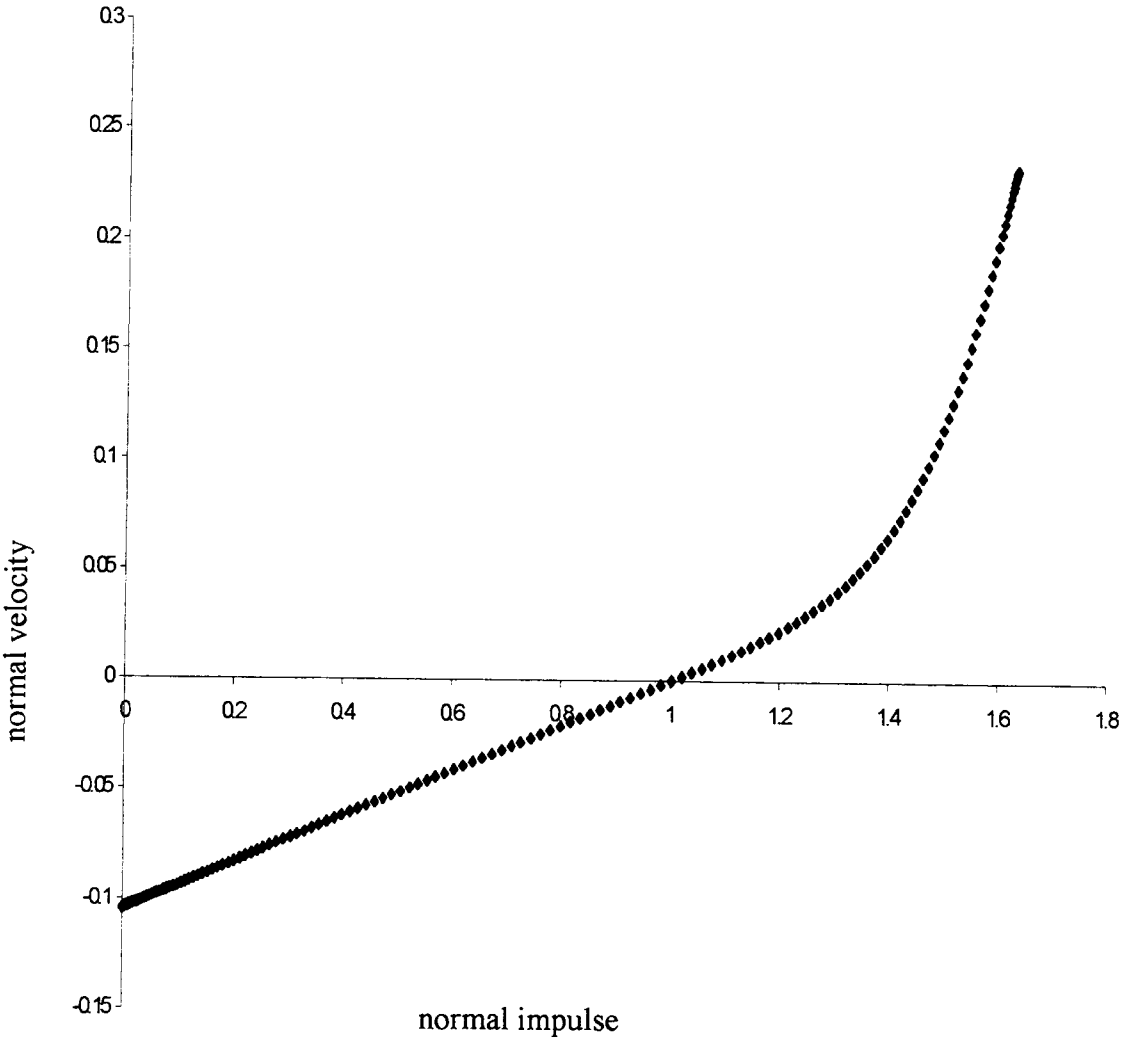

Figure 5.28 The normal velocity and the normal impulse of the rod impact for case b

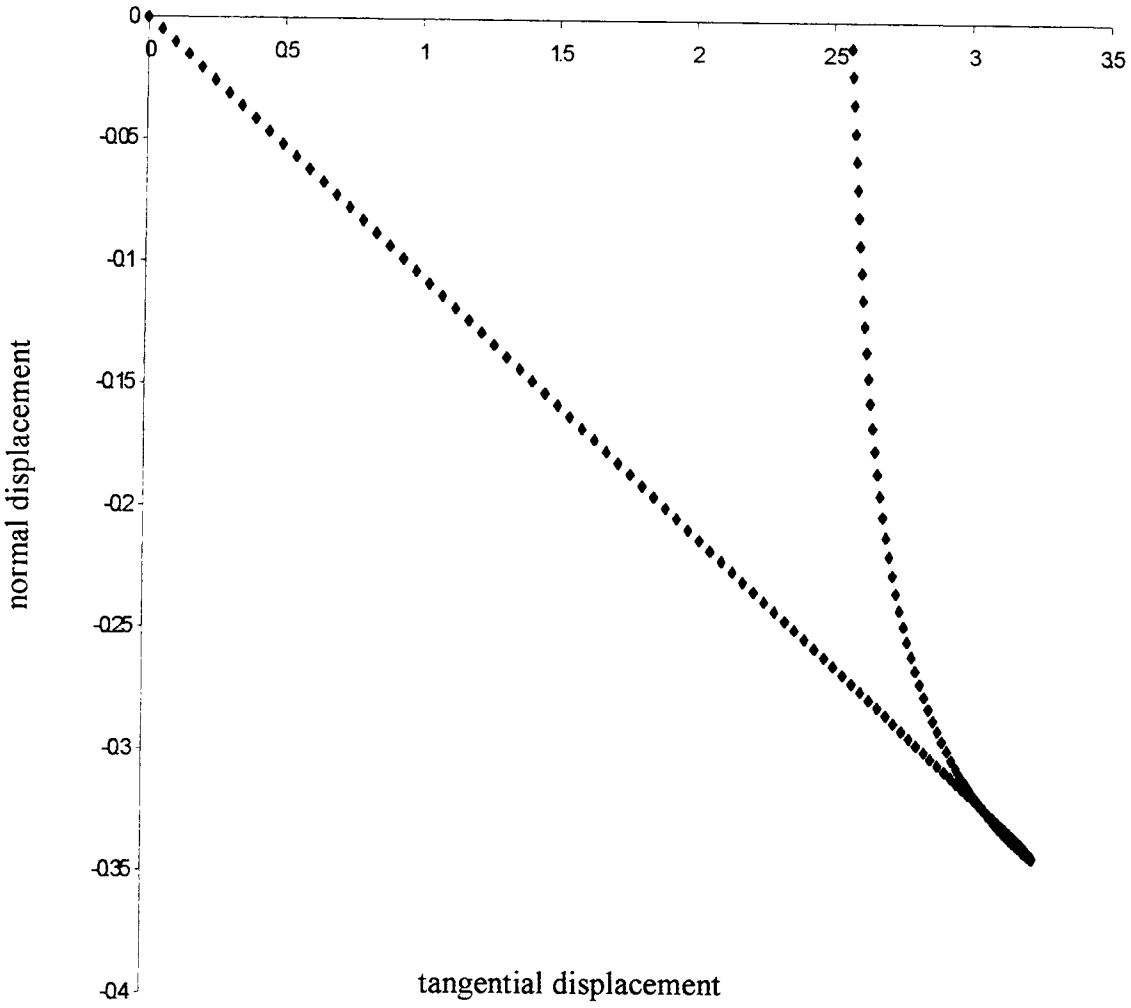

Figure 5.29 The normal displacement and tangential displacement for case b

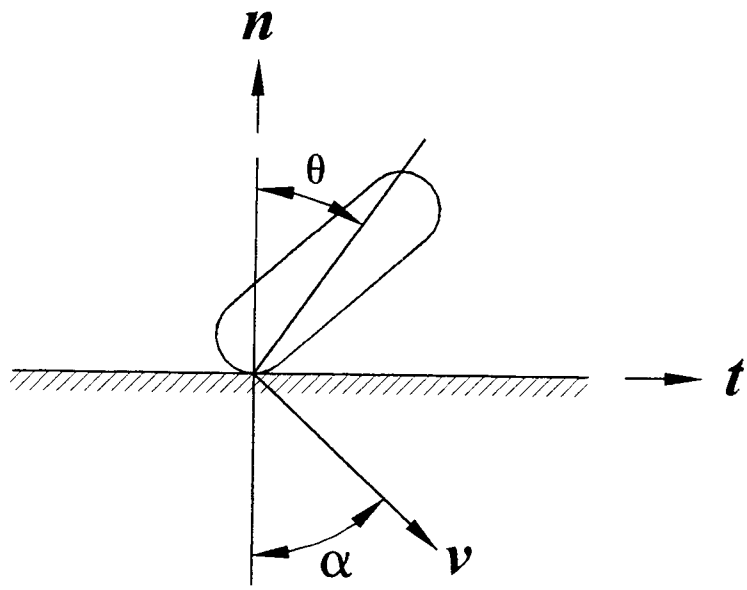

Figure 5.30 The rod impact of case c ($\theta = -0.62204$, $\tan\alpha = 1.07757$)

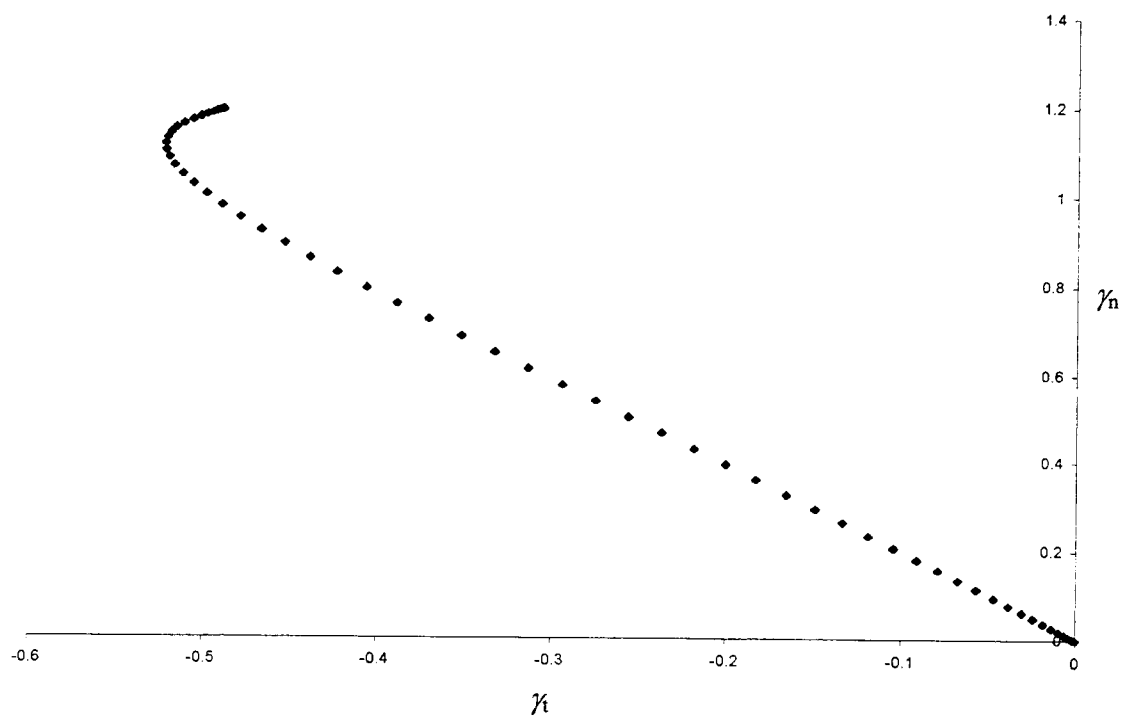

Figure 5.31 The normal impulse and tangential impulse of the rod impact for case c

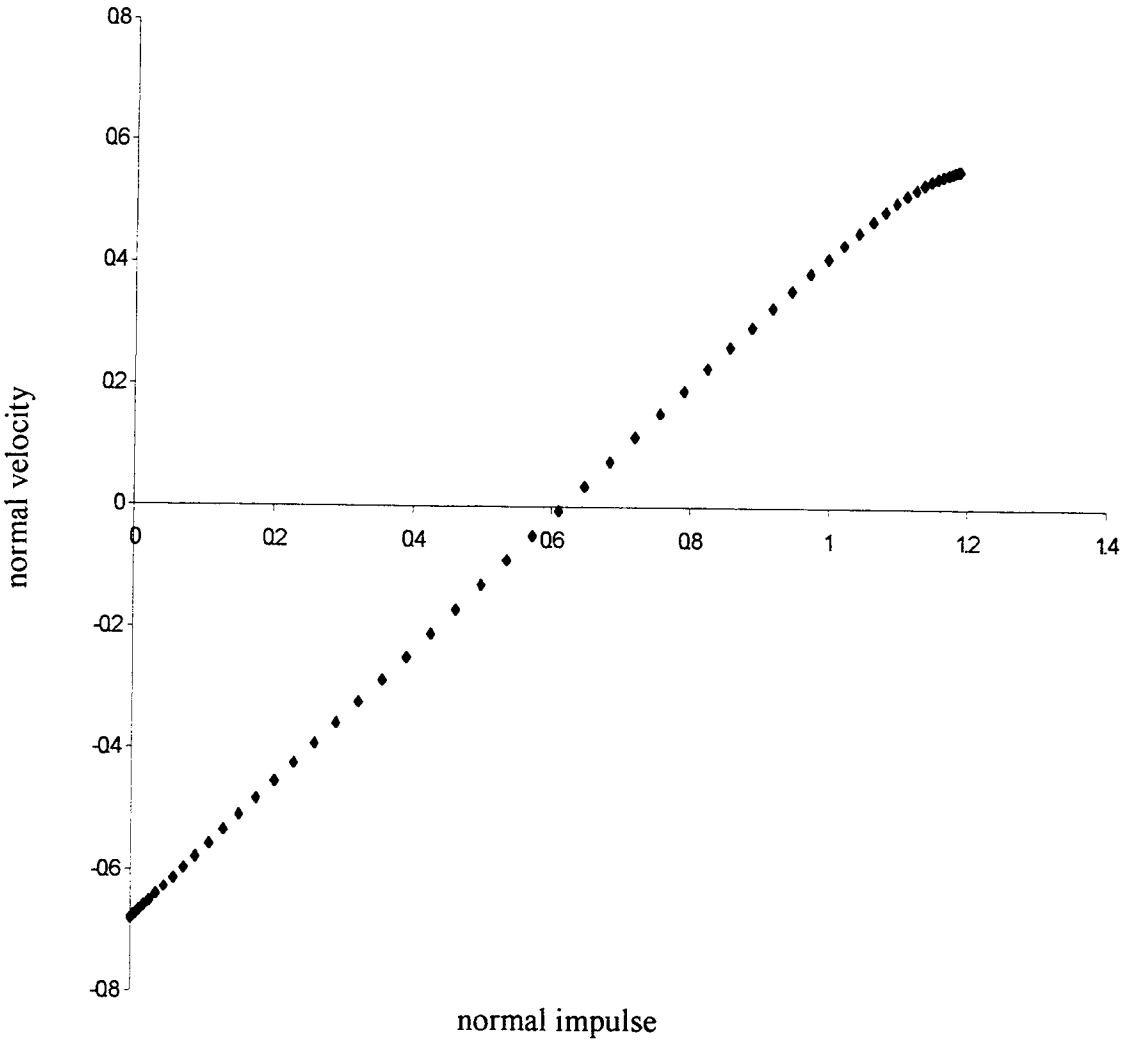

Figure 5.32 The normal velocity and the normal impulse of the rod impact for case c

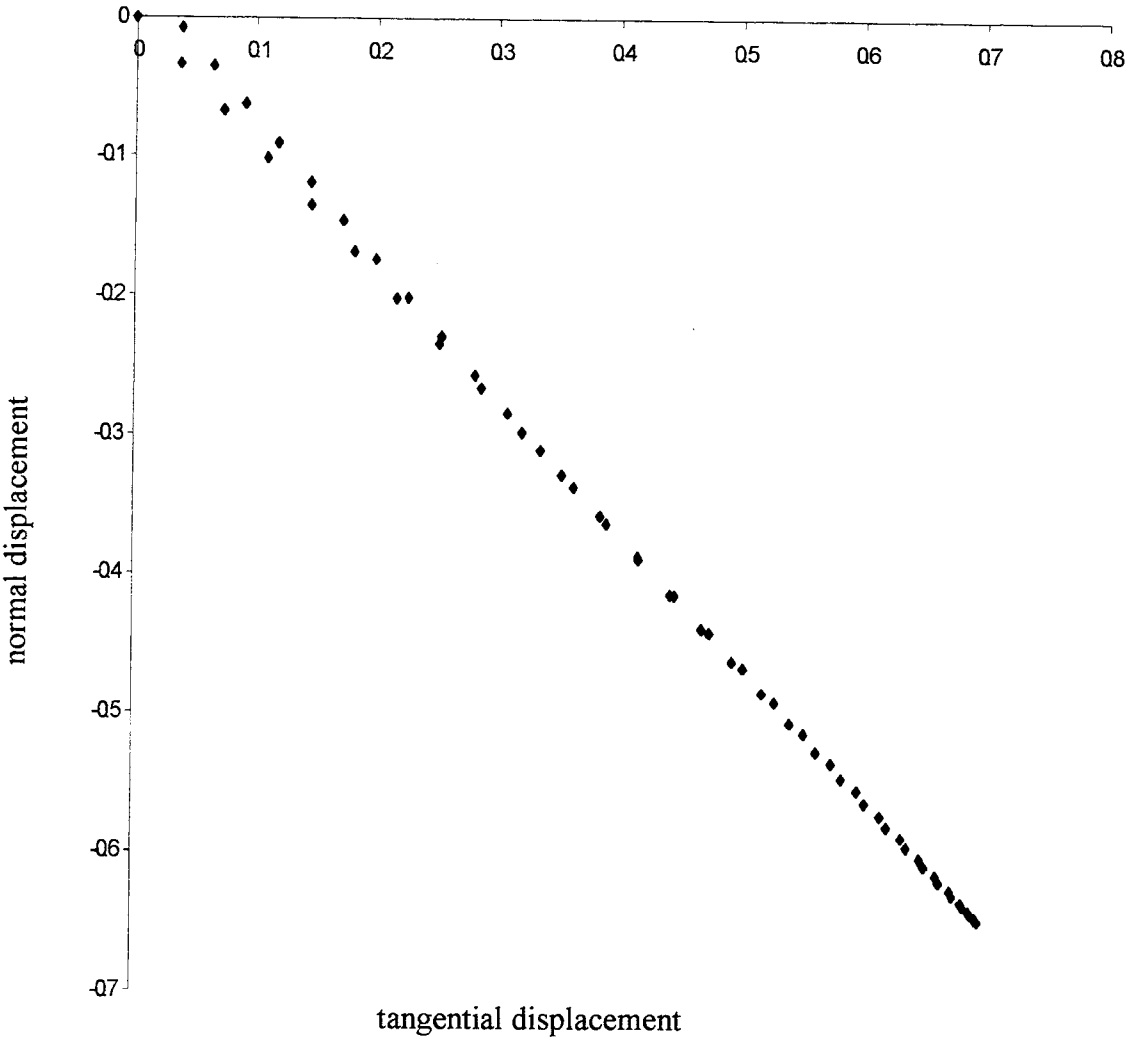

Figure 5.33 The normal displacement and the tangential displacement for case c

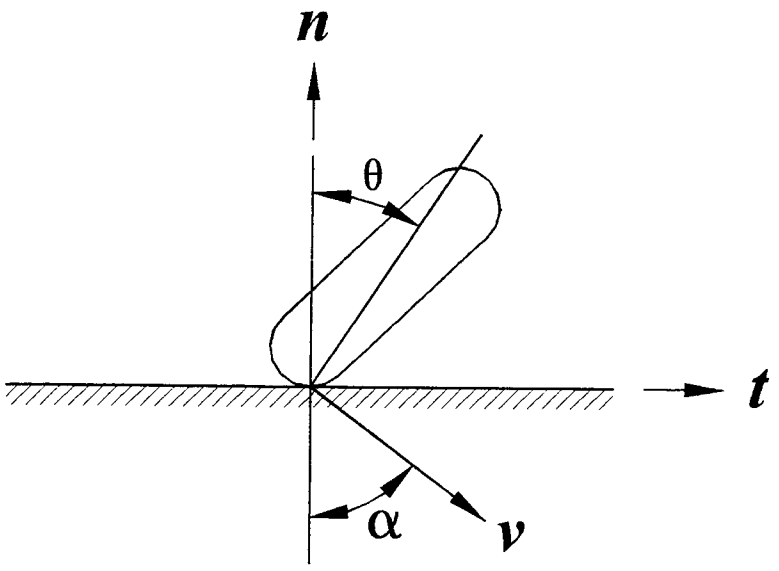

Figure 5.34 The rod impact of case d (θ = -0.59062, tanα = 1.35013)

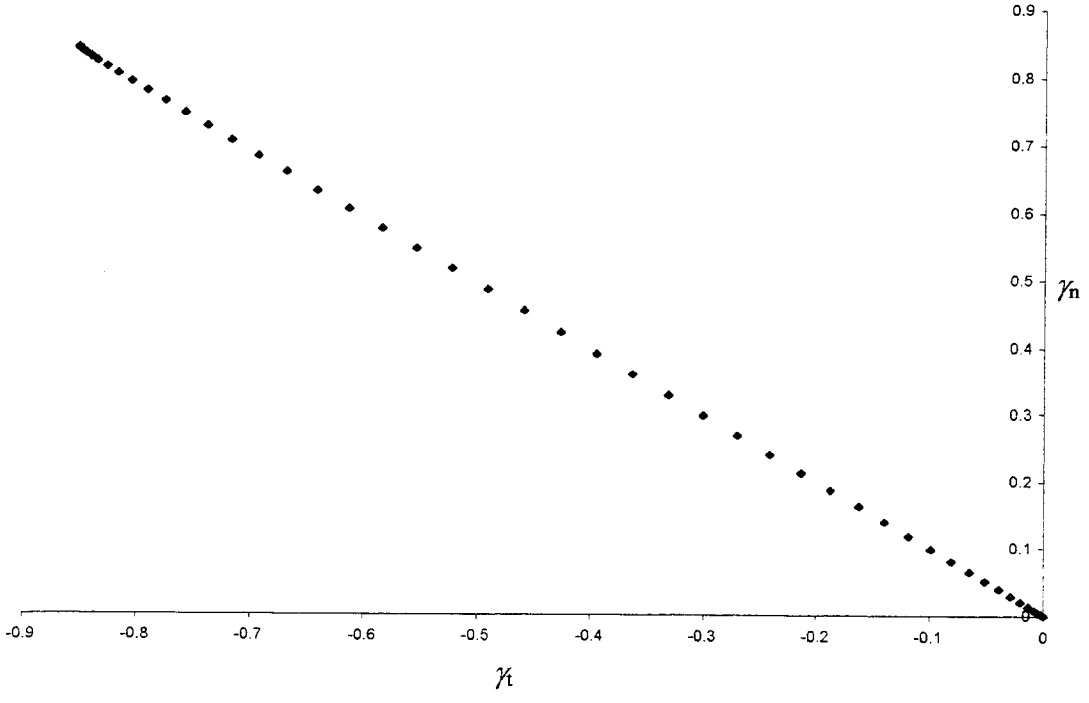

Figure 5.35 The normal impulse and the tangential impulse of the rod impact for case d

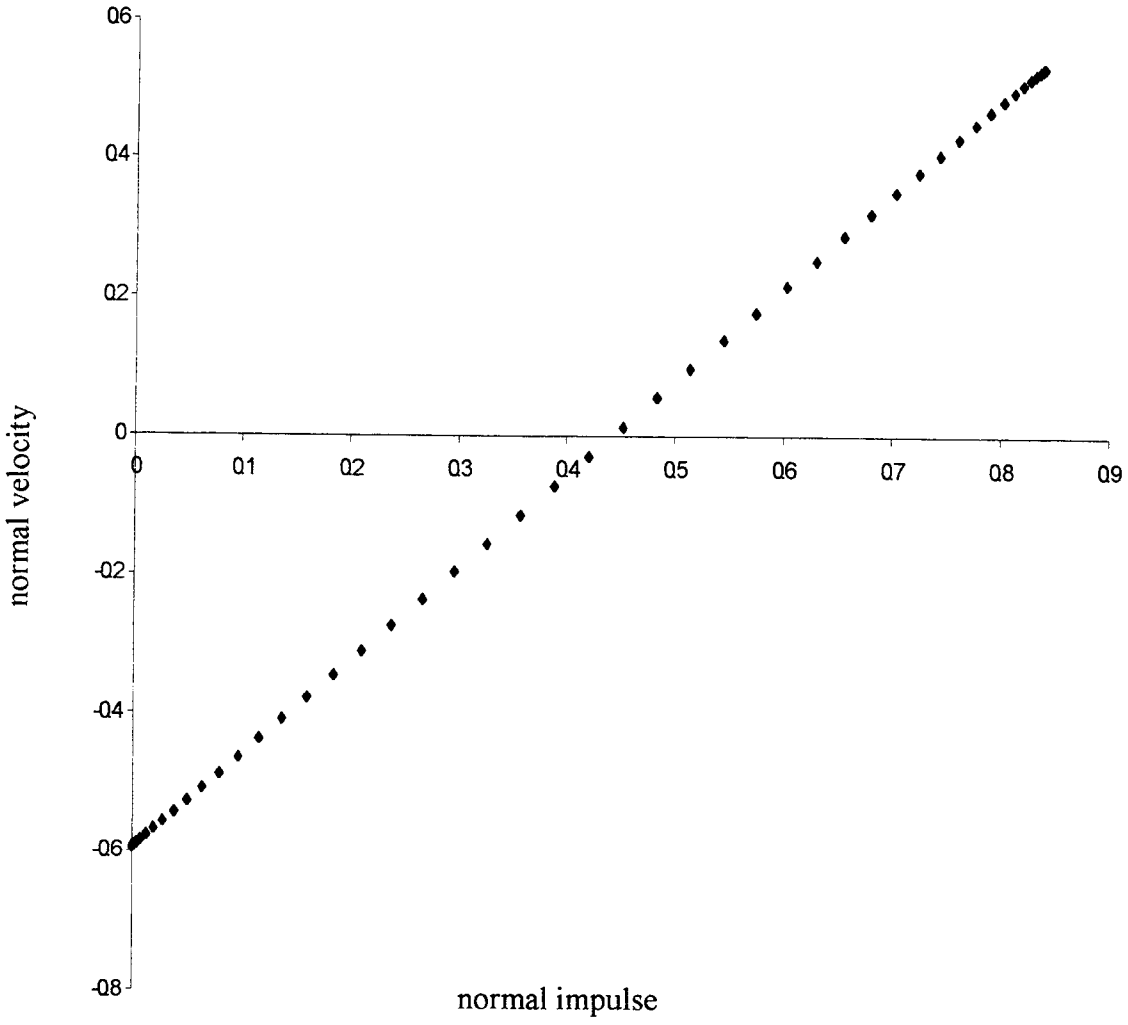

Figure 5.36 The normal velocity and the normal impulse of the rod impact for case d

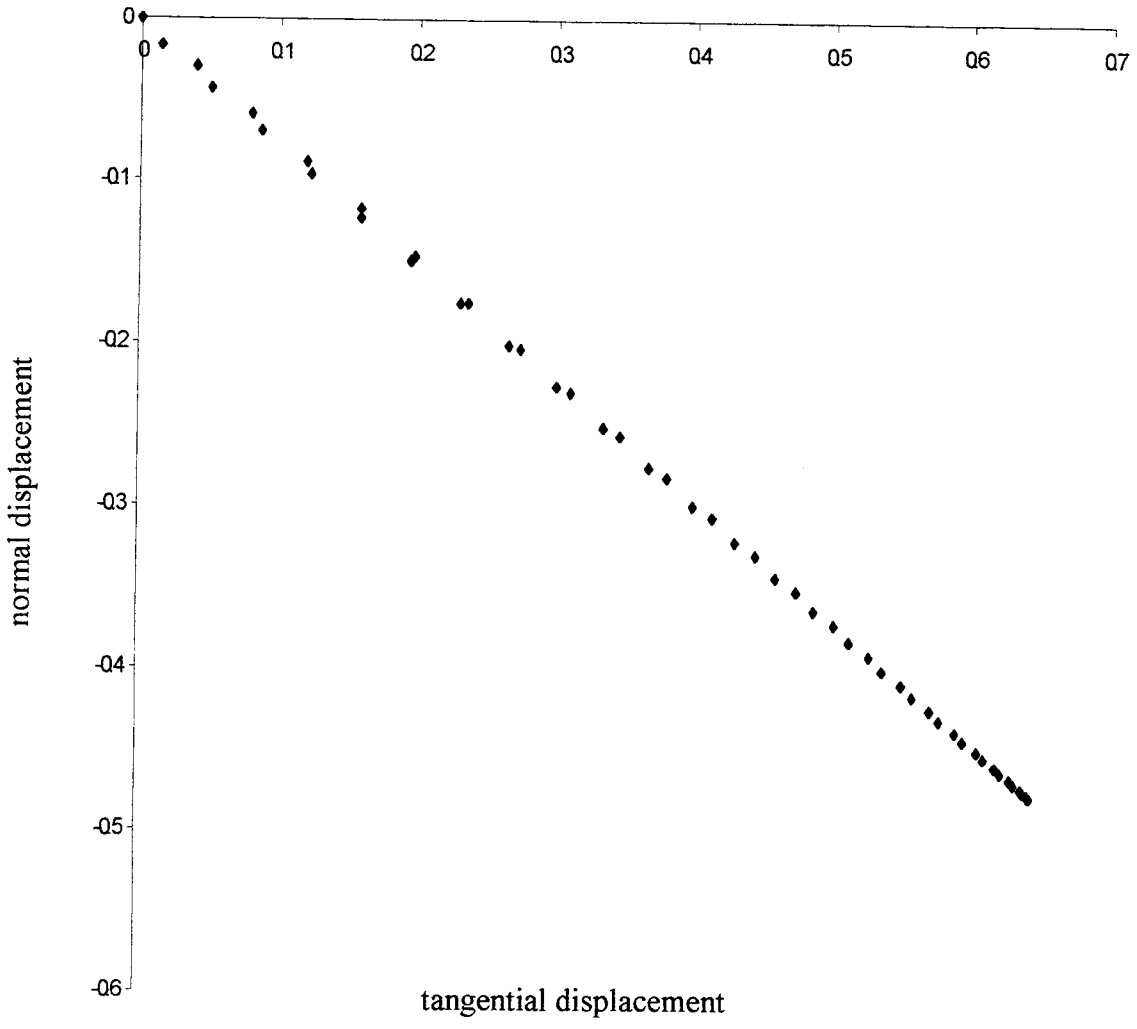

Figure 5.37 The normal displacement and the tangential displacement for case d

6. COLLISION PREDICITON SIMULATED BY DYNA3D

Finite element codes have been used to predict the collision of the two rigid bodies. Liu (1991) uses the ANSYS code developed by Swanson Analysis System, Inc. to analyze the post-collision of two rigid bodies. Although predictions from a finite element method which include wave propagation are closer to the real system than simplified prediction procedures based on rigid body mechanics, they sometimes are unstable under certain circumstances. Furthermore, the increase in computational load required for the use of this method is significant.

In this investigation the post-collision of two rigid bodies was predicted by using the DYNA3D (Hallquist, 1983) (Whirley, 1993) finite element code developed by the Lawrence-Livermore National Laboratory (LLNL). The introduction of DYNA3D is represented in this chapter. The example of the oblique impact of solid sphere is discussed in the following from results using the DYNA3D finite element code.

6.1 The DYNA3D Finite Element Code

DYNA3D is a nonlinear, explicit, finite element code for analyzing the transient dynamic response of three-dimensional solids and structures. The element formulations available include one-dimensional truss and beam elements, two-dimensional quadrilateral and triangular shell elements, and three-dimensional continuum elements. Many material models are available to represent a wide range of material behavior, including elasticity, plasticity, composites, thermal effects, and rate dependence.

In addition, DYNA3D has a sophisticated contact interface capability, including frictional sliding and single surface contact, to handle arbitrary mechanical interactions between independent bodies or between two portions of one body.

DYNA3D does not contain any significant model generation capability, and relies totally on external software for this task. The LLNL mesh generator, INGRID, (Hallquist et al., 1990) is widely used at LLNL and provides full support for all DYNA3D analysis options. INGRID is a generalized three-dimensional finite element mesh generator for modeling nonlinear systems. INGRID provides the capability to generate complex geometrical models using beam, shell and hexahedral elements. Similarly, boundary conditions, initial conditions and material properties can be specified for complex regions with a minimum of user input. Interactive graphics in INGRID offer the ability to probe and interrogate mesh structure, boundary conditions, slide surfaces, and radiation enclosures so that valid models can be easily constructed and rapidly verified.

DYNA3D writes up to three binary plot databases. The state data plot file family contains information for complete states at relatively infrequent intervals; 50 to 100 states of data are typical in a state database. The time history data plot file family contains information for only selected nodes and elements, but at much more frequent intervals; 1000 to 10,000 states of data are typical in time history database.

TAURUS (Hallquist and Spelce, 1991), a LLNL code, can be used to visualize results from DYNA3D. TAURUS uses a command-line based user interface with X-Windows graphics for portability. TAURUS can read any of the three binary plot databases produced by DYNA3D and allow plotting of color contours, fringes, deformed shapes, and time histories in an interactive graphics environment.

6.2 The Oblique Impact of Solid Spheres

The example of the oblique impact of a solid sphere discussed in chapter 5 is simulated by DYNA3d finite element code. This model consists of a solid sphere with a diameter of 0.1 m and a half-space surface. The INGRID finite element mesh is shown in Figure 6.1. The distribution of the nodes of the contact area is shown in Figure 6.2, where the node number 1712 is the incident contact node. Although the assumption used in the previous chapter considers that the solid sphere except near contact is modeled as rigid, the DYNA3d finite element code has difficulties to simulate a solid sphere containing both rigid and elastic parts together. Therefore, the simulation of the oblique impact of solid sphere by the DYNA3D finite element code is assumed that every element of the solid sphere is elastic and has identical material properties. The material properties used for the solid sphere are summarized in following,

the Poisson ratio $\nu = 0.3$,

the Young Modulus $E = 7E10\ N/m^2$

the density $\rho = 2700\ kg/m^3$

the coefficient of friction $\mu = 0.1$

the initial normal velocity $v_n = -0.5\ m/s$.

"Center velocity" is evaluated as total momentum divided by total mass, and "angular velocity" is evaluated as total central angular momentum divided by central moment of inertia. Rigid body velocity of the contact point is then

$$\bar{v}_p = \bar{v}_c + \omega \times r_{cp} \tag{6.1}$$

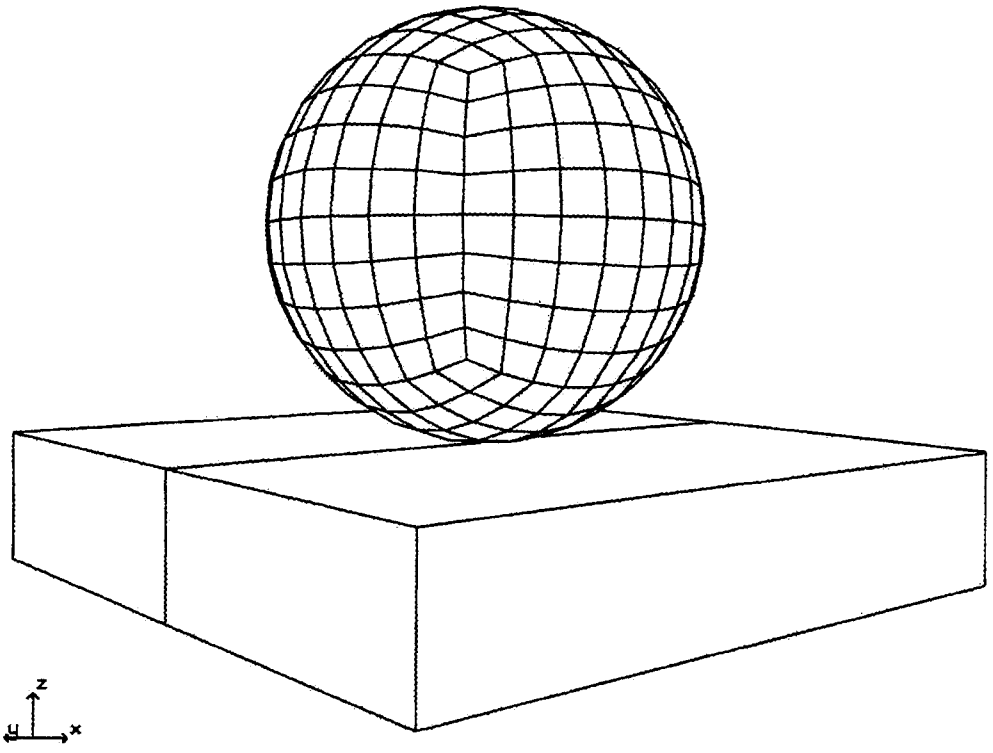

Figure 6.1 Model description of the oblique impact of solid sphere

1467	1509	1551	1593	1635	1677	1929	1971	2013	2055	2097
1474	1516	1558	1600	1642	1684	1936	1978	2020	2062	2104
1481	1523	1565	1607	1649	1691	1943	1985	2027	2069	2111
1488	1530	1572	1614	1656	1698	1950	1992	2034	2076	2118
1495	1537	1579	1621	1663	1705	1957	1999	2041	2083	2125
1502	1544	1586	1628	1670	1712	1964	2006	2048	2090	2132
1719	1754	1789	1824	1859	1894	2139	2174	2209	2244	2279
1725	1761	1796	1831	1866	1901	2146	2181	2216	2251	2286
1733	1768	1803	1838	1873	1908	2153	2188	2223	2258	2293
1740	1775	1810	1845	1880	1915	2160	2195	2230	2265	2300
1747	1782	1817	1852	1887	1922	2167	2202	2237	2272	2307

Figure 6.2 The distribution of nodes on the contact surface of the DYNA3D model

"Rigid body" displacement and acceleration are evaluated by time integration and differentiation. These will be compared with results from simplified model of chapter 5. There are total eight cases are simulated, the relative angle of incidence, Ψ_1, and initial tangential velocity, v_t, are listed in Table 6.1.

Ψ_1	0.5	1.0	2.0	3.0	4.0	5.0	6.0	7.0
v_t	0.0303	0.0607	0.1164	0.1821	0.2378	0.3035	0.3642	0.4249

Table 6.1 The numerical value of the angle of incidence and initial tangential velocity

The time histories of the normal displacement of the contact node 1712 and the rigid sphere for all eight cases are shown in Figure 6.3 and Figure 6.4 respectively. From the Figures, we can see there is no difference between cases for the normal displacement of either that of the contact node or that of the rigid sphere.

The nodal time history of the tangential displacement of the contact node 1712 and the rigid body displacement are shown in Figure 6.5 and Figure 6.6. From the results, we can see the larger the initial tangential velocity, the larger the tangential displacement. The comparison of the normal velocity between the nodal time history and the rigid body velocity are shown in Figure 6.7 and Figure 6.8. The normal rigid body velocity is very close to the prediction from the simplified coupled-conservative model. From Figure 6.8, we can see there is dissipation of the normal velocity, the normal velocity of separation is less than the incident normal velocity.

The time histories of the tangential velocity for the nodal velocity and the rigid body velocity are shown in Figure 6.9 and Figure 6.10. Although the tangential velocity of the contact node predicted from DYNA3D vibrates a lot, we still can see there is

reverse tangential velocity in small incident angle case from Figure 6.9. That is, the tangential velocity turns to opposite direction during contact. The rigid body acceleration gives us the idea of the interaction force. The normal and the tangential acceleration of the solid sphere are shown in Figure 6.11 and Figure 6.12 respectively. The time history of the tangential acceleration of the solid sphere is very close to that of the tangential force predicted by the simplified coupled-conservative model.

It will be of interest to know the time history of the internal energy and the kinetic energy change. From Figure 6.13 and Figure 6.14, we can see the internal energy it not different for different cases and there is some kinetic energy loss in all cases. The time history of the kinetic energy loss is shown in Figure 6.15.

The time histories of normal and tangential impulse are shown in Figure 6.16 and Figure 6.17. The results of the normal and tangential impulse are close to those predicted from the simplified coupled-conservative model. The relationship of the normal impulse and tangential impulse is shown in Figure 6.18. We can see the prediction is very similar to previous research. The normal and tangential forces can be given after integrating the relative impulse by MATHCAD program and are shown Figure 6.19 and Figure 6.20. Compared with the previous research, we see the DYNA3D finite element code gives pretty good prediction.

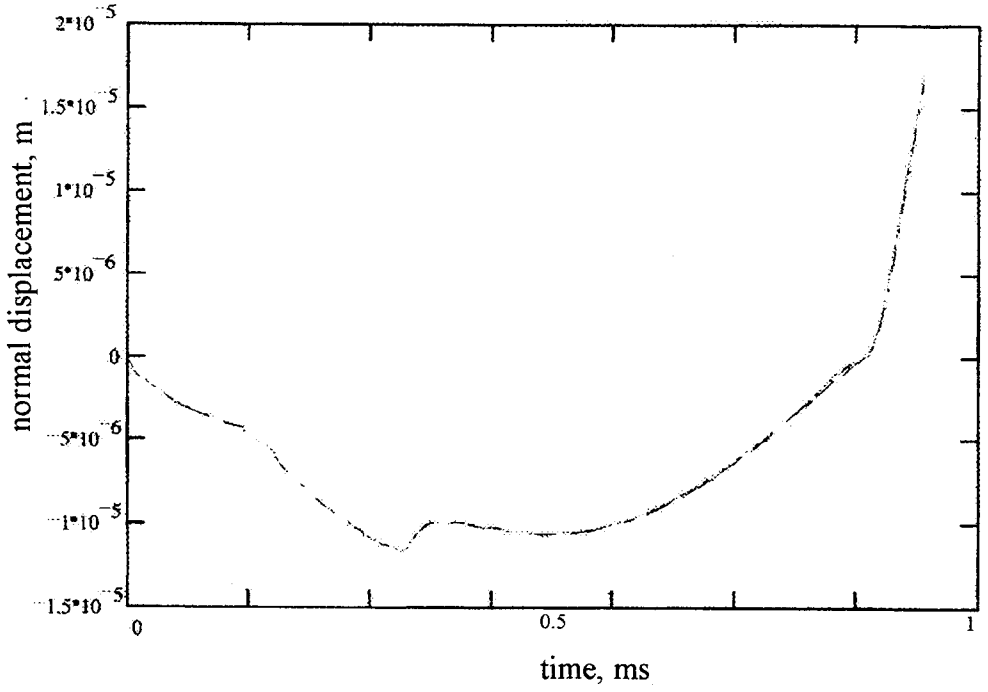

Figure 6.3 The time history of the normal displacement of contact node 1712

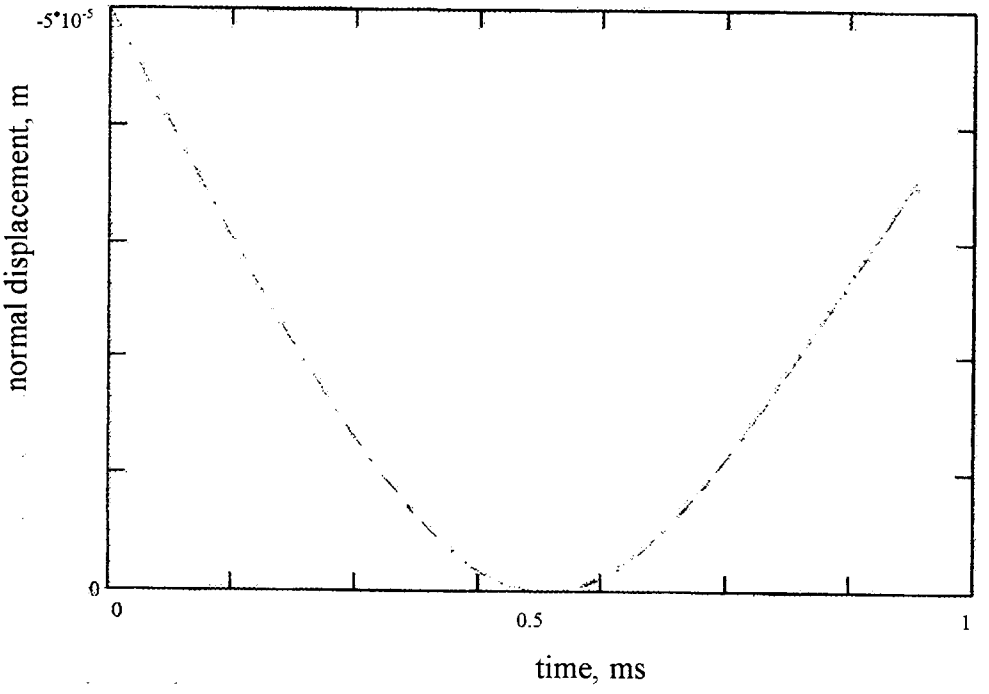

Figure 6.4 The time history of the normal rigid body displacement

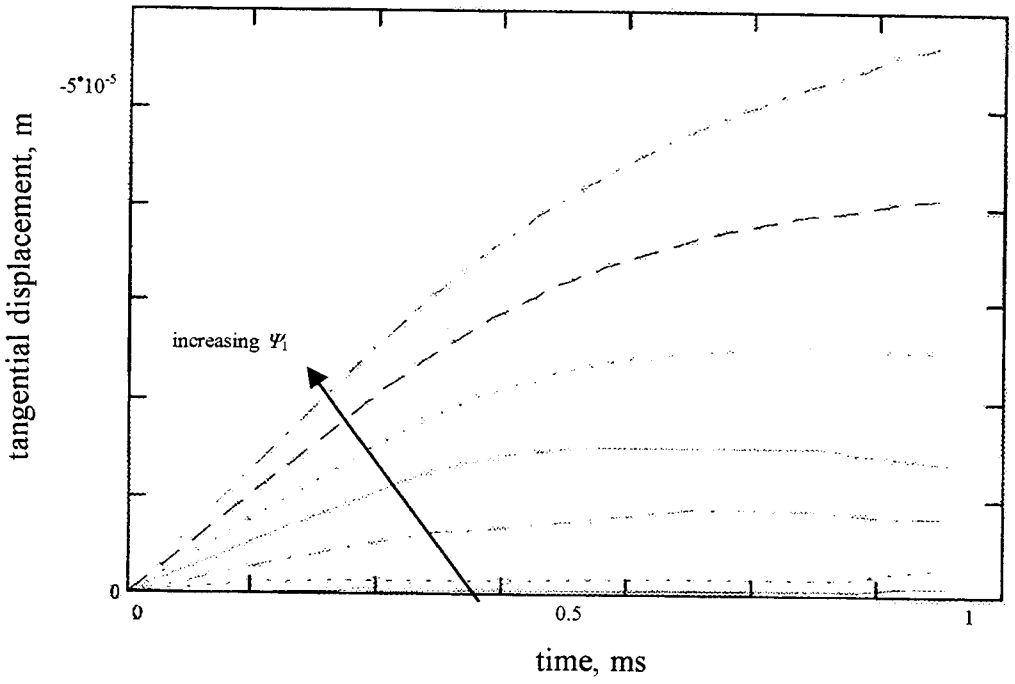

Figure 6.5 The time history of the tangential displacement of the contact node 1712 for different angles of incidence

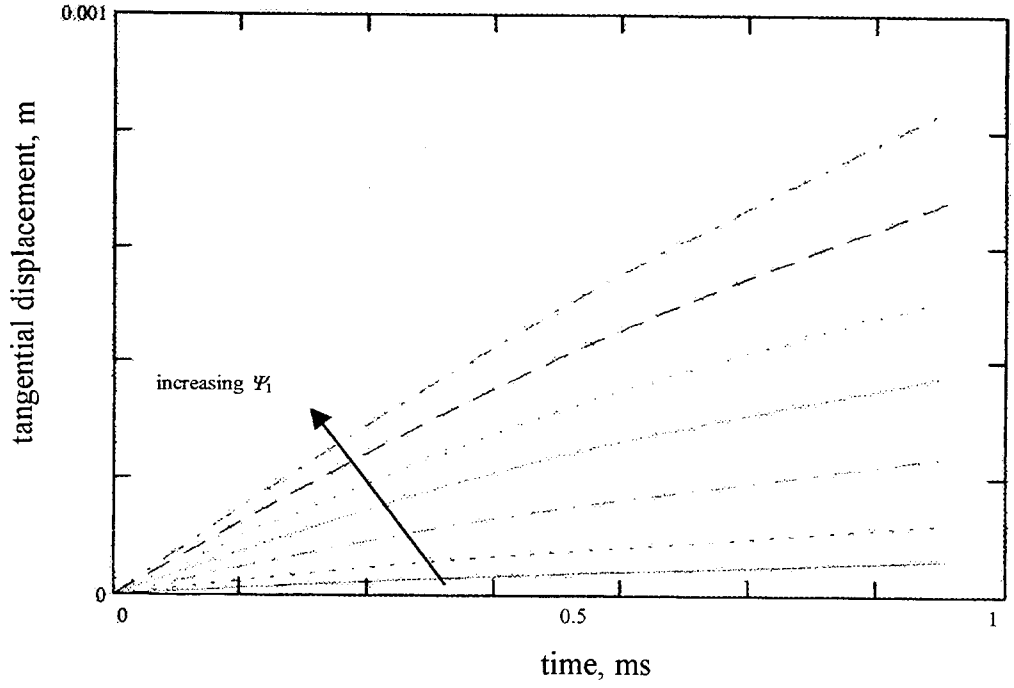

Figure 6.6 The time history of the tangential rigid body displacement

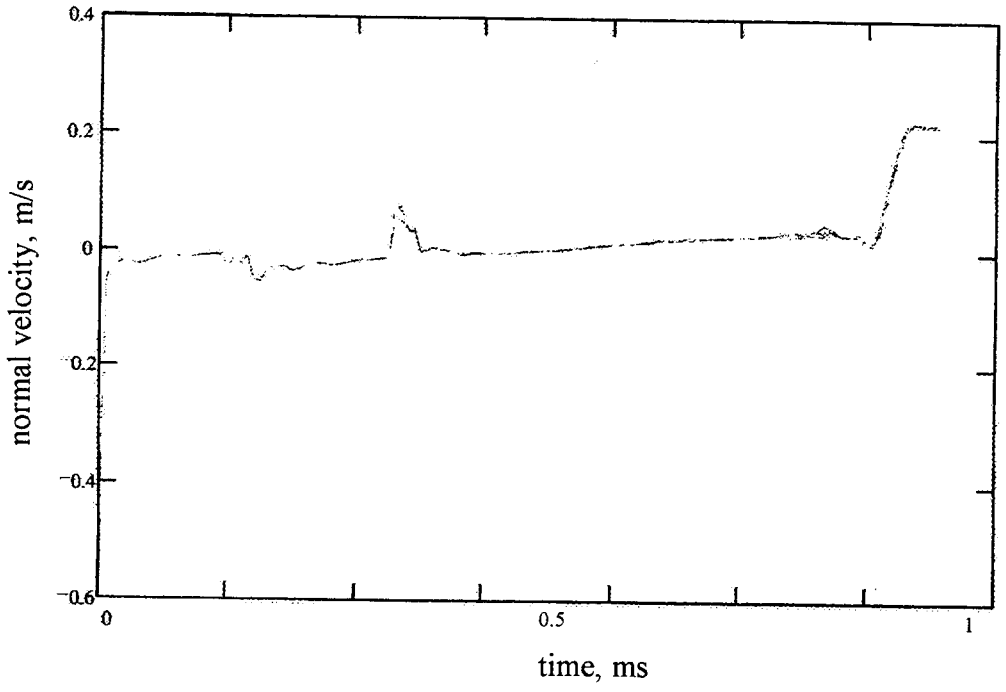

Figure 6.7 The time history of the normal velocity of the contact point

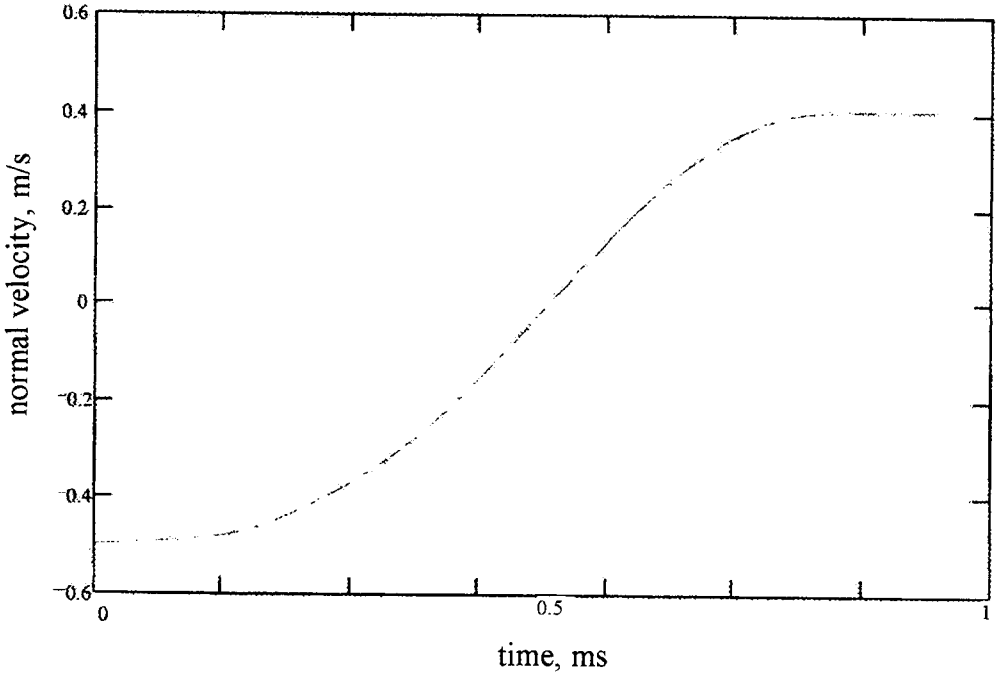

Figure 6.8 The time history of the normal rigid body velocity

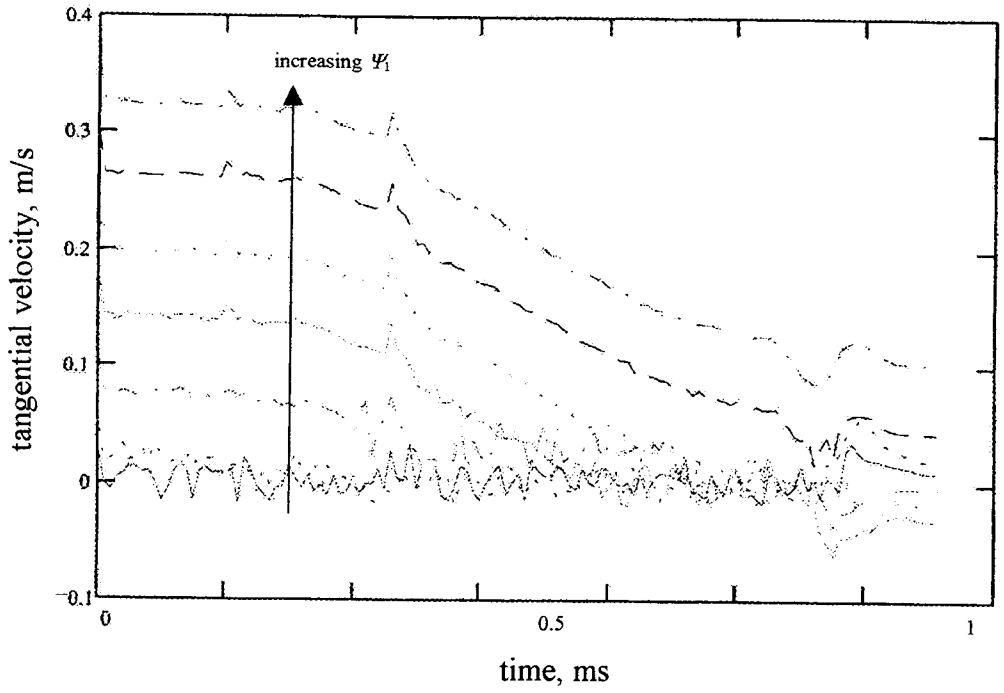

Figure 6.9 The time history of the tangential velocity of the contact point

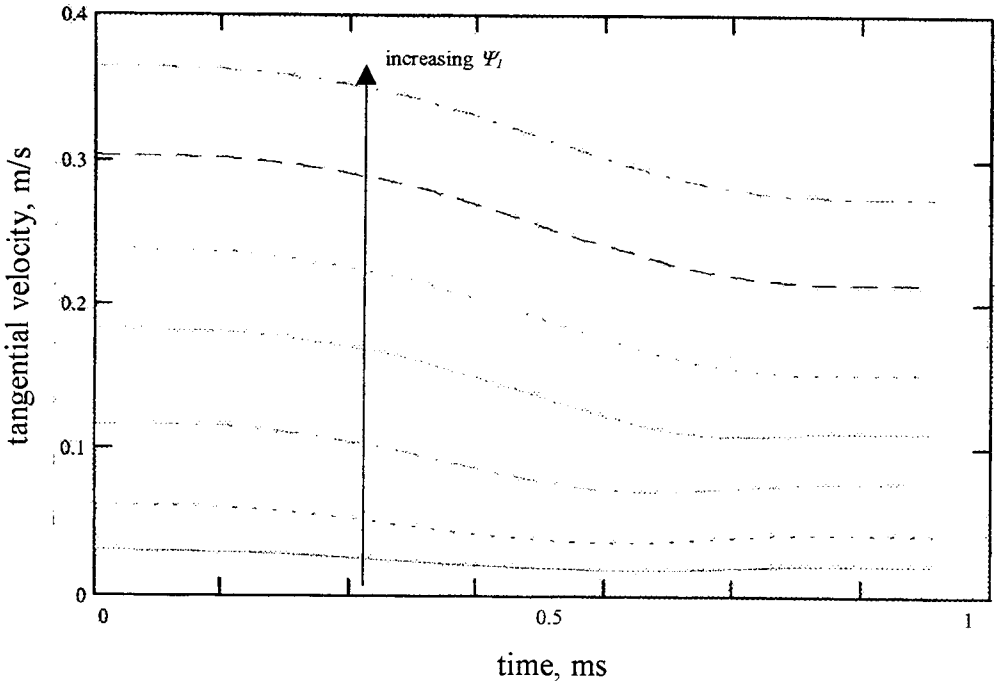

Figure 6.10 The time history of the tangential rigid body velocity

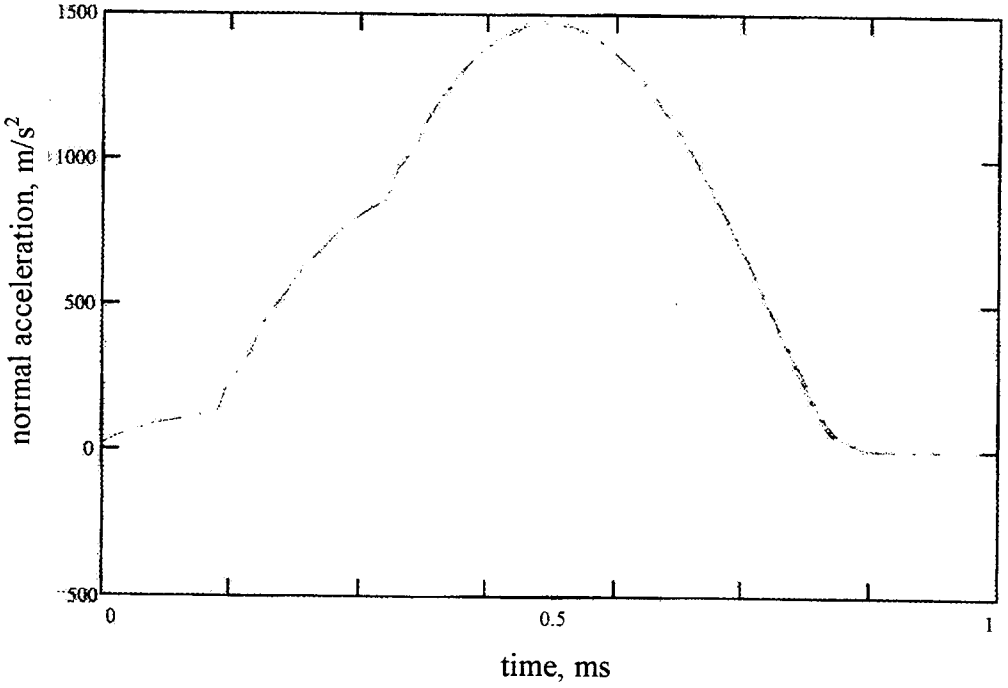

Figure 6.11 The time history of the normal rigid body acceleration

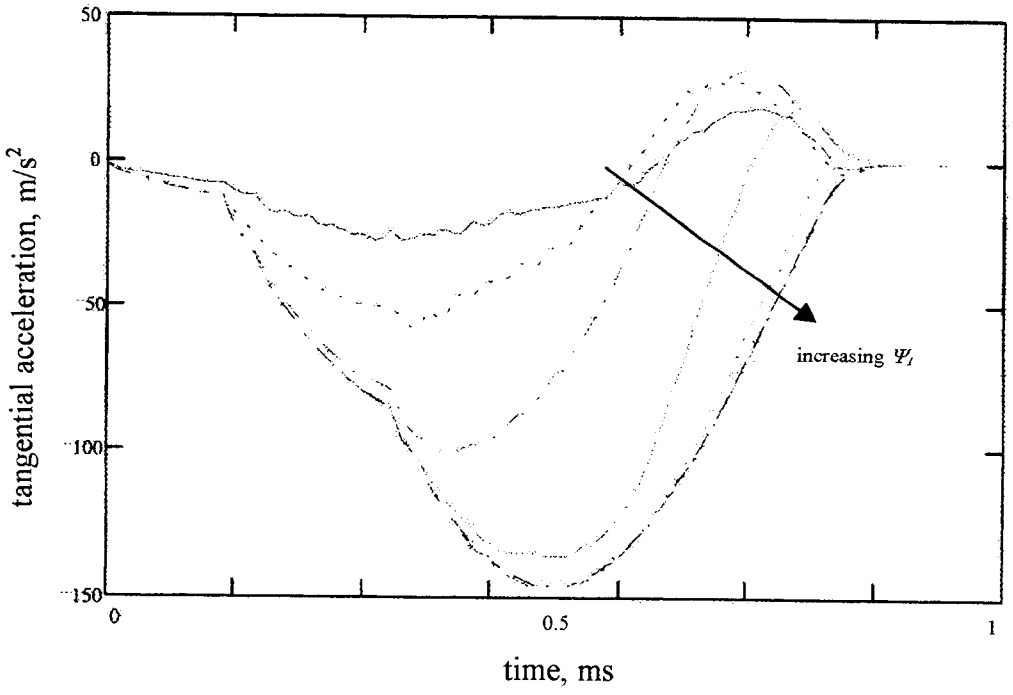

Figure 6.12 The time history of the tangential rigid body acceleration

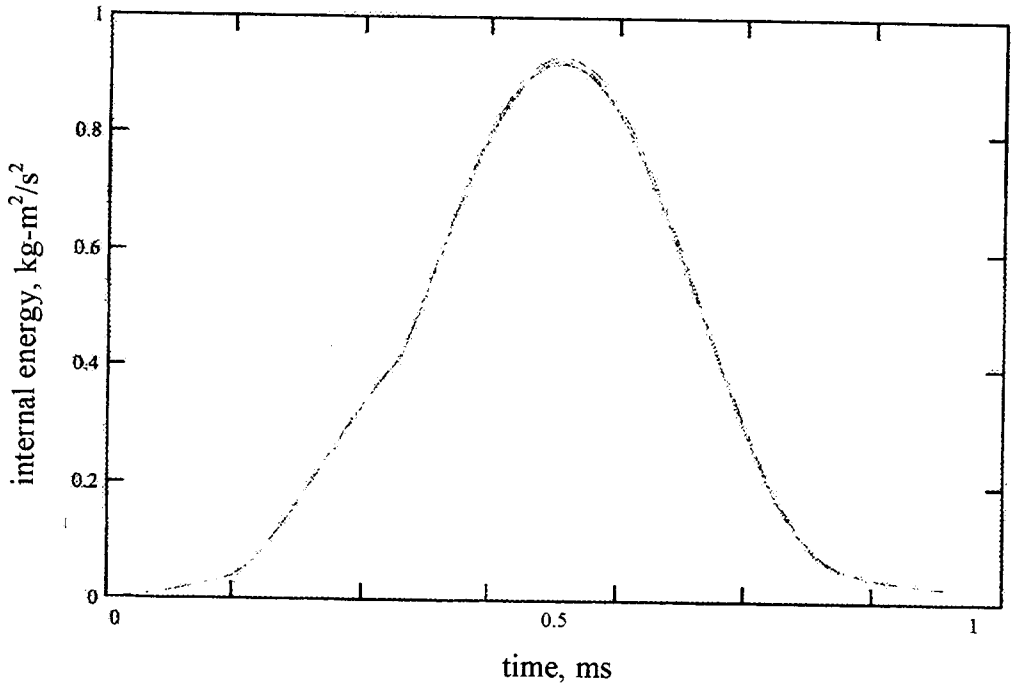

Figure 6.13 The time history of the internal energy of the rigid sphere

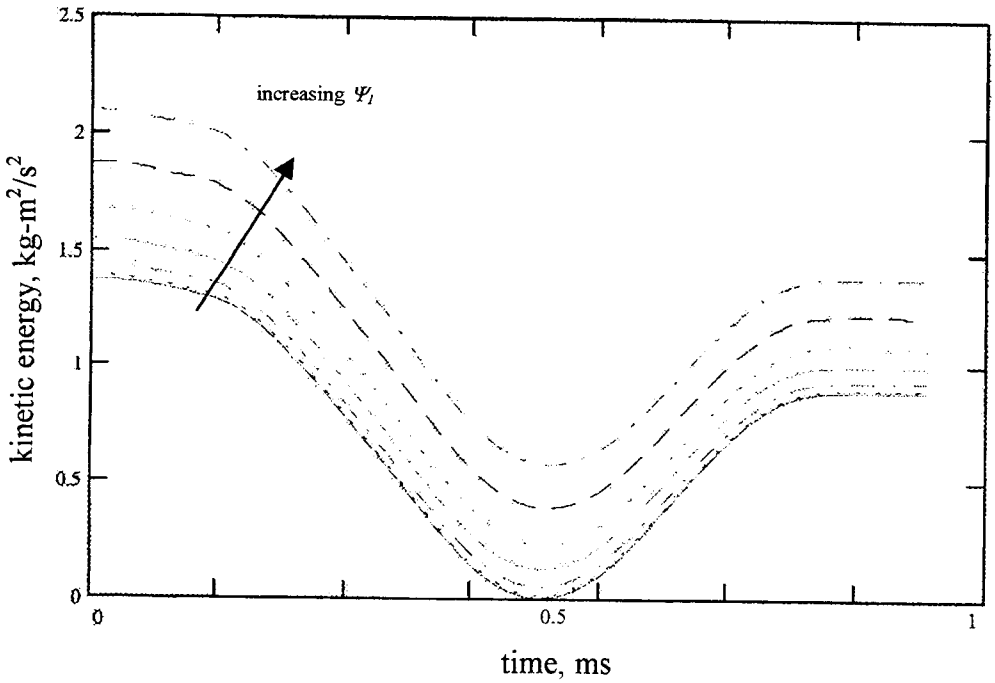

Figure 6.14 The time history of the kinetic energy of the rigid sphere

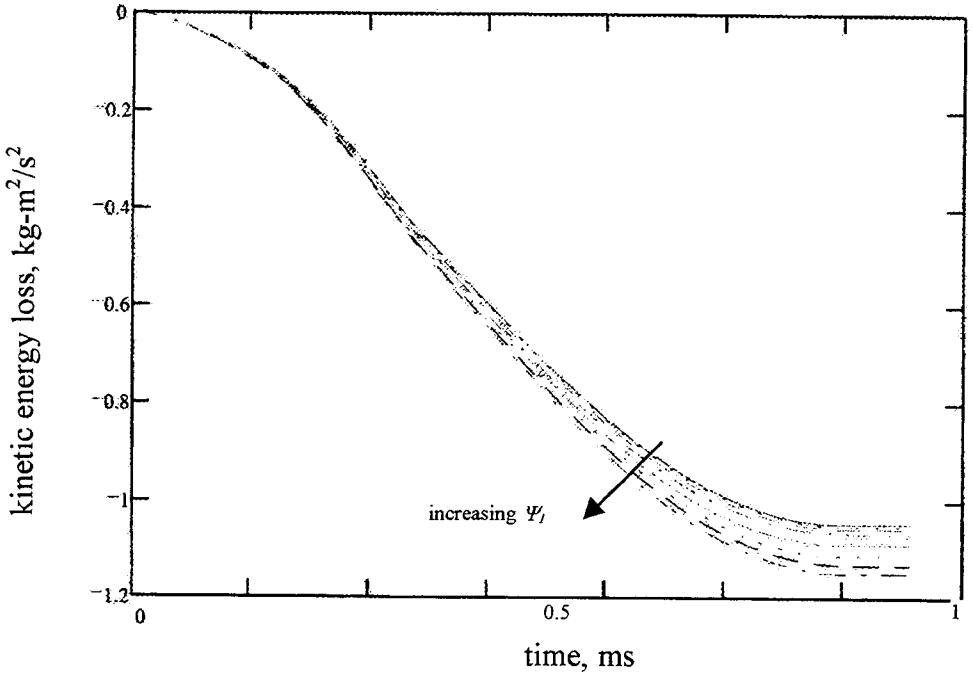

Figure 6.15 The time history of the kinetic energy loss of the rigid sphere

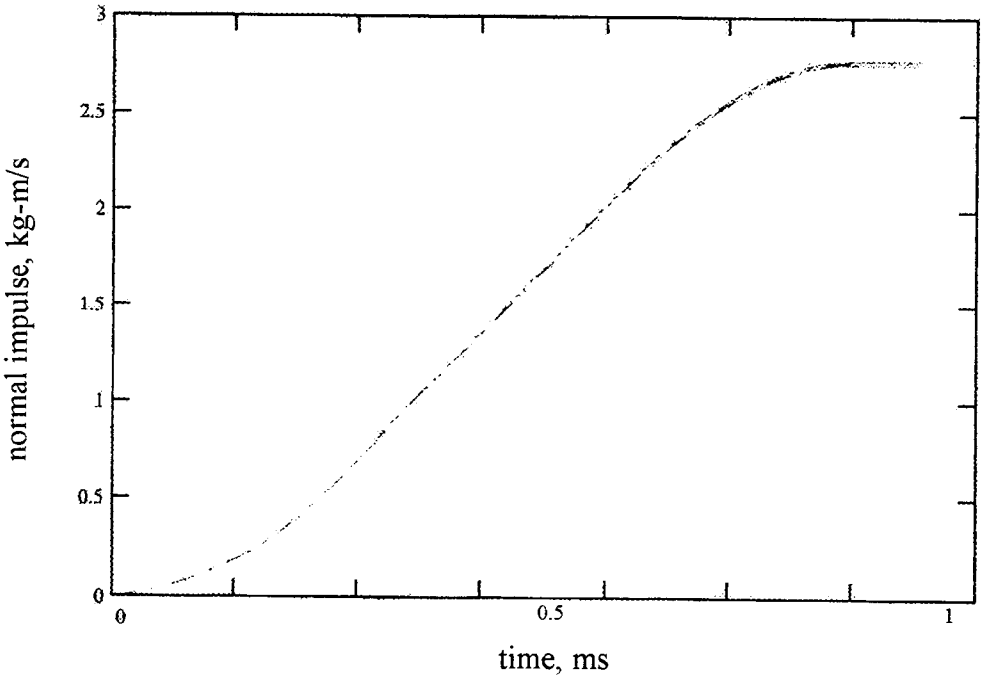

Figure 6.16 The time history of the normal impulse of the rigid sphere

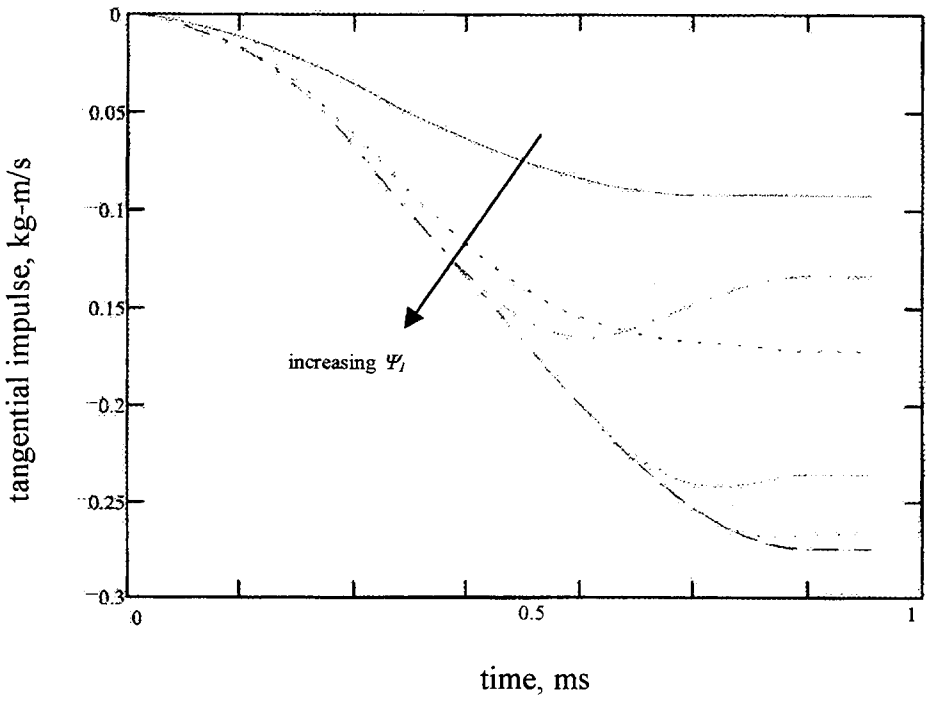

Figure 6.17 The time history of the tangential impulse of the rigid sphere

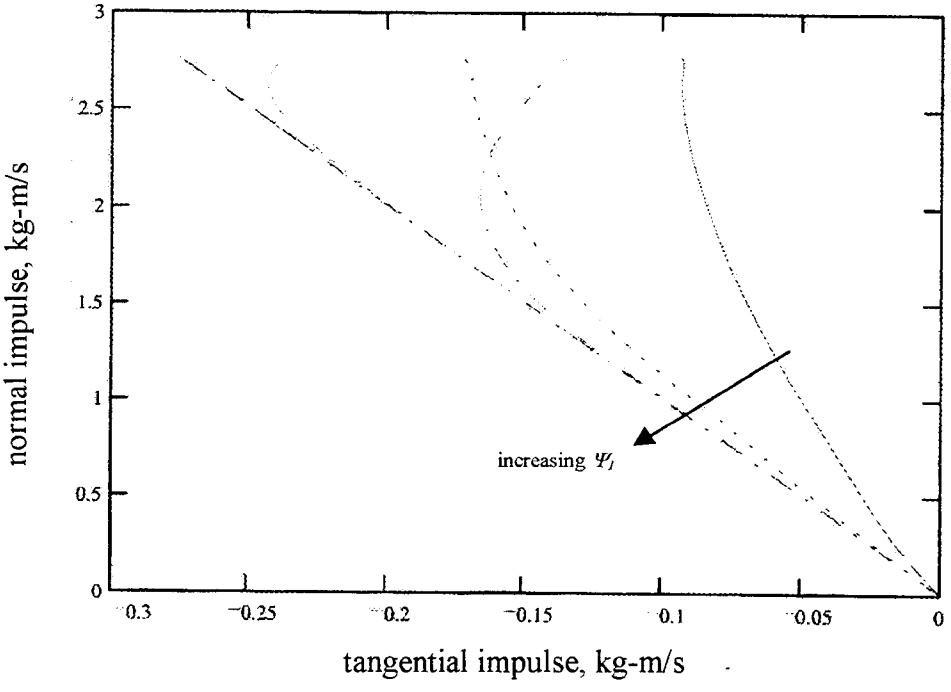

Figure 6.18 The relationship of the normal impulse and the tangential impulse of the rigid sphere

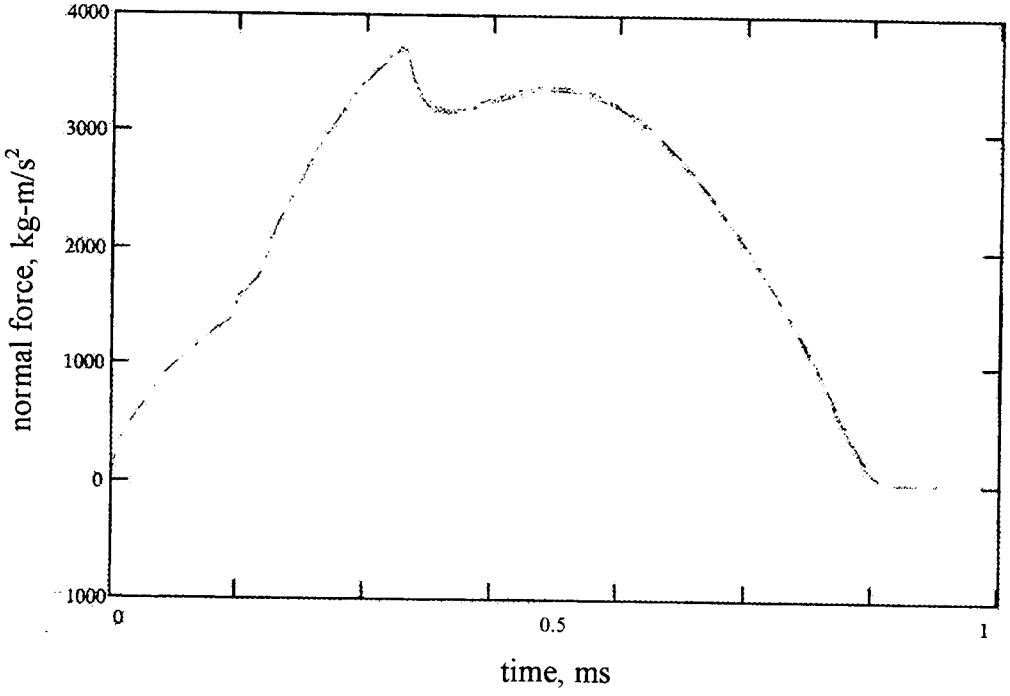

Figure 6.19 The time history of the normal force of the rigid sphere

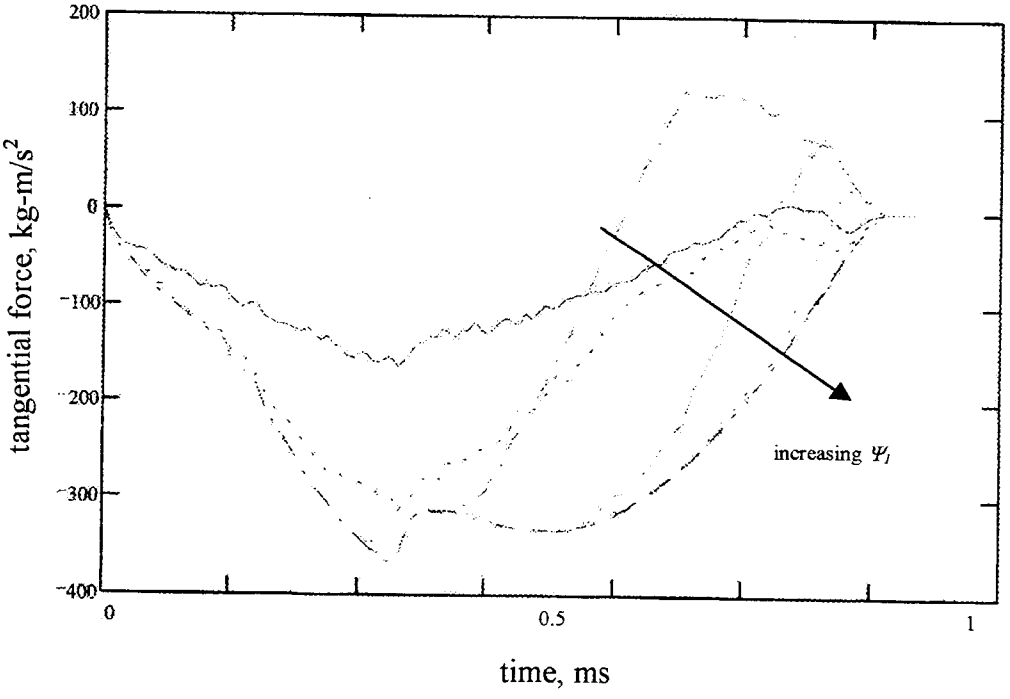

Figure 6.20 The time history of the tangential force of the rigid sphere

6.3 The Collision of the Rod with a Rigid Surface

The collision of the cylindrical rod with a rigid surface discussed in chapter 5 was simulated by DYNA3D also. This system consists of a cylindrical rod with $L/R = 5$ and a rigid half-space surface. The mesh of the model drawn by INGRID is shown in Figure 6.21. Since the initial velocity is small enough that the configuration of the system will not change during impact, the contact area is very small compared with the whole body of the cylinder rod, which is shown in Figure 6.22. The detail of the mesh between the contact area and the whole cylinder rod is shown in Figure 6.23. In order to have finer mesh at the contact surface and conserve the time consumed in calculation, the memory of the computer simultaneously, the mesh of the rod is divided into several parts with different mesh density. As seen in Figure 6.24, the different parts of the rod have different mesh sizes. This causes discontinuities between different parts of the rod, which gives rise to errors of calculation happens. In Figure 6.25 and Figure 6.26, the relationship of the normal impulse and tangential impulse for case a and case b as discussed in chapter 5.5 are shown respectively. Comparing these results with those of the simplified non-linear coupled conservative model, we can see the results of DYNA3D model is not as good as we expected. The reason maybe comes from the discontinuity between the different part of the mesh of the rod. The analysis of the cylinder rod impact has not been completed. The refinement of the finite element code and the increase of the memory of the computer need to be done in the future for improving the analysis of the cylinder rod impact.

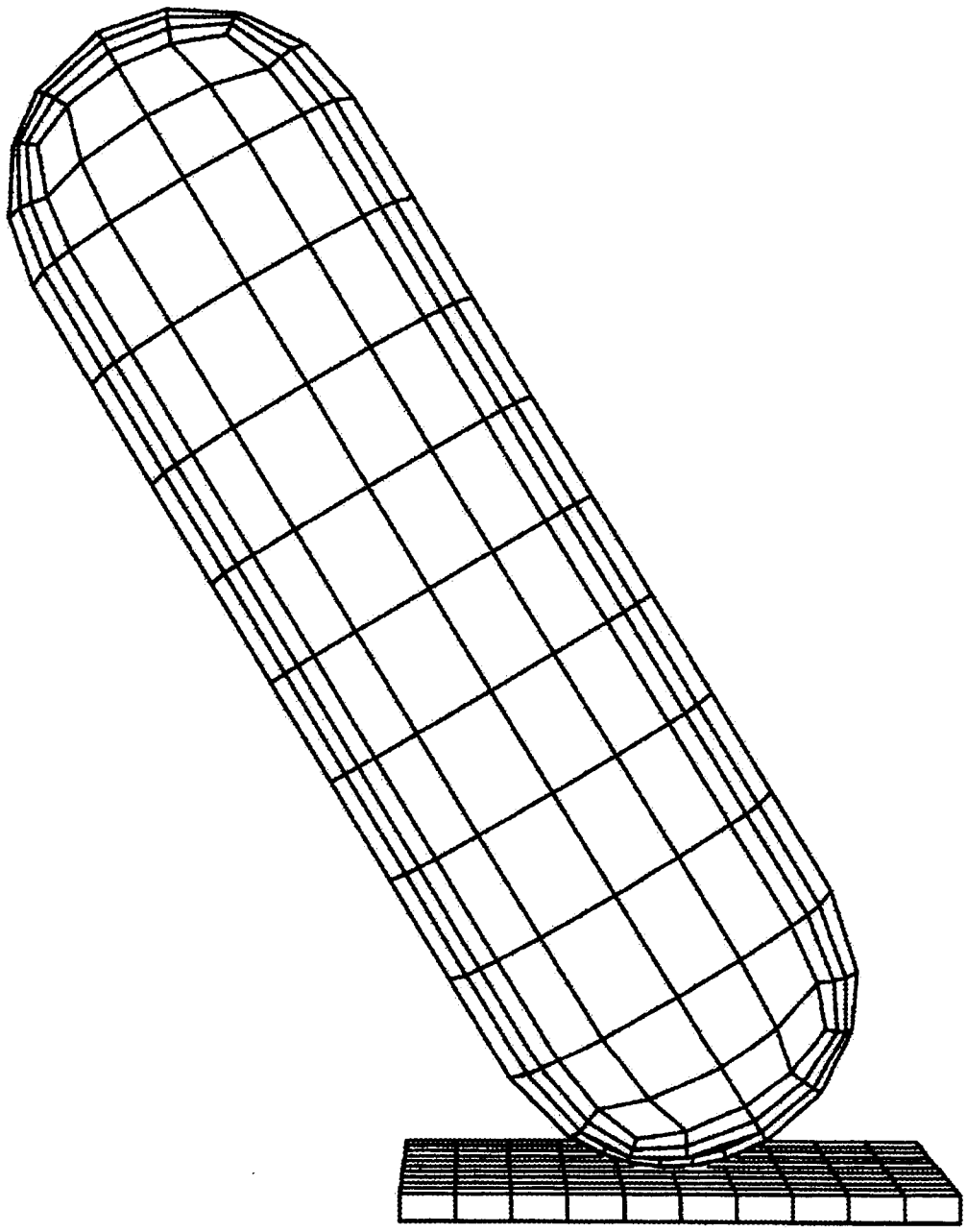

Figure 6.21 The model of the bar impact for DYNA3D finite element code

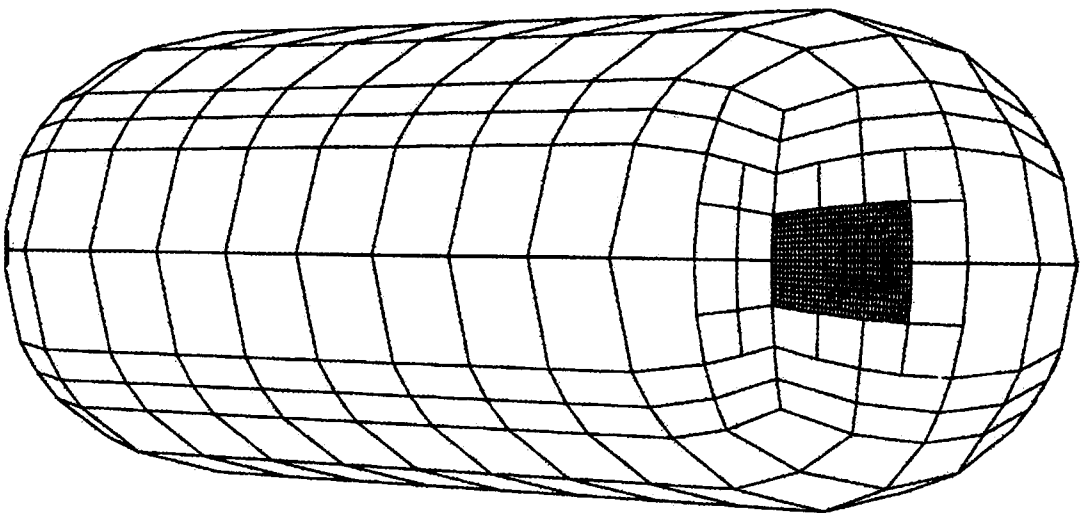

Figure 6.22 The contact surface of the bar impact

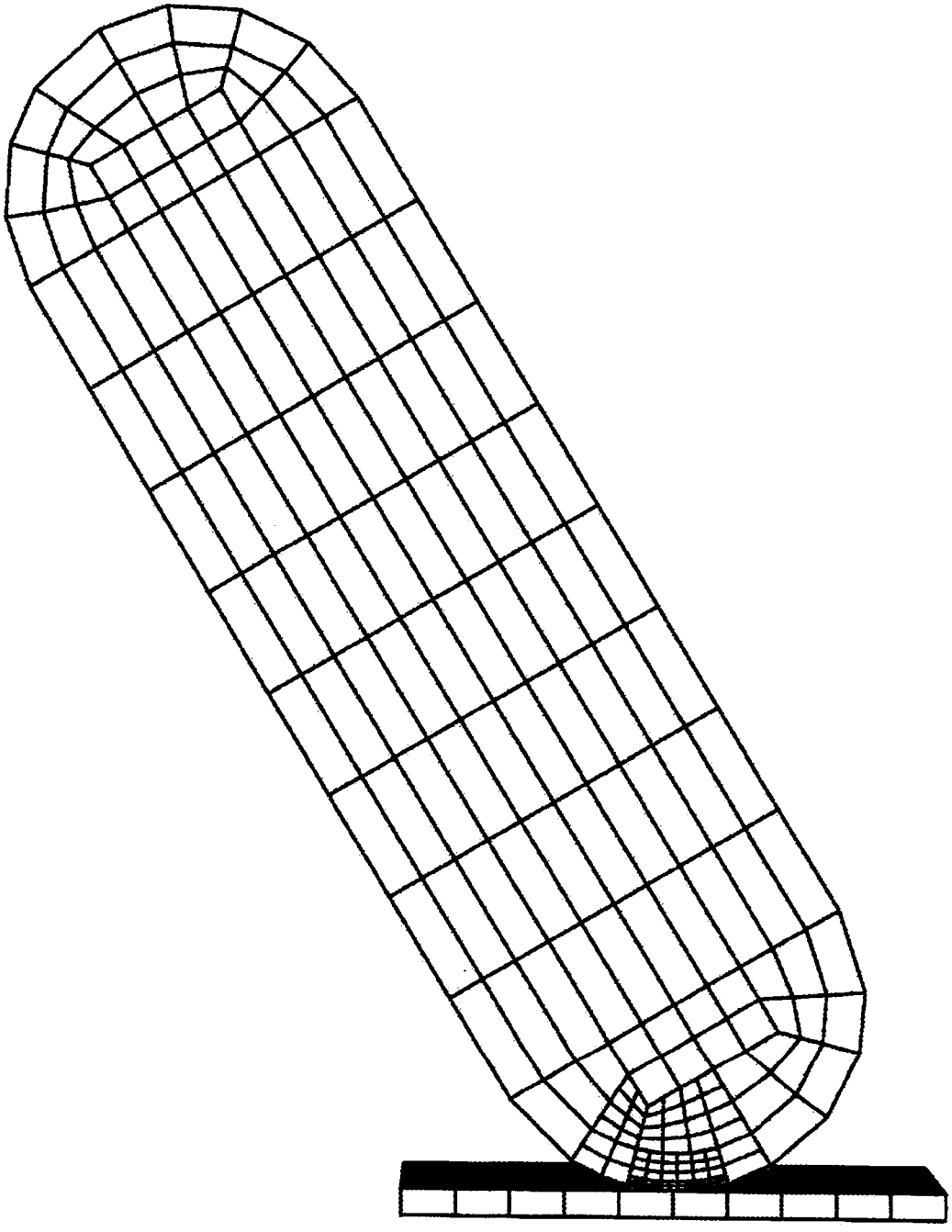

Figure 6.23 The mesh of the bar impact for the half of the bar

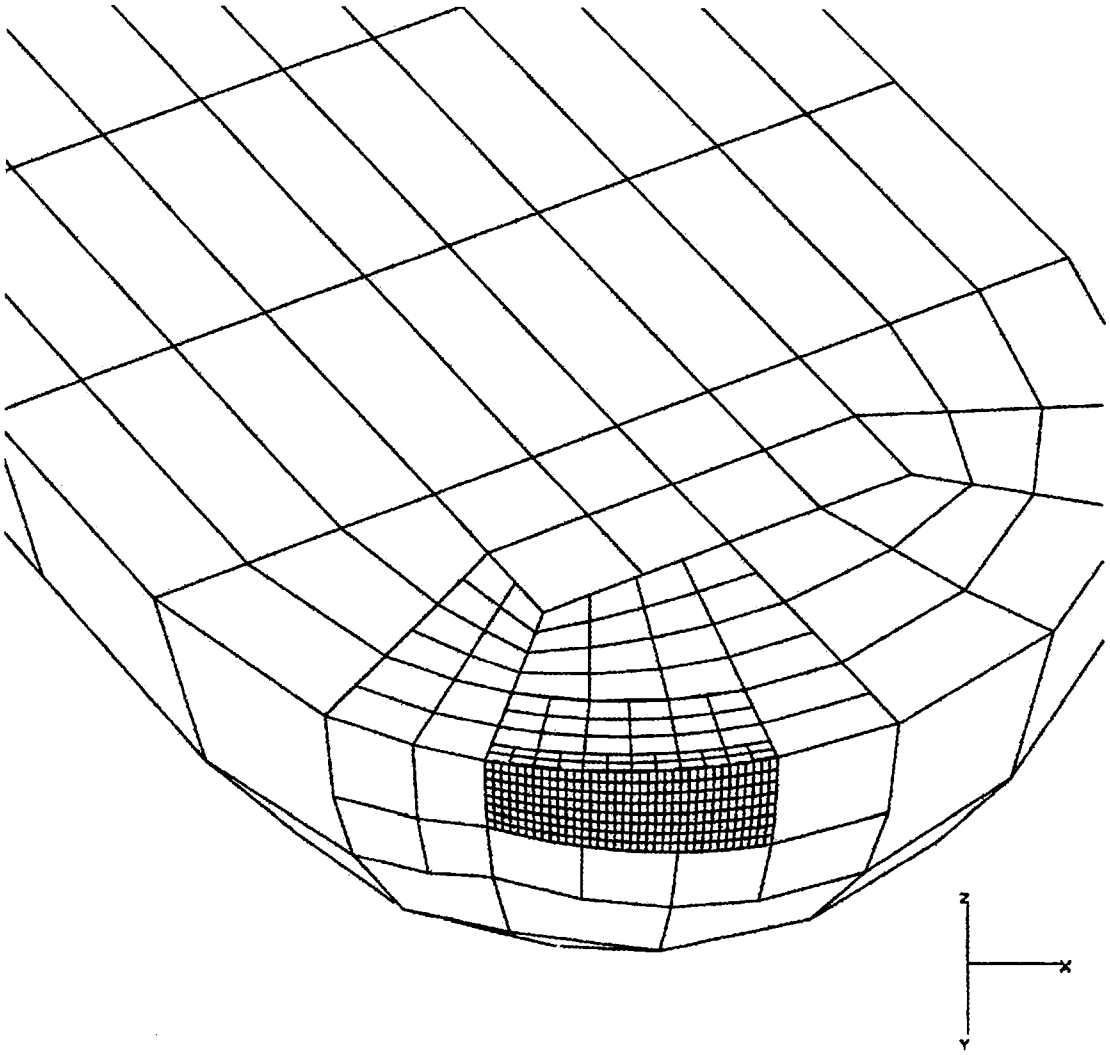

Figure 6.24 The detail mesh of the contact surface of the bar impact

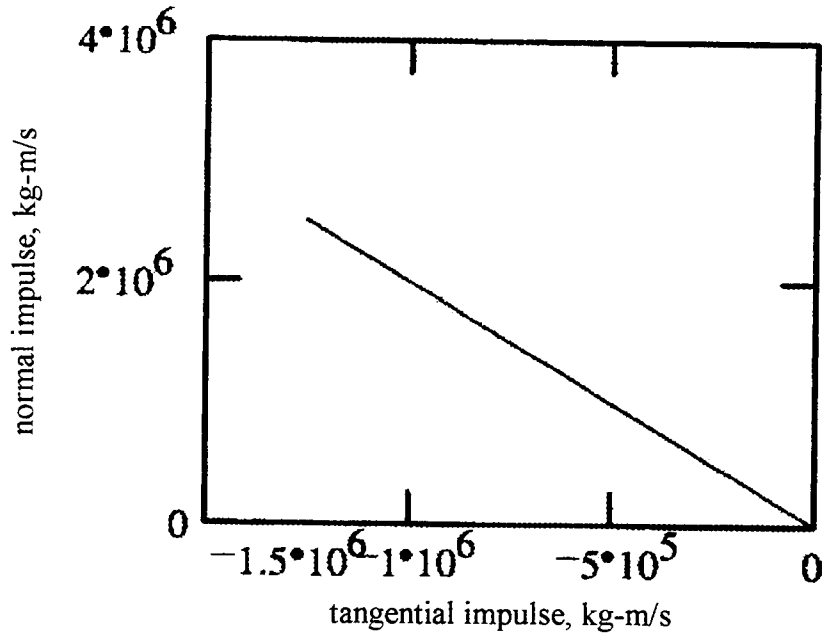

Figure 6.25 The normal impulse and the tangential impulse of the rod impact for case a

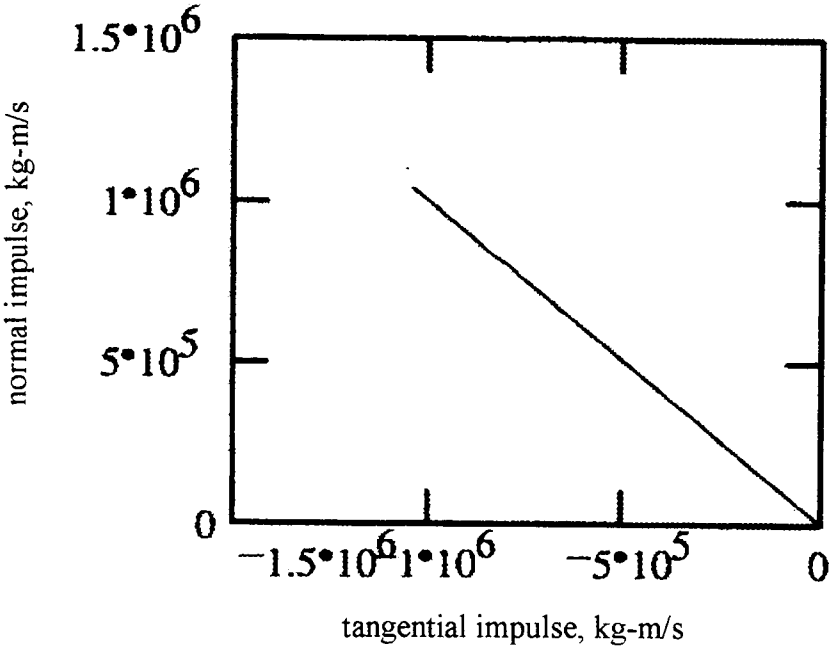

Figure 6.26 The normal impulse and the tangential impulse of the rod impact for case b

7. CONCLUSIONS

The analysis of the planar impact of two bodies in a mechanical system is refined by the consideration of the elastic deformations at contact surface. Each body was assumed to exert an instantaneous impulse on the other at the contact point and the configuration of the system remained unchanged during contact. From Hertz theory, the contact area was assumed to be circular and very small that is compared to the size of the bodies. A static analysis of the contact area was applied by introducing the compliance in both normal and tangential directions. In this simplified non-linear coupled-conservative model, the tangential compliance has its influence on the post-collision results. It was also assumed that the elastic potential energy is conservative. By the application of the spring, which represents the deformation on elastic half-space, the influence of the tangential traction upon normal pressure was represented. Therefore, from this analysis of the contact mechanism, the simplified contact mass-spring vibrating model can achieve the prediction of the elastic collision. The energy dissipation considered in the simplified model is due only to the friction. In this investigation of the simplified non-linear coupled-conservative model, the resultant equations were integrated with a numerical method.

This simplified model constitutes an effort to analyze the impact motions for general configurations analytically. It was determined that for a given Poisson ratio, ν, of colliding bodies, only four parameters, including the inertia coupling λ and θ, friction coefficient μ and the ratio of incident velocity $\tan\alpha$, can have an effect upon the prediction of the motion of mechanical collisions. Other material properties, including

Young's modulus and mass density, will thus not effect the collision motions. All slip and stick conditions of incident velocity at the initial state of impact for general configuration have been found in terms of inertia coupling parameters λ, θ and friction coefficient μ.

In this investigation, the DYNA3D program was used to predict the post-collision motion of elastic bodies and the results from DYNA3D are compared with those from simplified coupled-conservative model. The results of the oblique impact of the solid sphere from DYNA3D are close to the real system and satisfied. The more the elements and nodes the mesh has, the more accurate the program predicts. Since numerical method frequently limits the time increments and requires long running time in calculation, the computation with DYNA3D program is much more time and memory consuming. On the contrary, the simplified model provides a great advantage in simplicity and stability in many situations. In order to compare the results with those of the simplified coupled-conservative model, we need to recalculate the results of the DYNA3D from the post-processor, TAURUS, by running MathCad program. From TAURUS, since the results of the contact node are very unstable, the results of the rigid body output are used for comparison instead.

The results from the DYNA3D program for rod impact is not as good as we expected. The processing of DYNA3D program for rod impact has lots of difficulties. In order to have finer mesh at the contact surface and conserve the time consuming of calculation, the memory of the computer simultaneously and the assumptions of the model, the mesh of the rod is difficult to construct. The investigation of the elastic deformation of the contact surface needs fine mesh for accuracy. But concerning the

time consuming of calculation, we need to separate the rod into several parts with different mesh density. Therefore, between the different parts of the mesh, there are discontinuities in the mesh, which cause errors in the calculation.

The future work should be focused on the refinement of the discontinuity of the mesh for the DYNA3D finite element method. The ability of the capacity of calculation for the computer and the refinement of the software, such as the commercial version of the DYNA3D finite element code, will improve the accuracy of prediction for this investigation.

In the future, the simplified coupled-conservative model can be extended to deal with three-dimensional systems. The introduction of material damping can also be incorporated to account for internal dissipation.

BIBLIOGRAPHY

Aum, H. S. 1992. Parameters affecting mechanical collisions. Ph. D. Dissertation Oregon State University Corvallis Oregon.

Brach, R. M. 1984. Friction, restitution, and energy loss in planar collisions. ASME Journal of Applied Mechanics 51: 164-170.

Brach, R. M. 1989. Rigid body collision. ASME Journal of Applied Mechanics 56: 33-138.

Goldsmith, W. 1960. Impact. London: Cambridge.

Hallquist, J. O. 1983. Theoretical manual for DYNA3D. Lawrence Livermore National Laboratoy.

Hallquist, J. O., Christon, M. A. and Dovey, D. 1990. INGRID a 3-d mesh generator for modeling nonlinear systems user manual. Methods Development Group Lawrence Livermore National Laboratory.

Hallquist, J. O. and Spelce, T. 1991. TAURUS: an interactive post-processor for the analysis codes NIKE3D, DYNA3D, and TOPAZ3D. Methods Development Group Lawrence Livermore National Laboratory.

Hunter, S. C. 1957. Energy absorbed by elastic waves during impact. Journal of the Mechanics and Physics of Solids 5: 162-171. London: Pergamon Press Ltd.

Johnson, K. L. 1985. Contact mechanics, London: Cambridge.

Kane, T. R. and Levinson, D. A. 1985. Dynamics: theory and applications. New York: McGraw-Hill.

Keller, J. B. 1986. Impact with friction. ASME Journal of Applied Mechanics 53: 1-4.

Liu, Pao-Pao. 1991. Rebound predictions for elastic collision. Ph. D. Dissertation Oregon State University Corvallis Oregon.

Maw, N., Barber, J. R., and Fawcett, J. N. 1976. The oblique impact of elastic spheres. Wear Vol. 38 No. 1 pp. 101-114.

Maw, N., Barber, J. R. and Fawcett, J. N. 1981. The role of elastic tangential compliance in oblique impact. ASME Journal of Lubrication Technology 103: 74-80.

Mindlin, R. D. 1949. Compliance of elastic bodies in contact. ASME Journal of Applied Mechanics 71: 259-268.

Mindlin, R. D. and Deresiewicz, H. 1953. Elastic spheres in contact under varying oblique forces. ASME Journal of Applied Mechanics 75: 327-344.

Routh, E. J. 1905. Dynamics of a system of rigid bodies. London: Macmillan and Co.

Smith, C. E. 1991. Prediction rebounds using rigid body dynamics. ASME Journal of Applied Mechanics 58: 754-758.

Smith, C. E. and Liu, P. 1992. Coefficients of restitution. ASME Journal of Applied Mechanics 59: 963-969.

Stronge, W. J. 1990. Rigid body collisions with friction. London: Proc. R. Soc. 431:169-181

Stronge, W. J. 1994. Planar impact of rough compliant bodies. International Journal of Impact engineering 15: 435-450.

Timoshenko, S. P. and Goodier, J. N. 1970. Theory of elasticity. 3rd edn. New York: McGraw-Hill.

Whirley, R. G. and Engelmann, B. E. 1993. DYNA3D a nonlinear, explicit, three-dimensional finite element code for solid and structural mechancis-user manual. Methods Development Group Lawrence Livermore National Laboratory.

Whittaker, E. T. 1904. A treatise on the analytical dynamics of particles and rigid bodies. London: Cambridge.